PARAMETRIC INTERPOLATION METHOD FOR LONG-TERM EXTREME RESPONSE AND PROBABILISTIC FATIGUE PREDICTION OF OFFSHORE STRUCTURES

Juan Sebastián Monsalve Giraldo

Tese de Doutorado apresentada ao Programa de Pós-graduação em Engenharia Civil, COPPE, da Universidade Federal do Rio de Janeiro, como parte dos requisitos necessários à obtenção do título de Doutor em Engenharia Civil.

Orientador: Luis Volnei Sudati Sagrilo

Rio de Janeiro

Dezembro de 2018

PARAMETRIC INTERPOLATION METHOD FOR LONG-TERM EXTREME RESPONSE AND PROBABILISTIC FATIGUE PREDICTION OF OFFSHORE STRUCTURES

Juan Sebastián Monsalve Giraldo

TESE SUBMETIDA AO CORPO DOCENTE DO INSTITUTO ALBERTO LUIZ COIMBRA DE PÓS-GRADUAÇÃO E PESQUISA DE ENGENHARIA (COPPE) DA UNIVERSIDADE FEDERAL DO RIO DE JANEIRO COMO PARTE DOS REQUISITOS NECESSÁRIOS PARA A OBTENÇÃO DO GRAU DE DOUTOR EM CIÊNCIAS EM ENGENHARIA CIVIL.

Examinada por:

Prof. Luis Volnei Sudati Sagrilo, D.Sc.

Dr. Paulo Maurício Videiro, PhD.

Prof. Fernando Jorge Mendes de Sousa, D.Sc.

Prof. Breno Pinheiro Jacob, D.Sc.

Prof. Marcelo Igor Lourenço de Souza, D.Sc.

Prof. Celso Kazuyuki Morooka, PhD.

RIO DE JANEIRO, RJ-BRASIL

DEZEMBRO DE 2018

Monsalve Giraldo, Juan Sebastián

Parametric Interpolation Method for Long-Term Extreme Response and Probabilistic Fatigue Prediction of Offshore Structures / Juan Sebastián Monsalve Giraldo. – Rio de Janeiro: UFRJ/COPPE, 2018.

XV, 104 p.: il.; 29,7 cm.

Orientador: Luis Volnei Sudati Sagrilo

Tese (Doutorado) – UFRJ/ COPPE/ Programa de Engenharia Civil, 2018.

Referências Bibliográficas: p. 98-102.

1. Estruturas offshore. 2. Risers rígidos. 3. Fadiga probabilística. 4. Estatística de longo prazo da resposta. 5. Interpolação parabólica. 6. Interpolação exponencial. I. Sagrilo, Luis Volnei Sudati *et al*. II. Universidade Federal do Rio de Janeiro, COPPE, Programa de Engenharia Civil. III. Título.

Acknowledgments

I would like to express my sincere thanks to my supervisor Professor Luis Volnei Sudati Sagrilo, for his dedication, guidance, patience and instructions throughout this research project. He steered me in the right direction whenever he thought I needed it.

I would also like to thank the experts who were involved in this research project: Dr. Paulo Mauricio Videiro, Prof. Fernando José Mendes de Sousa and the researchers of CENPES/PETROBRAS that also contributed to the development of this thesis. Without their participation, this work could not have been successfully conducted.

I am thankful to the friends and colleagues of LACEO for their friendship and valuable professional support.

I must express my very profound gratitude to my wife Priscilla Maiolino, to my friends, family and to my parents Gloria Amparo Giraldo and Luis Ernesto Monsalve which even distant, always supported me. They provided me with unfailing continuous encouragement throughout my years of study and through the process of researching and writing this doctoral thesis.

Finally, I would like to thank CNPq (National Council for Scientific and Technological Development), COPPE (Alberto Luiz Coimbra Institute for Graduate Studies and Engineering Research) and PETROBRAS for financial support.

Juan Sebastián Monsalve Giraldo

December 2018

Resumo da Tese apresentada à COPPE/UFRJ como parte dos requisitos necessários para a obtenção do grau de Doutor em Ciências (D.Sc.)

MÉTODO DE INTERPOLAÇÃO PARAMÉTRICA PARA A PREDIÇÃO DA RESPOSTA EXTREMA DE LONGO PRAZO E DA FADIGA PROBABILÍSTICA DE ESTRUTURAS *OFFSHORE*

Juan Sebastián Monsalve Giraldo

Dezembro/2018

Orientador: Luis Volnei Sudati Sagrilo

Programa: Engenharia Civil

Este trabalho apresenta uma metodologia semi-analítica para avaliar eficientemente as integrais multidimensionais encontradas nas análises de resposta extrema de longo prazo e fadiga probabilística de estruturas *offshore*. Algumas metodologias tradicionais usadas tanto na avaliação da resposta extrema de longo prazo quanto na análise probabilística de fadiga de estruturas marinhas descritas na literatura são discutidas neste estudo. Além desses métodos, um novo procedimento para otimizar esses cálculos é desenvolvido e apresentado em detalhes neste trabalho. O método proposto baseia-se na interpolação paramétrica de variáveis que descrevem as séries temporais de respostas de curto prazo; por exemplo, os parâmetros estatísticos da distribuição de probabilidade de picos e os danos à fadiga de curto prazo. Este método de interpolação é então usado para avaliar eficientemente as integrais de convolução de longo prazo. Três exemplos são apresentados mostrando a eficiência e precisão do método proposto quando comparados com os métodos de integração completa (metodologia da "força bruta"). No primeiro exemplo, um modelo analítico de um grau de liberdade é analisado no domínio da frequência. No segundo exemplo, um *Steel Catenary Riser* (SCR) é avaliado com base em simulações no domínio do tempo. Na sequência, uma análise semelhante é realizada para um *Steel Lazy Wave Riser* (SLWR).

Abstract of Thesis presented to COPPE/UFRJ as a partial fulfillment of the requirements for the degree of Doctor of Science (D.Sc.)

PARAMETRIC INTERPOLATION METHOD FOR LONG-TERM EXTREME RESPONSE AND PROBABILISCTIC FATIGUE PREDICTION OF OFFSHORE STRUCTURES

Juan Sebastián Monsalve Giraldo

December/2018

Advisor: Luis Volnei Sudati Sagrilo

Department: Civil Engineering

This work presents a semi-analytical methodology to efficiently evaluate the multi-dimensional integrals found in the analyses of the long-term extreme response and probabilistic fatigue of offshore structures. Some traditional methodologies for long-term extreme response and probabilistic fatigue analysis of marine structures described in literature are discussed in this study. Besides these methods, a new procedure developed in this work for optimizing these calculations is explained in details. The proposed method is based on the parametric interpolation of parameters which describe the short-term time-series responses, e.g., statistical parameters of peaks probability distribution and short-term fatigue damage. This interpolation method is then used to efficiently evaluate the long-term convolution integrals. Three comprehensive examples are presented showing the efficiency and accuracy of the proposed method when compared with the complete long-term integration methods ("brute force" methodology). In the first example, an analytic model of a single degree of freedom is analyzed in the frequency domain. In the second one, a Steel Catenary Riser (SCR) is evaluated based on time-domain simulations. In the sequence, a similar analysis is performed for a Steel Lazy Wave Riser (SLWR).

Contents

List of Figures

List of Tables

Nomenclature

The following symbols are used in this work:

Latin:

a_n, b_n: Constants of parabolic interpolation method for non-Gaussian response processes

ALS: Accidental Limit State

CM: Mass Coefficient

d: Short-term (3-h) accumulated fatigue damage

DM: Drag Coefficient

D_{1-yr}: Annual fatigue damage

EC: Environmental Contour

f_{H_s}: Marginal probability density function of Hs

$f_{Hs,Tz}$: Joint probability distribution of Hs and Tz

FE: Finite Element

FEM: Finite Element Method

FL: Fatigue Life

FLS: Fatigue Limit State

$FPSO$: Floating Production, Storage and Offloading

$f_{R_E}^{L}$: Long-term extreme response peak distribution

$f_{R_E|\mathbf{s}}$: Short-term extreme response peak distribution

$f_{R|\mathbf{s}}$: Short-term response peaks probability distribution

$f_{\mathbf{s}}$: Joint probability distribution of the environmental parameters

F_R: Long-term response cumulative probability distribution

$F_{R_E}^{L}$: Long-term extreme cumulative response peaks distribution

$F_{R_E|\mathbf{s}}$: Short-term extreme cumulative response peaks distribution

$F_{R|\mathbf{s}}$: Short-term response peaks cumulative probability distribution

$f_{T_z|H_s}$: Conditional probability density function of Tz given Hs

h_s: Significant wave height

ID : Internal Diameter

IFORM : Inverse First Order Method

K : S-N curve parameter

m : S-N curve parameter

m_n : n^{th} moment of the response spectral density function

M_d : Design bending moment

M_k : Plastic bending moment resistance

N : Expected number of peaks

N_{Hs} : Number of divisions for H_S domain

N_L : Long-term expected number of peaks

Ns : Number of sea states

N_{Tz} : Number of divisions for T_Z domain

N_{yr} : Return period

OD : Outside Diameter

$p_b(t_2)$: Burst resistance

$p_c(t_2)$: Hoop buckling capacity

p_e : Local external pressure

p_{ld} : local internal design pressure

p_{min} : Minimum internal working pressure

PIM : Parametric Interpolation Method

r : Response parameter

RAO : Response Amplitude Operator

r_k : Characteristic response

s : vector containing the environmental parameters for a given short-term condition

SCR : Steel Catenary Riser

SLS : Serviceability Limit State

SLWR : Steel Lazy Wave Riser

S_η : Wave spectrum

t_p : Wave peak period

T_{ed} : Design effective axial tension

t_z : Zero-up-crossing wave period

TDP : Touch Down Point

TDZ : Touch Down Zone

T_k : Plastic axial force resistance

T_S : Short-term period

T_{ST} : Time length of a short term numerical simulation

u : Weibull location parameter

UF : Utilization Factor

u_G : Most probable value of Gumbel distribution

ULS : Ultimate Limit State

U_1 , U_2 : Standard Gaussian variables

Greek:

α : Weibull scale parameter

$\alpha(t_{z_i})$: Constant of linear-exponential interpolation method for non-Gaussian response processes

α_G : Parameter of the Gumbel distribution

α_n : Parameter of parabolic interpolation method which defines m_n for Gaussian and narrowband response processes

$\beta(t_{z_i})$: Constant of linear-exponential interpolation method for non-Gaussian response processes

β_0 : Parameter of exponential interpolation method which defines ν_o for Gaussian and narrowband response processes

β^+: Parameter of parabolic interpolation method which defines ν^+ for Gaussian and narrowband response processes

γ : JONSWAP peakedness parameter

γ_m : Safety factor related to uncertainties associated to the material properties

γ_{SC} : Safety factor related to uncertainties associated to a safety class

ε : Spectral bandwidth parameter

η : Sea surface elevation

θ_w : Wave incidence direction

λ : Weibull shape parameter

$\lambda(t_{z_i})$: Constant of linear-exponential interpolation method for non-Gaussian response processes

λ_{Hs}: Location parameter of lognormal distribution

μ: Peaks sample mean

ν: Peaks frequency

ν_0^+: Zero up-crossing frequency

$\overline{\nu}$: Long-term expected frequency of peaks

ξ: Critical damping ratio

ξ_{Hs}: Scale parameter of lognormal distribution

σ: Peaks sample standard deviation

Φ: Standard Gaussian cumulative distribution

ψ: Parameter of parabolic interpolation method which defines the short term fatigue damage for Gaussian and narrowband response processes

ω: Angular frequency

ω_n: Natural frequency

Chapter 1

Introduction

1.1 Context

The oil production in many countries, as in Brazil, is mainly located in offshore areas. An offshore oil production system is formed by several elements such as the platform, subsea equipment, mooring systems, risers, pipelines, among others. Regarding to the structure system, the platforms may be fixed (jackets and concrete platforms) or floating units. In relation to their function, offshore platforms may be for drilling, extraction, storage or/and processing.

In Brazil, the largest fixed platform is 170m high; however, in the North Sea there are taller jackets, up to 400m high. Nowadays, the offshore industry is exploring and producing in deep and ultra-deep waters, reaching even water depths of more than 3000m, in these cases floating platforms are used. There are different types of floating platforms; for instance FPSOs, TLPs, SPARs and semi submersibles. The most used platform in Brazilian basins is the FPSO (Floating, Production, Storage and Offloading unit) because it allows oil storage and offloading for other oil transport units in locations that are far from the coast where the use of pipelines for transportation would be very expensive.

The pipes which connect the subsea equipment to the floating units are called “risers”. They can be classified according to their function, configuration, and material. In relation to their function, risers may be of completion, oil production, oil or gas exportation and water or gas injection. Regarding the configuration, risers can be vertical, free-hanging catenary, lazy-wave, among others. In the vertical configuration the riser must be pulled up by applying a tension force at the top in order to prevent buckling. When risers are installed in free-hanging catenary configuration, as it is shown in Fig.1, top tensioners are not used and its shape follows a catenary curve from the top to the point where it touches the sea floor - TDP (Touch Down Point). In a lazy wave configuration, as it is shown in Fig.2, the geometry presents a double catenary,

obtained through the use of intermediate floaters. These elements reduce the riser movements mainly in the TDP region.

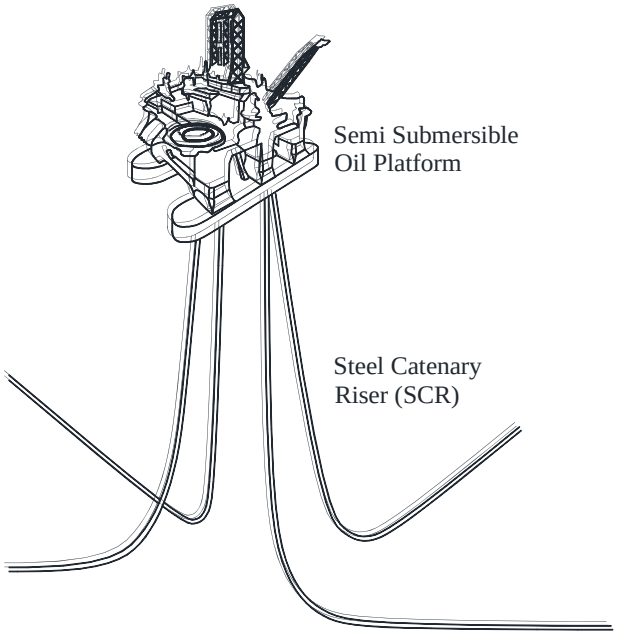

Figure 1. Semi-Submersible platform with SCRs (MONSALVE, 2014)

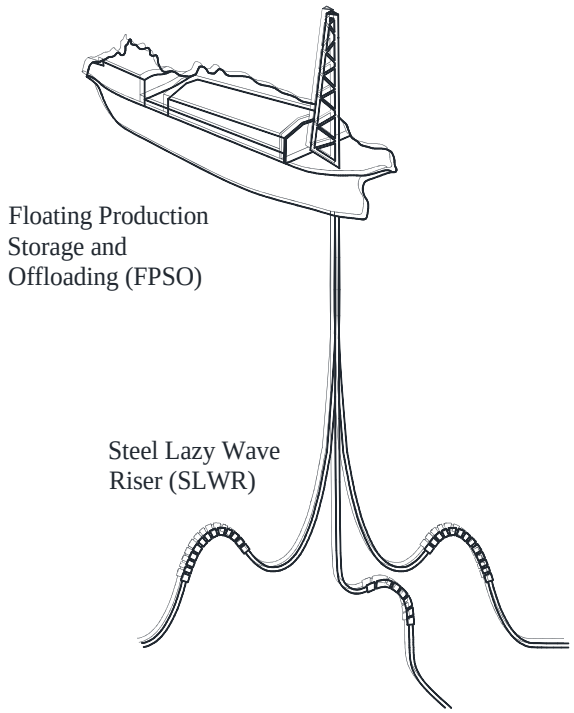

Figure 2. FPSO with SLWRs (MONSALVE, 2014)

In relation to the material which they are made, risers may be classified as rigid or flexible ones. A flexible riser is a composite structure composed of steel layers interspersed with polyethylene layers. A rigid riser is generally composed of steel, titanium or cladded-steel pipes. Rigid risers in catenary are connected to the platform by means of a flexible joint or a monolithic structure with a variable cross section. This latter structural element is known as stress joint and is used mainly to reduce the effects of high stresses caused by axial and bending load actions.

This work is focused on rigid risers; however, the analysis methodology developed in the next chapters may also be applied to other types of offshore structures.

Besides the functional loads (self-weight, fluid density, hydrostatic loading, etc.), in general, marine structures are subjected to stochastic environmental actions such as those generated by waves, wind and current. For this reason, the structural responses, i.e., motions, forces, stresses, etc, are essentially stochastic processes.

The environmental actions are represented by the vessel motions and by the wave and current loading acting directly on the structure. For riser, the wave loading acting on itself is usually neglected for deep waters.

Any marine structure design should carefully look at extreme and fatigue limit states. For both limit states, the ideal design methodology should be the one that considers the effect of all possible combinations of wind, wave and current that the structure will be submitted during its service life. Regarding extreme response verification, the method of long-term response analysis is considered as the best alternative to obtain the characteristic extreme response for the design and analysis of marine structures (SAGRILO *et al.*, 2011). In the case of probabilistic fatigue analysis, the total fatigue damage is computed by performing a complete integration of all predicted load cases represented by the long-term joint probability of the environmental parameters.

1.2 Motivation

The basis for the long-term response design methodology for extreme response verification is the long-term response probability distribution; likewise, the characteristic response value for design purposes is usually taken as the one associated to a given return period. Concerning the fatigue analysis, the annual fatigue damage can be estimated considering the contribution of all short-term environmental conditions

fatigue damages; hence, the estimated fatigue life is obtained as the inverse of this annual damage.

The estimation of both extreme response and fatigue damage are based on multi-dimensional integrals in the same integration domain, which is defined by the domain of the joint probability distribution of the environmental parameters. Traditional numerical integration techniques using constant integration intervals would require a huge demand for computational resources, since each integration point means a numerical simulation of the structure (usually, a long stochastic nonlinear finite element based simulation). This aspect is responsible for the use of other approaches in the everyday design practice. For instance, it is common practice to use short-term methodologies, such as the environmental contour method (see, for instance, BAARHOLM *et al*., 2010) for extreme responses and the irregular (or regular) wave scatter diagram (with or without some blockage scheme) for wave fatigue analysis (see, for instance, PEREIRA, 2018).

In general, the equations described above are valid for any marine structure and many studies are available in the technical literature dealing with the implementation of solutions techniques for both integrals and their application in practical cases. TRIM (1992) considered several approaches to predict long-term extreme responses of offshore structures and developed the averaged long-term peak distribution on a design storm approach. FARNES & MOAN (1994) studied the general theoretical basis for application of the direct long-term approach to offshore structures with non-Gaussian response. In addition, CRAMER (1994) presented a procedure for calculating the long term wave induced response of ship structures by obtaining the peak distribution of the response in each short-term period considering frequency domain analysis. BAARHOLM & MOAN (2000) applied the long-term method by determining nonlinear extremes of hull girder loads in ships. WINTERSTEIN *et al.* (1993) proposed the so-called environmental contour approach for approximately obtaining the N-yr long-term response. The environmental contour approach is largely used and recognized by some design standards (DnV-OS-F201, 2010). GAIDAI & NAESS (2008) proposed an approximation for efficiently calculating long-term extreme response statistics of drag dominated offshore structures subjected to severe sea states. Recently, some authors (NEJAD *et al*., 2013; GONG *et al*., 2014 and REN *et al*., 2015) have investigated the use of the long-term extreme response approach for modern offshore structures such as fixed and floating wind turbines.

Some authors have developed methods that seek to optimize the calculation of the long-term response. LOW & LANGLEY (2008) developed a hybrid approach in which the low-frequency motion is simulated in the time domain while the wave frequency motion is solved in the frequency domain at regular intervals. This method was implemented by LOW (2008) for predicting the long-term extreme vessel motions and line tensions. Afterwards, SAGRILO *et al*. (2011) proposed an improved approach to evaluate efficiently the long-term convolution integrals by means of a combination of the Inverse First Order Reliability Method (IFORM) and an Importance Sampling Monte Carlo Simulation approach (ISMCS). Recently, MONSALVE *et al.* (2018) proposed a hybrid parabolic interpolation-artificial neural network method for long-term extreme response estimation of steel risers. Their method solves the multi-dimensional integral of the long-term extreme response using two numerical procedures. The first one consists of a parabolic interpolation scheme to interpolate statistical parameters of the short-term integration points and the second one is an artificial neural network-based model used to speed-up the structure numerical simulations. VIDEIRO *et al*. (2019) also proposed a reduced integration scheme, based on the most contributive region of the integration domain, which require a small number of structure numerical simulations.

Probabilistic fatigue analysis is one of the most important limit states for the design of any marine structure. These structures are submitted to several dynamic environmental conditions causing a fatigue damage accumulation over the time. Nowadays, for instance, the complex and large numerical riser models and the very large number of sea state conditions presented in the wave scatter diagram, lead to high computational costs to perform the fatigue life evaluation of a single metallic riser. Then some techniques have proposed in the literature to efficiently and accurately solve the multidimensional integral associated to the long-term extreme response. LOW & CHEUNG (2012) presented two approaches, the Perturbation Method and the Asymptotic Method for efficient probabilistic analysis of mooring lines and risers, but their analyses were restricted to a single point of a riser section. MONSALVE *et al.* (2016) proposed the implementation of the Univariate Dimension Reduction Method (UDRM) to reduce the number of riser numerical simulations, obtaining interesting results.

So far, although both analyses are based on the same integration domain and some efficient methods have been proposed, the fatigue and extreme response

assessments based on a long-term approach have been treated separately. Then, in this work an integrated, efficient and accurate method which reduces the number of structure numerical simulations necessary to evaluate the long-term integrals is developed. The method uses an interpolation scheme to describe the behavior of the short-term response and short-term fatigue damage conditioned on a given wave period. Then, for each wave period of the integration domain, just a few structure numerical simulations are needed to describe the response behavior. Besides using the same integration domain points, this approach allows to solve both long term integrals (fatigue and extreme response) in an efficient and accurate way.

1.3 Objective

The main objective of this research work is to propose and develop an innovative method, based on long-term response analysis, to optimize the computer time demand for the calculation of both extreme responses and probabilistic fatigue of marine structures presenting nonlinear behavior and requiring long time-domain simulations in their design analyses, such as metallic risers used in the floating production units.

In order to fulfill this objective, the main idea was to develop an integrated methodology where the same reduced number of integration points (non-linear stochastic time-domain finite element-based analysis) are used in an interpolation scheme to efficiently solve the fatigue and extreme response long-term integrals associated to metallic risers analysis and design.

1.4 Text Organization

The next chapters of this work are organized as follows:

Chapter 2 describes the basic concepts about the short-term and long-term of environmental parameters. This chapter also presents a brief explanation about joint probability function of the environmental parameters.

Chapter 3 presents a theoretical background about short-term analysis including the following topics: short-term structural responses, crossing and peak frequencies, short-term peak distribution and short-term extreme peak distribution.

Chapter 4 presents a theoretical background about long-term analysis of ocean structures considering methods based on all short-term peaks, on all short-term extremes, and on short-term up-crossing rates.

Chapter 5 presents a theoretical background about probabilistic fatigue of ocean structures.

Chapter 6 presents the proposed method which is the main focus of this research work, the so-called Parametric Interpolation Method (PIM), for long-term extreme response and probabilistic fatigue prediction of marine structures.

Chapter 7 presents three comprehensive examples for long-term extreme response prediction and probabilistic fatigue using the proposed approach. In the first case, a single degree of freedom model is studied based on frequency domain analysis. In the second example, a SCR (Steel Catenary Riser) is evaluated based on nonlinear time-domain simulations. Finally, a similar analysis is performed for a SLWR (Steel Lazy Wave Riser).

Chapter 8 presents the final remarks concerning the study performed and some indications for further research topics are also addressed in this chapter

Bibliography presents the list of references which this study was based on.

Chapter 2

Short-term/long-term description of the environmental parameters

2.1 Environmental parameters

Ocean structures are subjected to environmental loads induced by waves, wind and currents. This work is focused on wave loads, however, more information about the other environmental loads can be found in CHAKRABARTI (2005). For extreme and fatigue analyses, an appropriate current profile will be used together with the wave load cases analyzed. Indirectly, the wind effect on the risers will be considered by means of an static offset.

Ocean waves are considered as a succession of pseudo-stationary ergodic processes of short duration where each event corresponds to a specific sea sate (CHAKRABARTI, 2005). Each sea state has a short-term duration period usually taken as 3 hours. In this period, the wave elevation is assumed to be a Gaussian stationary and ergodic random process.

Each sea state is characterized by the wave environmental parameters: the significant wave height (H_s), the zero-up-crossing wave period (T_z) or wave peak period (T_p) and the wave incidence direction Θ_w. The significant wave height (H_s) is defined as the average value of the one third highest individual waves identified in sea surface elevation record $\eta(t)$ and T_z is the mean value of the periods of all individual waves identified in the wave record. Additionally, a frequency domain representation of the wave record is always adopted by means of a wave spectrum $S_\eta(\omega)$ (see, for example, NEWLAND, 1993). T_p is the period associated to the modal frequency of the wave spectrum. The most used spectral models to represent sea elevations records are Pierson-Moskowitz (PIERSON & MOSKOWITZ, 1964) and JONSWAP (HASSELMANN *et al.*, 1973) spectra formulas.

The long-term modelling of the environmental parameters is considered as a sequence of stationary short-term periods. In the specific case of waves, it is considered as a sequence of sea states as shown schematically in Fig. 3.

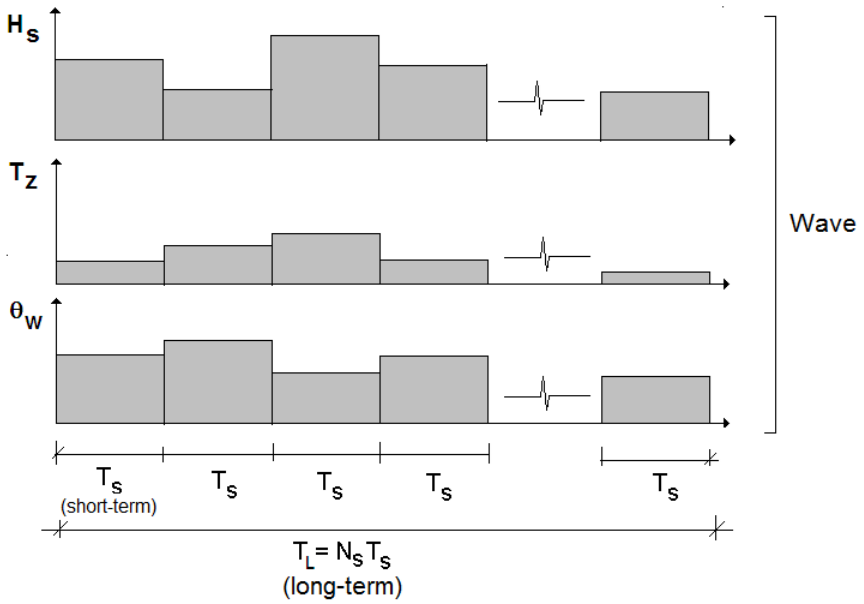

Figure 3. Characterization of short and long-term wave environmental parameters (SAGRILO, 2016)

2.2 Joint probability function of wave parameters

The joint probability density function $f_S(\mathbf{s})$ of the wave environmental parameters $\mathbf{S}=(H_s, T_z, \Theta_w)$ is defined so that the product $f_S(h_s, t_z, \theta_w)dh_s\, dt_z\, d\theta_w$ represents the probability that a set of sampled values of H_s, T_z, and θ_w will be within the region surrounded by $h_s < H_s < h_s + dh_s$, $t_z < T_z < t_z + dt_z$, and $\theta_W < \Theta_W < \theta_W + d\theta_W$ (CLOUGH & PENZIEN, 1993).

This definition requires that

$$\int_{-\infty}^{\infty}\int_{-\infty}^{\infty}\int_{-\infty}^{\infty} f_S(h_s, t_z, \theta_w)dh_s\, dt_z\, d\theta_w = 1 \qquad (2.1)$$

In practical terms, it is common to model the wave incidence direction by a discrete probability distribution. In this way the joint probability function of wave environmental parameters can be written as

$$f_S(h_s, t_z, \theta_w) = f_{Hs,Tz|\theta_w}(h_s, t_z|\Theta_w = \theta_i)p(\theta_i) \qquad (2.2)$$

where $f_{Hs,Tz|\theta_w}(h_s, t_z|\Theta_w = \theta_i)$ is the joint probability density of H_s and T_z conditioned on the wave incidence direction $\Theta_w = \theta_i$ and $p(\theta_i)$ is frequency of waves coming from this direction.

For sake of simplification from now on the incidence direction will be dropped from the representation of the joint distribution of H_s and T_z and it will be simply represented by $f_{Hs,Tz}(h_s, t_z)$ for a given wave direction. In this way, the marginal probability density function of H_s, i.e., $f_{H_s}(h_s)$, is defined such that $f_{H_s}(h_s)dh_s$ is the chance that a sampled value of H_s will be in the range $h_s < H_s < h_s + dh_s$ regardless of the value of T_z. Likewise, the marginal probability density function $f_{T_z}(t_z)$ is defined so that $f_{T_z}(t_z)dt_z$ is the chance that a sampled value of T_z will be in the range $t_z < T_z < t_z + dt_z$ regardless of the value of H_s. These marginal probability density functions are given by (CLOUGH & PENZIEN, 1993):

$$\begin{aligned} f_{H_s}(h_s) &= \int_{-\infty}^{\infty} f_{H_s,T_z}(h_s, t_z)dt_z \\ f_{T_z}(t_z) &= \int_{-\infty}^{\infty} f_{H_s,T_z}(h_s, t_z)dh_s \end{aligned} \tag{2.3}$$

The conditional probability density function $f_{H_s|T_z}(h_s|t_z)$ is defined such that $f_{H_s|T_z}(h_s|t_Z)dh_s$ is the chance that H_s will be in the range $h_s < H_s < h_s + dh_s$ when (or given that) $T_Z = t_z$. In the same way, the conditional probability density function $f_{T_z|H_s}(t_z|h_s)$ is defined such that $f_{T_z|H_s}(t_z|h_s)dt_z$ is the chance that T_Z will be in the range $t_z < T_Z < t_z + dt_z$ when $H_S = h_s$. These conditional density probability distributions are given by (CLOUGH & PENZIEN, 1993):

$$\begin{aligned} f_{H_s|T_z}(h_s|t_z) &= \frac{f_{H_s,T_z}(h_s, t_z)}{f_{T_z}(t_z)} \\ f_{T_z|H_s}(t_z|h_s) &= \frac{f_{H_s,T_z}(h_s, t_z)}{f_{H_s}(h_s)} \end{aligned} \tag{2.4}$$

Based on the equations described above the $H_s - T_z$ joint probability distribution can also be written in one of the following forms:

$$f_{H_s,T_z}(h_s,t_z) = f_{T_z}(t_z) f_{H_s|T_z}(h_s|t_z)$$
$$f_{H_s,T_z}(h_s,t_z) = f_{H_s}(h_s) f_{T_z|H_s}(t_z|h_s) \tag{2.5}$$

The latter expression in Eq. (2.5) is the most common form utilized in practice. In cases where the wave period is represented by T_P instead of T_Z the treatment described also applies by just changing T_Z for T_P.

2.3 Scatter diagram

For a given sea location of interest, the collected wave data are firstly separated by the wave direction sector. For each direction, the corresponding wave scatter diagram is obtained by counting the jointly observed pairs of the H_s and T_z values in the corresponding bins of a two-dimensional H_s-T_z graph. In this graph the sea state characterization is represented by (N_{Hs} x N_{Tz}) bins where N_{Hs} and N_{Tz} are the number of H_s and T_z intervals, respectively, used to represent all observed sea state parameters. Each bin is represented by its central point (H_{S_i}, T_{Z_j}). The total number of observed samples in each bin is divided by the total number of observations in the given direction characterizing then the relative probability of occurrence $p_{i,j}$ of sea states for each bin (see, for instance, MONSALVE, 2014). A simple scatter diagram is shown in Table 1.

In terms of the joint probability distribution of H_s and T_z, the probability of occurrence $p_{i,j}$ can be expressed as:

$$p_{i,j} \approx f_{H_s,T_z}(h_{si}, t_{z_j}) \Delta hs \Delta tz \tag{2.6}$$

where Δhs and Δtz are the intervals sizes of the wave scatter diagram used for the characterization of H_S and T_Z data, respectively. Then, an empirical representation of the joint probability distribution of H_S and T_Z is given by

$$f_{H_s,T_z}(h_{Si}, t_{Z_j}) = \frac{p_{i,j}}{\Delta hs \Delta tz} \tag{2.7}$$

Table 1. Example of a scatter diagram (the value inside each cell means the probability of occurrence)

H_s(m)	T_z(s)									
	3.95	**4.85**	**5.75**	**6.65**	**7.55**	**8.45**	**9.35**	**10.25**	**11.15**	**12.05**
0.683	4.06E-03	6.01E-04	3.11E-05	5.70E-07	3.39E-09	1.01E-11	3.47E-13	4.82E-15	0.00E+00	0.00E+00
1.348	9.10E-02	2.34E-01	9.76E-02	1.20E-02	4.67E-04	7.03E-06	2.40E-07	3.34E-09	1.80E-11	3.62E-14
2.013	9.58E-03	1.36E-01	1.95E-01	7.48E-02	8.38E-03	3.38E-04	1.16E-05	1.60E-07	8.66E-10	1.74E-12
2.678	3.24E-04	1.50E-02	5.09E-02	4.37E-02	1.08E-02	8.51E-04	2.91E-05	4.04E-07	2.18E-09	4.39E-12
3.343	7.97E-06	9.24E-04	5.99E-03	1.02E-02	4.66E-03	6.09E-04	2.08E-05	2.89E-07	1.56E-09	3.14E-12
4.008	1.94E-07	4.81E-05	5.70E-04	1.52E-03	1.16E-03	2.33E-04	7.98E-06	1.11E-07	5.98E-10	1.20E-12
4.672	5.17E-09	2.44E-06	4.63E-05	1.90E-04	2.22E-04	6.41E-05	2.19E-06	3.04E-08	1.64E-10	3.30E-13
5.338	1.56E-10	1.29E-07	3.68E-06	2.20E-05	3.69E-05	1.46E-05	5.01E-07	6.95E-09	3.75E-11	7.55E-14
6.002	5.41E-12	7.31E-09	2.99E-07	2.49E-06	5.76E-06	3.02E-06	1.03E-07	1.44E-09	7.74E-12	1.56E-14
6.668	2.15E-13	4.51E-10	2.55E-08	2.85E-07	8.78E-07	5.92E-07	2.02E-08	2.81E-10	1.52E-12	3.05E-15

In order to have probabilistic information regarding wave parameters beyond those observed in the field it is necessary to fit a theoretical model to represent the joint probability distribution of H_S and T_Z. There is not a general rule for the choice of this theoretical model. As stated before, the most common model used in the literature (CLOUGH & PENZIEN, 1993) is the conditional distribution model:

$$f_{H_s,T_z}(h_s,t_z) = f_{H_s}(h_s) f_{T_z|H_s}(t_z|h_s) \tag{2.8}$$

In this model, usually the Weibull or Lognormal models, depending on the data behavior, are used for representing the marginal distribution of H_s, i.e., $f_{H_s}(h_s)$, and conditional Lognormal distribution is used to represent the conditional distribution of T_z on H_s values, i.e., $f_{T_z|H_s}(t_z|h_s)$.

Alternatively, a joint probability model for H_S and T_Z can be established based on the Nataf Transformation method (MANUEL *et al.*, 2018; SILVA, 2018). This model uses just the marginal distributions of these two parameters, which are fitted independently of each other, and the correlation coefficient between them. Further details on this approach can be found in PAPALEO (2009), MOSQUERA (2015), MANUEL (2018) and SILVA (2018).

Chapter 3

Short-term response analysis

3.1 Short-term structural response

In a short-term analysis, the marine structure is subjected to the action of short-term wave loads. As explained in the previous chapter, waves are random Gaussian processes and consequently the loads produced by them are transformed stochastic processes that can be Gaussian in case of a linear transformation or non-Gaussian (nonlinear) otherwise. For example, first order floater motions prescribed at the top of a riser are assumed to be linear transformations and then modelled as Gaussian processes. On the other hand, due to the nonlinear drag term, the Morison wave hydrodynamic loading acting on a riser is non-Gaussian. For some structures, such as risers and mooring lines, response parameters as axial tension and stresses along their length are usually non-Gaussian processes due to nonlinear structural behavior of such structures.

For a short-term period the structural analysis can be approached in two different ways, depending on the degree of nonlinearity between the wave elevation and the structure´s response. It can be performed in time domain or frequency domain, where the latter case only applies to linear responses.

In the time domain procedure, the load caused by a short-term wave is represented by a time series and is applied on the structure; subsequently, a numerical method, such as the finite element method (FE), is used to obtain the structural responses (displacements, internal forces, stresses, etc.) which are also represented by time series. Fig. 4 shows schematically the approach of structural analysis in time domain.

In the case of linear responses, i.e., a linear relation between the ocean elevation $\eta(t)$ and the structural response $R(t)$, it is possible to obtain the response spectrum for a short-term period, characterized by wave spectrum $S_\eta(\omega)$ (or $S_\eta(\omega, H_S, T_Z) = S_\eta(\omega, \mathbf{S})$), in very simple way as (see, for example, CHAKRABARTI, 1987):

$$S_R(\omega, \mathbf{S}) = RAO(\omega)^2 \times S_\eta(\omega, \mathbf{S}) \tag{3.1}$$

where RAO means Response Amplitude Operator and $RAO(\omega)$ corresponds to the response amplitude for a regular wave having an amplitude equal to 1 meter and frequency ω (or period equal to $2\pi/\omega$). $RAO(\omega)$ is obtaining by means of standard structural analysis tools. Eq. (3.1) is schematically represented in Fig. 5 and it synthetizes the so-called frequency domain methodology.

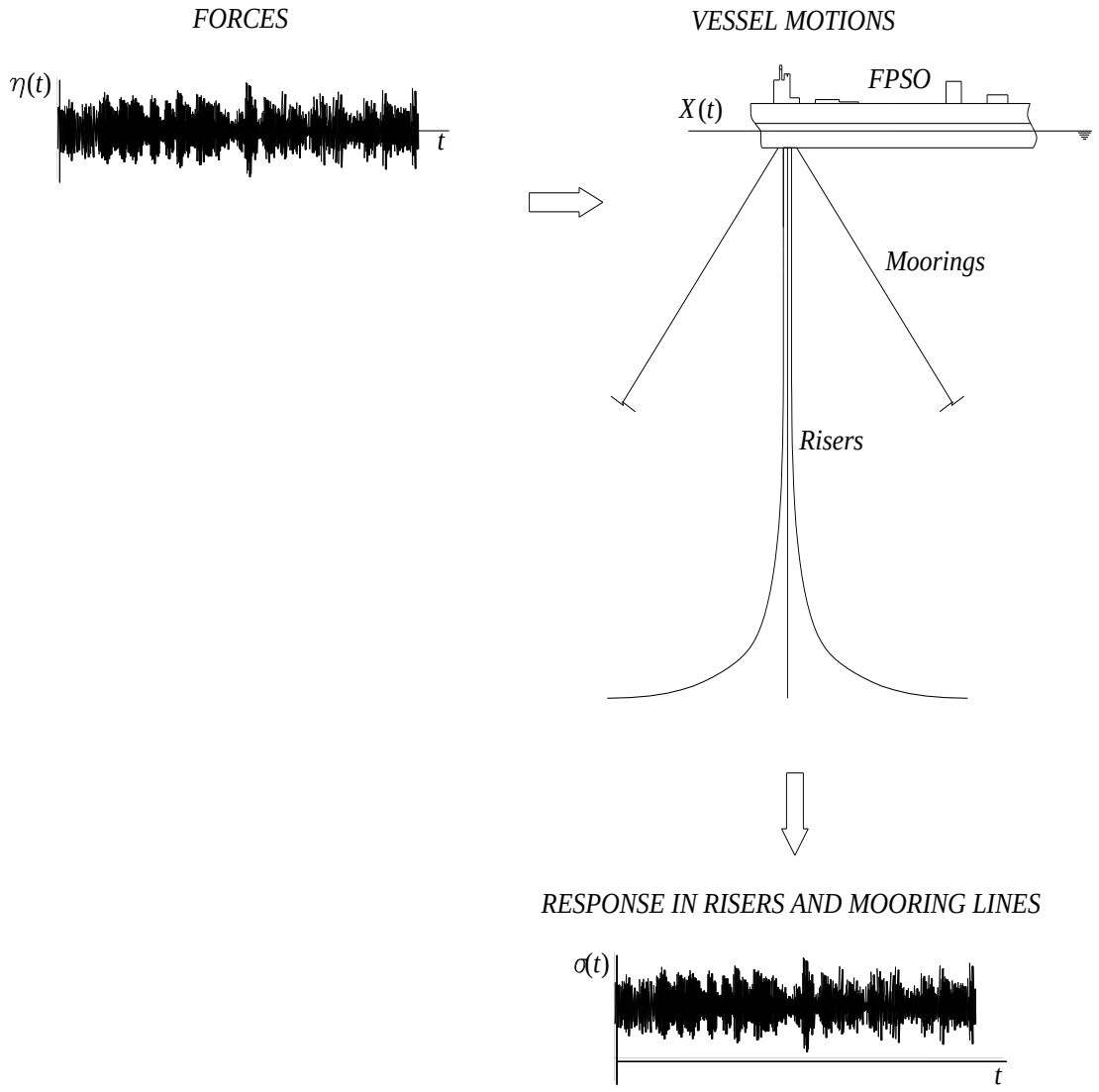

Figure 4. Time domain stochastic analysis representation in moorings and risers

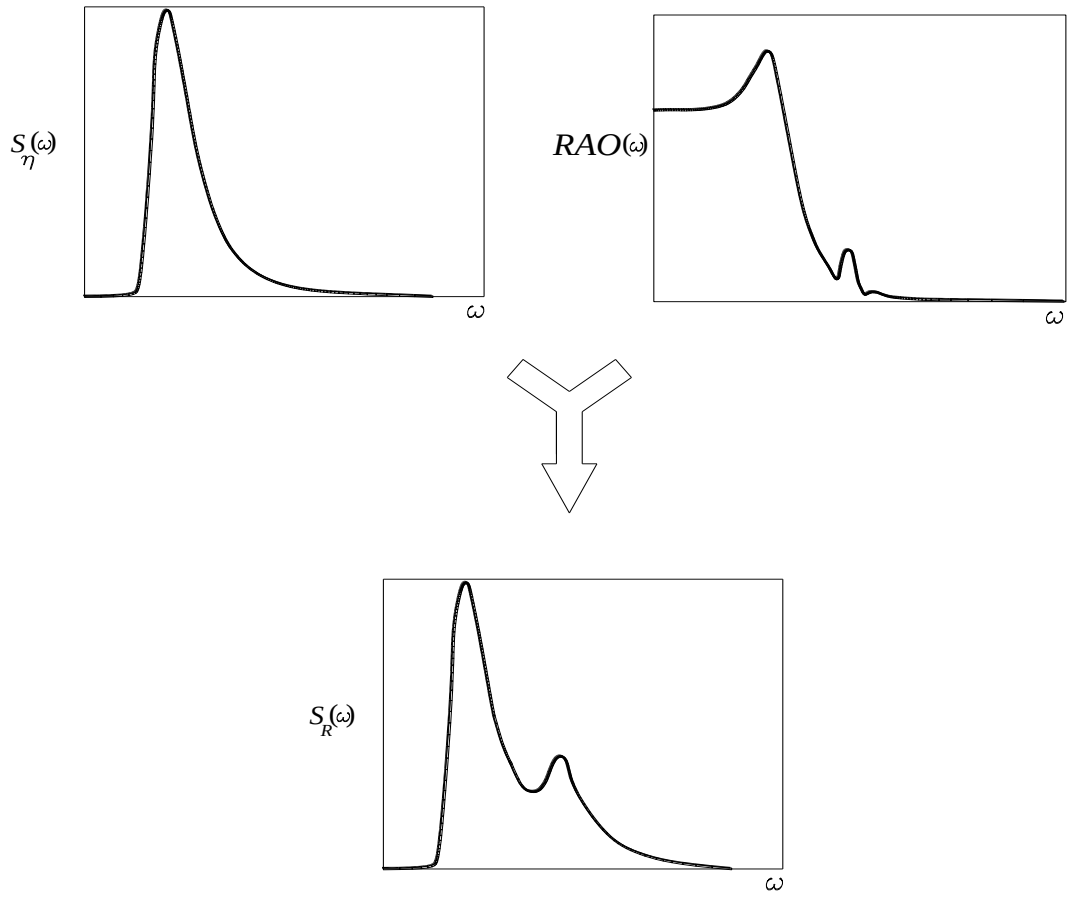

Figure 5. Frequency domain stochastic analysis representation of vessel movements

For nonlinear responses, due to wave loading transformation or nonlinear structural behavior or both, it is not possible to perform frequency domain analyses and the practical way is to use nonlinear stochastic time domain simulations, as schematically shown in Fig. 4. A random time history of the wave elevation is generated and then the random hydrodynamic forces acting on the structure are computed. Using a nonlinear time domain solver the required responses are also obtained in the form of random time-series. This basically constitutes the main steps of a time-domain stochastic analysis of marine structures.

One of the most important aspects of stochastic analysis of marine structures, using either frequency approach or time domain simulations, is the statistical representation of the structural response. This statistical representation has the goal of characterizing the probability functions of the response process itself, its peaks and its extreme value in the short-term. This representation is needed to estimate extreme response characteristic values; besides, it is also important to perform fatigue analyses.

Another useful parameter in stochastic analysis of marine structures is the spectrum of a response parameter of interest, i.e., $S_R(\omega, \mathbf{S})$. In the frequency domain approach its definition is straightforward (see Eq. 3.1) while for response time series is obtained by means of a Fourier analysis (see, for example, NEWLAND, 1993)

As mentioned before, the structural responses of marine structures subjected to short-term wave loading are not necessarily Gaussian distributed. The statistical characterization for a Gaussian process is well-known in literature; however this is not the case for non-Gaussian processes (VARGAS-BAZÁN, 2012). In last case there are several possible ways of dealing with this topic as it will be shown later in this work.

3.2 Crossing and peaks frequencies

The up-crossing and peak frequencies of a random process are parameters of large use in the context of its statistical characterization. The up-crossing frequency of a short-term stationary random process $S(t)$ is calculated by dividing the number of identified crossings at a given level "a" (giving that $\frac{dS(t)}{dt} \geq 0$ at the crossing) by the simulated (or measured) duration T_{ST} of this process:

$$\nu_a^+ = \frac{N^+(a; T_{ST})}{T_{ST}} \tag{3.2}$$

The zero up-crossing frequency ν_o^+ is obtained when a = 0. The frequency of maxima (or peak frequency) is determined dividing the number of peaks of maxima (points where $\frac{dS(t)}{dt} = 0$, $\frac{dS(t+\Delta t)}{dt} < 0$ and $\frac{dS(t-\Delta t)}{dt} > 0$ for $\Delta t \to 0$) by the duration T_{ST} of the process:

$$\nu_m^+ = \frac{N^m(T_{ST})}{T_{ST}} \tag{3.3}$$

It must be observed, that for a zero mean process, negative and positive peaks can be identified as shown in Fig. 6.

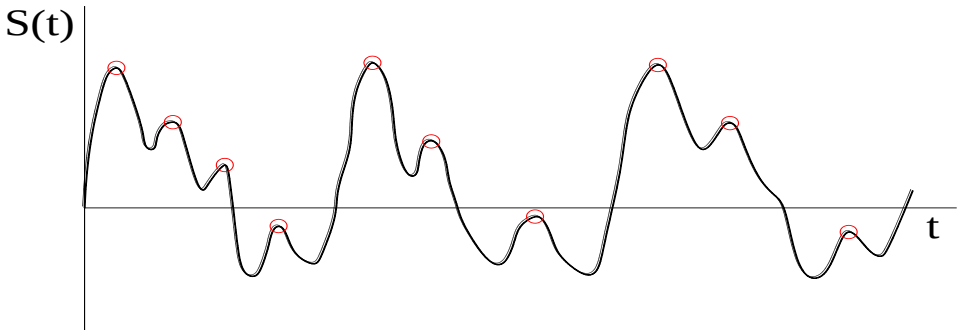

Figure 6. Peaks of a time-series

For short-term stationary and ergodic Gaussian random processes with zero mean, the zero up-crossing frequency and the peak frequency are, respectively, defined as (see, for instance, NAESS and MOAN, 2013):

$$\nu_0^+(\mathbf{s}) = \frac{N_0^+}{T_{ST}} = \frac{1}{2\pi}\sqrt{\frac{m_2(\mathbf{s})}{m_0(\mathbf{s})}}$$
$$\nu_m^+(\mathbf{s}) = \frac{N_m^+}{T_{ST}} = \frac{1}{2\pi}\sqrt{\frac{m_4(\mathbf{s})}{m_2(\mathbf{s})}} \qquad (3.4)$$

where $m_n(\mathbf{s})$ is the n[th] moment of the response spectral density function $S_R(\omega,\mathbf{s})$ about the origin, given the short-term environmental parameters $\mathbf{S}=\mathbf{s}=(h_s, t_z)$, and is defined as:

$$m_n(\mathbf{s}) = \int_0^\infty \omega^n S_R(\omega,\mathbf{s})d\omega \qquad (3.5)$$

Note that the zero[th] spectral moment $m_0(\mathbf{s})$ corresponds also to the variance of the stochastic process (see, for instance, FALTINSEN, 1990). In practical terms, the time length of a numerical simulation T_{ST} is usually different of the short-term period T_S.

3.3 Short-term peaks distribution

The short-term peak cumulative probability distribution of a response parameter of a marine structure is the function $F_{R|\mathbf{S}}(r|\mathbf{s})$ that describes the probability of the peaks

(or maxima) (represented hereafter as R) of such a response parameter to be less or equal to a specific value R=r in a short-term term environmental condition $\mathbf{S}=\mathbf{s}=(h_s, t_z)$. The corresponding probability density function is $f_{R|\mathbf{S}}(r|\mathbf{s})=\frac{dF_{R|\mathbf{S}}(r|\mathbf{s})}{dr}$.

For a stationary Gaussian process, the conditional peak probability distribution, given a short-term condition $\mathbf{S}=\mathbf{s}$, corresponds to the Rice distribution whose probability density function is given by (see, for instance, FALTINSEN, 1990; NAESS and MOAN, 2013; CLOUGH and PENZIEN, 1993):

$$f_{R|\mathbf{S}}(r|\mathbf{s})=\frac{\varepsilon(\mathbf{s})}{\sqrt{m_0(\mathbf{s})}\sqrt{2\pi}}\exp\left(-\frac{1}{2}\frac{r^2}{m_0(\mathbf{s})\varepsilon(\mathbf{s})^2}\right)+\frac{r}{m_0(\mathbf{s})}\sqrt{1-\varepsilon(\mathbf{s})^2}\exp\left(-\frac{1}{2}\frac{r^2}{m_0(\mathbf{s})}\right)\Phi\left(\frac{r}{\sqrt{m_0(s)}\varepsilon(\mathbf{s})}\sqrt{1-\varepsilon(\mathbf{s})^2}\right) \tag{3.6}$$

where $\Phi(.)$ is the standard Gaussian cumulative distribution and ε is the spectral bandwidth parameter which is defined as:

$$\varepsilon(\mathbf{s})=\sqrt{1-\frac{m_2(\mathbf{s})^2}{m_0(\mathbf{s})\,m_4(\mathbf{s})}} \tag{3.7}$$

The spectrum and the process itself is said to be narrow-banded when this parameter is close to zero and broad-banded when it approaches to 1.

Note that for the case of a narrow-banded stationary Gaussian process, the Rice distribution becomes the Rayleigh distribution:

$$f_{R|\mathbf{S}}(r|\mathbf{s})=\frac{r}{m_0(\mathbf{s})}\exp\left(-\frac{1}{2}\frac{r^2}{m_0(\mathbf{s})}\right)$$
$$F_{R|\mathbf{S}}(r|\mathbf{s})=1-\exp\left(-\frac{1}{2}\frac{r^2}{m_0(\mathbf{s})}\right) \tag{3.8}$$

In the case of non-Gaussian responses there is not a general theoretical solution for the peaks distribution as for the case of Gaussian ones. In this case, the peaks distribution is usually defined by fitting a probability distribution model to the sample of identified peaks in the response time-history obtained by a numerical time domain

simulation. The most used probability model is the Weibull probability distribution in its various different representations (NASCIMENTO, 2009). The general form of the Weibull cumulative probability function for the short-term response peaks is given by

$$F_{R|\mathbf{s}}(r|\mathbf{s}) = 1 - \exp\left(-\left(\frac{r - u(\mathbf{s})}{\alpha(\mathbf{s})}\right)^{\lambda(\mathbf{s})}\right) \tag{3.9}$$

where $u(\mathbf{s})$, $\lambda(\mathbf{s})$ and $\alpha(\mathbf{s})$ are, respectively, the location, shape and scale parameters of the distribution. The form represented in Eq. (3.9) is known as the three-parameter (3P) Weibull distribution, however when $u(\mathbf{s}) = 0$ it is known as two-parameter (2P) Weibull distribution. There are various ways of fitting a Weibull distribution to a sample of response peaks. For instance, NASCIMENTO (2009) studied 5 different methodologies for this purpose:

- **Weibull-2P:** Two-parameter model of Weibull distribution where the method of moments based on the sample mean and standard deviation is used to define the distribution parameters.

- **Weibull-3P Skewness:** The three parameters of the distribution are obtained by the method of moments using the mean, standard deviation and coefficient of asymmetry of the response time-series peaks sample.

- **Weibull-3P Kurtosis:** The three parameters of the distribution are computed by the method of moments using the mean, standard deviation and coefficient of kurtosis of the response time-series peaks sample.

- **Weibull-Tail:** Two-parameter distribution which is adjusted by means of a regression method considering only the time-series peaks sample higher than some exceedance levels

- **Weibull-PoT (Peaks over a Threshold):** A three-parameter Weibull is fitted by the method of moments (using sample mean, standard deviation

and skewness) for a sub-sample of peaks exceeding a given peak threshold.

Based on the NASCIMENTO (2009) study, the Weibull-2P approach is adopted in this work to represent the peaks of short-term responses time-series. The considerations and equations related to this method are explained in details in Chapter 6.

3.4 Short-term extreme peak distribution

Assume that $R_1, R_2, \ldots, R_n$ are peaks statistically independent and identically distributed, then the short-term extreme response peak distribution, given a short-term condition $\mathbf{S} = \mathbf{s}$ of duration T_S, is:

$$F_{R_E|\mathbf{S}}(r|\mathbf{s}) = P(R_1 \le r \cap R_2 \le r \cap \ldots \cap R_N \le r) = \left[F_{R|\mathbf{S}}(r|\mathbf{s})\right]^N \tag{3.10}$$

where $F_{R|\mathbf{S}}(r|\mathbf{s})$ is the short-term peaks cumulative probability distribution (defined above) and N is the expected number of peaks in the period T_S, i.e., $N = \nu_m^+(\mathbf{s})T_S$, where $\nu_m^+(\mathbf{s})$ is short-term frequency of maxima.

The derivative of Eq. (3.10) represents the short-term conditional probability density function of the extreme (largest) response peak:

$$f_{R_E|\mathbf{S}}(r|\mathbf{s}) = \frac{\partial F_{R_E|\mathbf{S}}(r|\mathbf{s})}{\partial r} = N\left[F_{R|\mathbf{S}}(r|\mathbf{s})\right]^{N-1}\frac{\partial F_{R|\mathbf{S}}(r|\mathbf{s})}{\partial r} = N\left[F_{R|\mathbf{S}}(r|\mathbf{s})\right]^{N-1} f_{R|\mathbf{S}}(r|\mathbf{s}) \tag{3.11}$$

It can be shown (CHAKRABARTI, 1987; ANG and TANG, 1984) that for large N, the extreme peak distribution converge to Gumbel distribution when $F_{R|\mathbf{S}}(r|\mathbf{s})$ is either the Rice distribution (Gaussian response process) or the Weibull distribution (non-Gaussian response process). The Gumbel density and cumulative probability distribution are, respectively, given by

$$f_{R_N|\mathbf{S}}(r|\mathbf{s}) = \exp\left(-\alpha_G(\mathbf{s})\left(r-u_G(\mathbf{s})\right)-\exp\left(-\alpha_G(\mathbf{s})\left(r-u_G(\mathbf{s})\right)\right)\right)$$
$$F_{R_N|\mathbf{S}}(r|\mathbf{s}) = \exp\left(-\exp\left(-\alpha_G(\mathbf{s})\left(r-u_G(\mathbf{s})\right)\right)\right) \tag{3.12}$$

where $\alpha_G(\mathbf{s})$ and $u_G(\mathbf{s})$ are the parameters of the distribution ($u_G(\mathbf{s})$ corresponds also to the most probable value of this distribution). In the case of a Gaussian process these two parameters are, respectively, given by

$$\alpha_G(\mathbf{s}) = \frac{\sqrt{2\ln(\nu_0(\mathbf{s})T_S)}}{\sqrt{m_0(\mathbf{s})}} \tag{3.13}$$

$$u_G(\mathbf{s}) = \sqrt{m_0(\mathbf{s})}\sqrt{2\ln(\nu_0(\mathbf{s})T_S)} \tag{3.14}$$

In the case of a non-Gaussian process where the response peaks are modelled by a Weibull distribution (see Eq. 3.9) the Gumbel distribution parameters are respectively given by

$$\alpha_G(\mathbf{s}) = \frac{\lambda(\mathbf{s})}{\alpha(\mathbf{s})}\left[\ln\left(\nu^+(\mathbf{s})T_S\right)\right]^{\frac{\lambda(\mathbf{s})-1}{\lambda(\mathbf{s})}} \tag{3.15}$$

$$u_G(\mathbf{s}) = u(\mathbf{s}) + \alpha(\mathbf{s})\left[\ln\left(\nu^+(\mathbf{s})T_S\right)\right]^{\frac{1}{\lambda(\mathbf{s})}} \tag{3.16}$$

where $u(\mathbf{s})$, $\lambda(\mathbf{s})$ and $\alpha(\mathbf{s})$ are the Weibull distribution parameters and $\nu^+(\mathbf{s})$ is the frequency of peaks for the environmental condition $\mathbf{S}=\mathbf{s}$.

Chapter 4

Long-term extreme response analysis

In the previous chapter the statistical description of the short-term response has been described. However, the most critical (or extreme) response associated to a long term period is of the major concern for the design of marine structures. Design codes are usually based on characteristic responses associated to a return period of 100 years.

There are many ways of characterizing the long-term extreme response, most of them based on the long-term extreme environmental condition e.g. 100-yr storm sea state, etc. Nevertheless, depending on the dynamic properties, for some structures the most critical responses can be associated to other environmental conditions. Then the most appropriate methodology to take this aspect into account is the long-term response analysis (SAGRILO *et al*., 2011, NAESS and MOAN, 2013). Another aspect which is incorporated in the long-term response methodology is that the marine structure is designed to reach a certain failure probability. Instead, when a structure is designed using extreme environmental conditions, project criteria which are recommended by technical standards are used; for instance, a combination of winds, waves and currents of different probabilities of occurrence.

For a marine structure, the long term response is described by the contribution of all short-term responses. In literature there are many methods to perform long-term analysis (see for instance, SAGRILO *et al*., 2011), i.e., to obtain the long-term extreme distribution, which can be categorized in (a) methods based on all short-term peaks, (b) methods based on all short-term extremes, and (c) the method based on short-term up-crossing rates. Despite the different approaches followed, when no simplifications are used, all methods conduct to the same result. Then, in what follows it will be described the methodology based on the short-term peaks distribution which was the one used in the present work.

4.1 Long-term distribution based on short-term peaks distributions

The probability of a peak R being below a level r in the long term is given by:

$$P(R \le r) = F_R(r) = P(R \le r|\mathbf{S} = \mathbf{s}_1)P(\mathbf{s}_1) + P(R \le r|\mathbf{S} = \mathbf{s}_2)P(\mathbf{s}_2) + \ldots + P(R \le r|\mathbf{S} = \mathbf{s}_{Ns})P(\mathbf{s}_{Ns}) \quad (4.1)$$

where each short-term environmental condition is defined as $\mathbf{S} = \mathbf{s}_i$ and $P(\mathbf{s}_i)$ is the probability of occurrence of each one of these events. $P(R \le r) = F_R(r)$ is the long-term cumulative probability distribution of the response peaks, $P(R \le r|\mathbf{S} = \mathbf{s}_i) = F_{R|\mathbf{S}}(r|\mathbf{s}_i)$ is the conditional cumulative probability distribution of the response peaks given a short-term environmental event $\mathbf{S} = \mathbf{s}_i$ (defined in the previous chapter) and N_s is the number of short-term environmental conditions within the long term period considered.

Eq. (4.1) can be rewritten as follows:

$$F_R(r) = \sum_{i=1}^{Ns} F_{R|\mathbf{S}}(r|\mathbf{s}_i)P(\mathbf{s}_i) = \int_S F_{R|\mathbf{S}}(r|\mathbf{s}) f_{\mathbf{S}}(\mathbf{s})\, d\mathbf{s} \quad (4.2)$$

where $f_{\mathbf{S}}(\mathbf{s})$ is the joint probability distribution of the environmental parameters for the location considered. The corresponding probability density function is given by

$$f_R(r) = \int_S f_{R|\mathbf{S}}(r|\mathbf{s}) f_{\mathbf{S}}(\mathbf{s})\, d\mathbf{s} \quad (4.3)$$

Note that Eq. (4.2) does not consider that the number of peaks of the response may be different in each short-term condition. Based on this observation, BATTJES (1970) developed a model including this factor in the long-term distribution of the response peaks which is given by

$$F_R(r) = \int_S \frac{\nu^+(\mathbf{s})}{\bar{\nu}^+} F_{R|\mathbf{S}}(r|\mathbf{s}) f_{\mathbf{S}}(\mathbf{s})\, d\mathbf{s} \quad (4.4)$$

where $\bar{\nu}^+$ is the long-term mean peak frequency given by

$$\bar{\nu}^{+} = \int_{S} \nu^{+}(\mathbf{s})\, f_{\mathbf{S}}(\mathbf{s})\, d\mathbf{s} \tag{4.5}$$

The corresponding probability density function associated to the cumulative probability function defined by Eq. (4.4) is

$$f_{R}(r) = \int_{S} \frac{\nu^{+}(\mathbf{s})}{\bar{\nu}^{+}} f_{R|\mathbf{S}}(r|\mathbf{s})\, f_{\mathbf{S}}(\mathbf{s})\, d\mathbf{s} \tag{4.6}$$

The total number of peaks in the long-term is

$$N_{L} = \bar{\nu}^{+} T_{S} Ns \tag{4.7}$$

where Ts is the short-term period duration (3-h in the present work).

Considering all peaks, independently of the environmental condition, as statistically independent, the extreme long term response peak distribution is given by

$$\begin{aligned} F_{R_E}^{L}(r) &= [F_{R}(r)]^{N_L} \\ f_{R_E}^{L}(r) &= N_{L}[F_{R}(r)]^{N_L - 1} f_{R}(r) \end{aligned} \tag{4.8}$$

In most practical applications there is a specific interest in the most probable value r_c of the long-term extreme response parameter R, i.e., the long-term distribution is not necessarily required in practical design applications (it is required for reliability analysis of marine structures). Note that the extreme peak r_c corresponds to the maximum value assumed by the long-term probability density function and it can be obtained by equating its derivative to zero, i.e., $\frac{\partial f_{R_E}^{L}(r)}{\partial r} = 0$. In this way, the following equation is found:

$$\frac{\partial f_{R_E}^{L}(r)}{\partial r} = N_L(N_L-1)[F_R(r_c)]^{N_L-2} f_R(r_c)^2 + N_L[F_R(r_c)]^{N_L-1}\frac{\partial f_R(r_c)}{\partial r} = 0 \qquad (4.9)$$

Assuming that the long-term response peaks distribution has an exponential decay in the direction of the extreme, the extreme value distribution converges to the Type I asymptotic extreme distribution (ANG and TANG, 1984). Under this hypothesis, for large values of r the following relation is met:

$$\frac{f_R(r)}{1-F_R(r)} = -\frac{\partial f_R(r)/\partial r}{f_R(r)} \qquad (4.10)$$

From the above equation, the following expression is obtained:

$$f_R(r)^2 = -\frac{\partial f_R(r)}{\partial r}(1-F_R(r)) \qquad (4.11)$$

By substituting Eq. (4.11) into Eq. (4.9) the following equation is obtained:

$$N_L(1-N_L)[F_R(r_c)]^{N_L-2}(1-F_R(r_c))\frac{\partial f_R(r_c)}{\partial r} + N_L[F_R(r_c)]^{N_L-1}\frac{\partial f_R(r_c)}{\partial r} = 0 \qquad (4.12)$$

As $\frac{\partial f_R(r_c)}{\partial r} \neq 0$ and $N_L \neq 0$, Eq. (4.12) reads:

$$(1-N_L)[F_R(r_c)]^{N_L-2} + N_L[F_R(r_c)]^{N_L-1} = 0 \qquad (4.13)$$

From the above equation, it is possible to identify the following relationship between the long-term distribution of the response peaks and the most probable extreme value r_c corresponding to N_S environmental conditions which is given by

$$F_R(r_c) = 1 - \frac{1}{N_L} \qquad (4.14)$$

4.2 General comments

Although the long-term equations seem to be simple, it is important to notice that a multi-dimensional integral over the domain of the environmental conditions must

be solved in order to obtain the extreme value distribution or even its most probable value. Considering only the wave parameters in **S** and just one wave incidence direction, the long-term cumulative probability function can be discretized as

$$F_R(r) = \sum_{i=1}^{N_{Hs}} \sum_{j=1}^{N_{Tz}} F_{R|H_S,T_Z}\left(r|h_{s_i}, t_{z_j}\right) f_{H_S,T_Z}\left(h_{s_i}, t_{z_j}\right) \Delta t_Z \Delta h_S \tag{4.15}$$

where N_{Hs} and N_{Tz} are the number of divisions used for H_S and T_Z, respectively, in order to cover all integration domain region that contributes to the response; Δt_Z and Δh_S are the corresponding integration intervals; $\left(h_{s_i}, t_{z_j}\right)$ is the central point of each discrete integration area; $f_{H_S,T_Z}\left(h_{s_i}, t_{z_j}\right)$ is the corresponding $H_S - T_z$ joint probability density function and $F_{R|H_S,T_Z}\left(r|h_{s_i}, t_{z_j}\right)$ is short-term response peaks cumulative distribution for the short-term condition $\mathbf{S} = \left(h_{s_i}, t_{z_j}\right)$.

It must be observed that the number of numerical simulations required to solve Eq. (4.15) is equal to $N_{Hs} x N_{Tz}$ for each wave incidence direction. Considering that a nonlinear time-domain simulation of metallic riser in a modern computer can take 2-3 hours, the computer costs are very large to solve such equation using this standard (or "Brute force") procedure. Therefore, an efficient integration approach is very demanding for solving this long-term integral.

Chapter 5

Fatigue analysis

The cyclic loads acting on a marine structure generate stress variations that can lead to the fatigue failure. This failure is caused by a crack generation or propagation of an existing crack, such as the micro cracks presented in welded joints.

There are two methods to estimate the useful life of a structural component which is under the effect of cyclic stress variations. In the first methodology, the crack propagation analysis is performed by using Fracture Mechanics; for instance, the Paris-Erdogan law (ETUBE, 2001; NAESS and ENGESVIK, 1985). In the second methodology, the evaluation of fatigue life is calculated by means S-N curves and the Miner's rule. The former approach is mainly used for an existing structure while the latter is largely used in the design of new structures. This work is focused on the S-N methodology for the fatigue assessment of a marine structural component.

An S-N curve defines the relationship between a stress range variation and the corresponding number of cycles that leads a certain structural component to the fatigue failure. In practical terms, these curves, in a double-logarithmic graph, can be linear or bilinear S-N curves, as it is shown in Fig. 7. To select an appropriate S-N curve for the design of a structural component, the engineer must consider some properties such as (DNV-RP-F204, 2010):

- Welding type
- Construction details
- Manufacturing process
- Stress concentration factors
- Environment to which the structure will be exposed to: air, free corrosion and cathodic protection in seawater, etc.

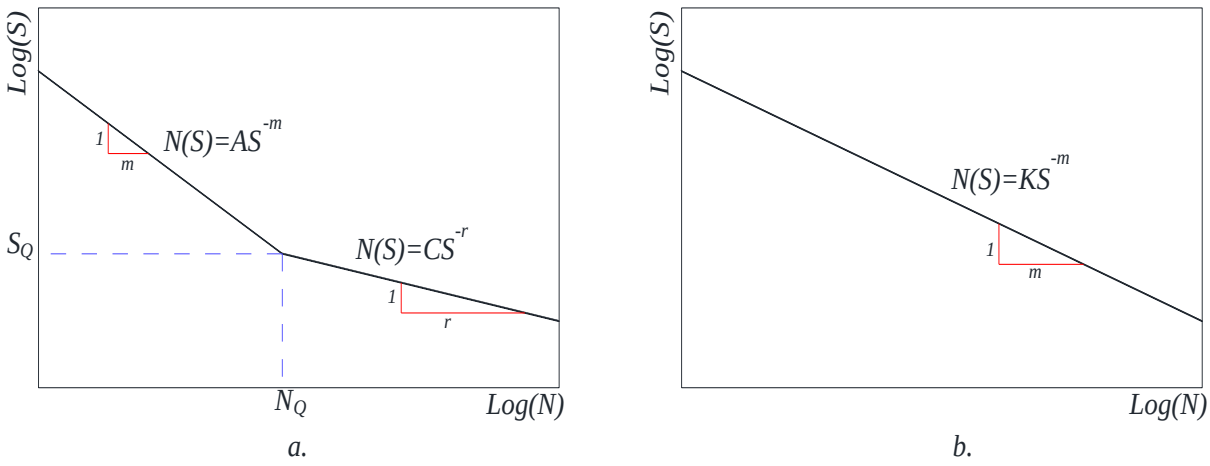

Figure 7. Definition of a S-N curve. a. bilinear, b. one-slope (DNV-RP-F204, 2010)

The mathematical equation that describes a one-slope S-N curve is the following:

$$N(\bar{S}) = K\bar{S}^{-m} \tag{5.1}$$

where $\bar{S}$ is the stress range, $N(\bar{S})$ is the number of stress cycles of range $\bar{S}$ that leads to fatigue failure, K and m are the curve parameters obtained experimentally

A bilinear S-N curve is defined as

$$N(\bar{S}) = \begin{cases} A\bar{S}^{-m} \text{ for } \bar{S} > S_Q \\ C\bar{S}^{-r} \text{ for } \bar{S} < S_Q \end{cases} \qquad S_Q = \left(\frac{A}{C}\right)^{\frac{1}{(m-r)}} \tag{5.2}$$

where S_Q is the stress range inflexion point.

If the long-term stress loading can be characterized by the stress ranges $\bar{S}_r = (\bar{S}_1 \quad \bar{S}_2 \quad \cdots \quad \bar{S}_N)$, where the i^{th} range occurs n_i times, according to the Miner's rule (DNV-RP-F204, 2010), the total induced fatigue damage is given by

$$d = \sum_{i=1}^{Ni} \frac{n_i}{N(\bar{S}_i)} \tag{5.3}$$

The Miner´s rule assumes that the fatigue failure occurs when the fatigue damage reaches the unity. In practice, additional safety factors (SF) are often used to consider uncertainties (DNV-RP-F204, 2010). Then, if the long-term period used to identify the stress ranges $\overline{S}_r$ is 1-yr, the design fatigue life is given by

$$VU = \frac{1}{d \times SF} \tag{5.4}$$

Regarding the modeling and analysis of marine structures, the fatigue damage is computed for each short-term condition and then appropriately accumulated for a long-term period of usually 1-yr. In what follows, methods for short and long-term fatigue estimation will be described.

5.1 Short-term fatigue damage assessment

In general, there are two distinct ways for computing the short-term term fatigue damage: spectral and cycle counting-based methods. The spectral methods are based on the spectral density of the short-term stress process while the cycle counting-based methods use a stress time history to identify and count the stress cycles.

Rayleigh (or Narrow-band spectrum) approach (WIRSCHING *et al*., 1987; NOLTE *et al*., 1976), Wirsching correction method (WIRSCHING, 1987) and Dirlik method (DIRLIK, 1985) are some examples of methodologies belonging to the class of spectral methods. The most traditional method in the class of cycle counting approaches is the well-know Rainflow method. In what follows only the methods used in the present work will be described, i.e., the Rayleigh or narrow-band stress spectrum approach and the Rainflow method.

5.1.1 Spectral Method: Narrow-band stress spectrum approach

This approach assumes that the stress spectrum is Gaussian and also narrow-banded and it is largely used in the case of linear structural analysis. As it was mentioned in Chapter 3, when the stress response process is Gaussian and also narrow-banded, the stress peaks distribution follows a Rayleigh distribution. This distribution depends only on the parameters which are obtained from the stress spectrum. For an

idealized narrow-banded stress approach, as shown in Fig. 8, each mean up-crossing represents an harmonic stress cycle with a stress range twice its amplitude (peak value).

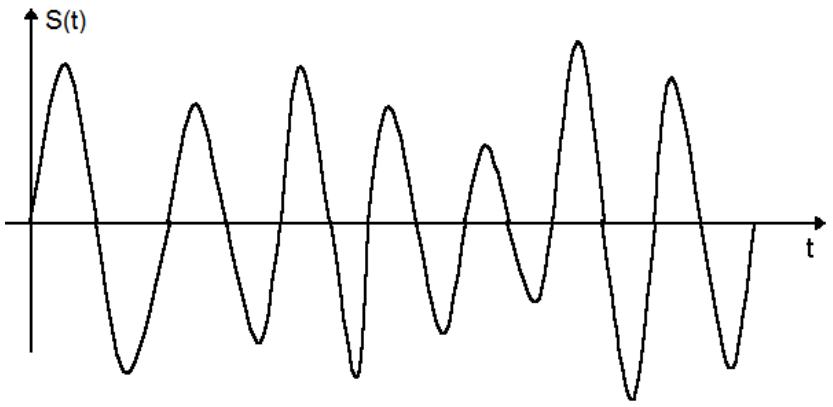

Figure 8. Narrow-banded Gaussian stress process time history

The total number of cycles for a narrow-banded Gaussian stress process can be calculated in terms of the short-term period T_s and the mean up-crossing frequency ν_o:

$$N_c = \nu_o T_S \tag{5.5}$$

The short-term stress peaks probability distribution is expressed by Eq. (3.8), then the number of stress cycles having peaks in the interval $[\sigma_i, \sigma_i + \Delta\sigma]$ in the short term period T_s with the environmental parameters $S = s_i$ is given by

$$n_i = \nu_o(s_i)\, T_s f_{\sigma|\mathbf{s}}(\sigma_i|\mathbf{s} = s_i)\,\Delta\sigma \tag{5.6}$$

By substituting the one-slope SN curve equation (Eq. (5.1)) and the Eq. (5.6) into Eq. (5.3) and considering $\Delta\sigma \to 0$, the short-term fatigue damage is given by:

$$d(\mathbf{s}_i) = \lim_{\Delta\sigma\to 0}\sum_{i=1}^{Ni}\frac{\nu_o(\mathbf{s_i})T_S f_{\sigma|\mathbf{s}}(\sigma_i|\mathbf{s}=s_i)\Delta\sigma}{N(2\sigma_i)} = \frac{\nu_o(\mathbf{s_i})T_S}{K}\int_0^{\infty}\sigma^m f_{\sigma|\mathbf{s}}(\sigma|\mathbf{s}=s_i)ds = \frac{\nu_o(\mathbf{s_i})T}{K}E(\sigma^m|\mathbf{s}_i) \tag{5.7}$$

Note that $E\left(\sigma^m \middle| \mathbf{s}_i\right)$ is the expected value of the stress peaks up to the exponent m in the short-term environmental condition $\mathbf{S} = \mathbf{s}_i$.

The Eq. (5.7) can be worked out, as detailed in WIRSCHING *et al.*(1987) and NOLTE *et al.* ,(1976), resulting in

$$d(\mathbf{s}_i) = \frac{\nu_0(\mathbf{s}_i) T \left(2\sqrt{2}\right)^m \left(m_0(\mathbf{s}_i)\right)^{\frac{m}{2}}}{K} \Gamma\left(1 + \frac{m}{2}\right) \tag{5.8}$$

where $\Gamma(.)$ is the Gamma function and

$$\nu_0(\mathbf{s}_i) = \frac{1}{2\pi} \sqrt{\frac{m_2(\mathbf{s}_i)}{m_0(\mathbf{s}_i)}} \tag{5.9}$$

with $m_i(\mathbf{s}_i)$ being i^{th} moment of the stress spectrum associated to the short-term condition $\mathbf{S} = \mathbf{s}_i$.

In the case of a bilinear S-N curve, the short-term fatigue damage for a narrow-banded Gaussian stress process can be also calculated applying Miner's rule leading to

$$d(\mathbf{s}_i) = T_s \nu_0(\mathbf{s}_i) \left[\frac{\left(2\sqrt{2m_0(\mathbf{s}_i)}\right)^r}{C} \Gamma_1(S_Q) + \frac{\left(2\sqrt{2m_0(\mathbf{s}_i)}\right)^m}{A} \Gamma_2(S_Q) \right] \tag{5.10}$$

where, C, A, r, m and S_Q are the bilinear S-N curves parameters and $\Gamma_1(S_Q)$ and $\Gamma_2(S_Q)$ are incomplete gamma functions defined as follows:

$$\Gamma_1(S_Q) = \int_0^{\zeta(S_Q)} t^{r/2} e^{-t} dt \tag{5.11}$$

$$\Gamma_2(S_Q) = \int_{\zeta(S_Q)}^{\infty} t^{m/2} e^{-t} dt \tag{5.12}$$

considering the following term:

$$\zeta(S_Q) = \frac{S_Q^2}{2m_0(\mathbf{s}_i)} \tag{5.13}$$

The use of this approach is straightforward in the case where the stress process can be assumed to be a linear transformation of the sea surface elevation, since the result of this analysis is the stress spectrum. In this case, it must observed that in the case of a wide-banded spectrum the calculation is not strictly correct. There are some approaches to take into account the stress spectrum bandwidth in the fatigue estimates, for instance, see WIRSHING and LIGHT (1980).

This frequency domain based procedure can also be used for those cases where the stress process is defined by means of a stress time series. In this case, the stress spectrum can be obtained through a Fourier analysis and them the calculation follows as described above. It should be noted that in this case, besides the spectrum bandwidth, the assumption (usually not true) that the stress process is Gaussian is also implicit in the calculation process.

5.1.2 Cycle Counting Approach: Rainflow Method

Rainflow is a method developed by MATSUISKI & ENDO (1968) to identify and count stress ranges directly from a stress time series. This method does not have restrictions regarding the stress process because it works directly with stress time-series. There are many Rainflow cycle counting algorithms reported in literature (ARIDURU, 2004). In this work the one described in the design standard ASTM E 1049 (2005) has been implemented and used in the fatigue analysis calculations.

After analyzing a stress time-series, obtained by means of a numerical simulation for the short-term environmental condition $\mathbf{S} = \mathbf{s}_i$, the result of a Rainflow algorithm is a sequence of stress ranges as

$$\overline{\mathbf{S}}_r(\mathbf{s}_i) = \left(\overline{S}_1 \quad \overline{S}_2 \quad \cdots \quad \overline{S}_N\right) \tag{5.14}$$

and their associated number of occurrences $(n_1 \quad n_2 \quad \cdots \quad n_N)$. Then the short-term fatigue damage is given by

$$d(\mathbf{s}_i) = \frac{T_{SL}}{T_S} \sum_{i=1}^{N} \frac{n_i}{N(\bar{S}_i)} \tag{5.15}$$

where $N(\bar{S}_i)$ is the allowable number of stress cycles for the stress range $\bar{S}_i$ given by S-N curve, T_{SL} and T_S are, respectively, the length of simulated stress time-series and the short-term period.

5.2 Long-term probabilistic fatigue analysis

As already described in Chapter 2, ocean waves are a succession of pseudo-stationary ergodic processes of short duration where each event corresponds to a specific sea state. Then, the fatigue damage assessment of any marine structure must take into account this long-term variability.

The most common technique to consider all the variability of sea states in the long-term is to use the wave scatter diagram which contain the observed relative frequency and direction of each sea state, represented by a pair **S**=(H_s,T_z), in a given sea location. Considering $\gamma_{i,j}$ as the relative frequency occurrence of a sea state defined by $H_S = h_{S_i}$ and $T_z = t_{z_j}$ and that the short-term period is 3-h, the number of occurrences $n_{i,j}$ of this sea sate in a period of one year may be calculated as:

$$n_{i,j} = 2920\, \gamma_{i,j} \tag{5.16}$$

Considering $d_{i,j}$ as the short term fatigue damage induced by the short-term environmental condition $\mathbf{S} = (h_{S_i}, t_{Z_j})$, the annual fatigue damage D_{1-y} is then:

$$D_{1-yr} = \sum_{i=1}^{N_{Hs}} \sum_{j=1}^{N_{Tz}} n_{i,j} d_{i,j} = 2920 \sum_{i=1}^{N_{Hs}} \sum_{j=1}^{N_{Tz}} d_{i,j} \gamma_{i,j} \tag{5.17}$$

The frequency of occurrence of a given sea state may also be calculated using the joint probability distribution of H_s and T_z (see Chapter 2) as follows:

$$\gamma_{i,j} = f_{Hs,Tz}\left(h_{S_i}, t_{Z_j}\right)\Delta hs\,\Delta tz \tag{5.18}$$

Thus, the equation for calculating the annual fatigue damage can be re-written as:

$$D_{1-yr} = 2920\sum_{i=1}^{N_{Hs}}\sum_{j=1}^{N_{Tz}} d_{i,j} f_{Hs,Tz}\left(hs_i, tz_j\right)\Delta hs\Delta tz \tag{5.19}$$

The above equation can be re-written in a more elegant way by making $\Delta h_s \rightarrow 0$ and $\Delta t_z \rightarrow 0$:

$$D_{1-yr} = 2920\int_0^{\infty}\int_0^{\infty} d(hs,tz) f_{Hs,Tz}(hs,tz)\,dhs\,dtz \tag{5.20}$$

where $d(h_s,t_z)$ is the fatigue damage for a short-term sea state.

5.3 General comments

As already mentioned for the case of extreme response analysis, the number of structure numerical simulations to perform the fatigue analysis for a single wave direction incidence is $N_{Hs}xN_{Tz}$. Considering, for instance, the case of a metallic riser connected to a floating unit in deep water subjected to many wave incidence directions, the fatigue analysis can be extremely demanding in terms of computer resources. So, this aspect make clear that some more efficient approaches should be investigated in order to estimate the long-term fatigue damage of a marine structure.

One aspect that has not been explored in literature, is the fact that in long-term extreme and fatigue analyses the integration domain (environmental data) is the same. This aspect allows the development of an integrated procedure where both analyses can be performed simultaneously.

Besides the development of interpolation methods for the analysis of extreme and fatigue of metallic risers, the aspect mentioned above will also be explored in the present work.

Chapter 6

Parametric Interpolation Method (PIM)

The focus of this work is the long term extreme and fatigue analyses of metallic risers considering the long-term variability of the wave environmental parameters. For sake of simplicity a short-term condition will be represented in what follows by a pair of H_S and T_z values, i.e, $\mathbf{s} = (h_s, t_z)$.

The structural model type employed in this development considers the floater and the lines uncoupled. As it is of common practice, only the first order induced floater motions were considered. As described later, a single current profile is used in the analyses and the wind effect on the floater is represented by an static offset dependent on H_S.

The idea developed in this work to speed up the long term extreme and fatigue analyses was to use parametric equations to interpolate the short-term parameters for each integration point of the integration domain. Hereafter, it will be described the procedures developed for both fatigue and extreme long-term analyses.

6.1 Parametric Interpolation Method (PIM) for long-term extreme response analysis of marine structures

For the present work the long-term response peaks distribution, i.e. Eq. (4.4), can be simply written as:

$$F_R(r) = \int_{t_z}\int_{h_s} \frac{\nu^+(h_s, t_z)}{\overline{\nu}^+} F_{R|(H_s,T_z)}(r|h_s, t_z)\, f_{H_s,T_z}(h_s, t_z)\, dh_s\, dt_z \qquad (6.1)$$

where $f_{H_s,T_z}(h_s, t_z)$ is the joint probability density function of H_s and T_z.

Hereafter some details related to Eq. (6.1) will be presented for the case where the short-term peaks distributions are related Gaussian and non-Gaussian response

processes. Then, later, a method to improve the efficiency of numerical evaluation of the long-term integral is proposed.

6.1.1 Gaussian and narrowband response processes

When the response process is considered Gaussian and narrow banded, the short-term cumulative probability function for the response peaks is given by the Rayleigh distribution, (see Eq. (3.8)), and can be re-written as:

$$F_{R|(H_s,T_z)}(r|h_s,t_z) = 1 - \exp\left(-\frac{1}{2}\frac{r^2}{m_0(h_s,t_z)}\right) \tag{6.2}$$

The frequency of maxima for a given short-term condition and the average long-term frequency of maxima for a Gaussian process are given, respectively, by:

$$\nu^+(h_s,t_z) = \frac{1}{2\pi}\sqrt{\frac{m_4(h_s,t_z)}{m_2(h_s,t_z)}} \tag{6.3}$$

$$\overline{\nu}^+ = \int_{t_z}\int_{h_s} \nu^+(h_s,t_z)\, f_{H_s,T_z}(h_s,t_z)\, dh_s\, dt_z \tag{6.4}$$

where $m_n(h_s,t_z)$ is the n^{th} order spectral moment of the response spectral density.

The proposed method seeks to analyze the behavior of the short-term peaks probability distribution parameters and peaks frequency in order to develop parametric equations to optimize the extreme response calculation. Note that for the present case, narrowband Gaussian process, both the peak up-crossing rate and the Rayleigh distribution function depend only on the moments of the response spectral density. Consequently, the prediction of these parameters by means of some parametric equations as function of (H_s, T_z, or both) will reduce the number of simulations required to solve the bi-dimensional long-term integral described by Eq. (6.1).

For a linear case where frequency domain analysis can be used, the spectral density of the response process for a given short-term condition $\mathbf{S} = \mathbf{s} = (h_s,t_z)$ can be obtained by crossing the response amplitude operator (RAO) with the sea surface elevation spectral density $S_\eta(\omega,h_s,t_z)$ as follows:

$$S_R(\omega, h_s, t_z) = RAO_R^2(\omega) S_\eta(\omega, h_s, t_z) \tag{6.5}$$

The corresponding spectral moments of the response process are obtained using the following equation:

$$m_n(h_s, t_z) = \int_0^\infty \omega^n S_R(\omega, h_s, t_z) d\omega \tag{6.6}$$

For the sake of simplicity, it is assumed that the wave spectrum is represented by the Pierson–Moskowitz modified model (PIERSON & MOSKOWITZ, 1964):

$$S_\eta(\omega, h_s, t_z) = \frac{4\pi^3 h_s^2}{\omega^5 t_z^4} \exp\left(\frac{-16\pi^3}{\omega^4 t_z^4}\right) \tag{6.7}$$

By substituting Eq. (6.7) into Eq. (6.5), the spectral density of the response process is expressed as:

$$S_R(\omega, h_s, t_z) = \frac{4\pi^3 h_s^2}{\omega^5 t_z^4} \exp\left(\frac{-16\pi^3}{\omega^4 t_z^4}\right) RAO_R^2(\omega) \tag{6.8}$$

Thus, by substituting Eq. (6.8) into Eq.(6.6), the n^{th} spectral moment of the response spectrum can be expressed as follows:

$$m_n(h_s, t_z) = \frac{4\pi^3 h_s^2}{t_z^4} \int_0^\infty \omega^{n-5} \exp\left(\frac{-16\pi^3}{\omega^4 t_z^4}\right) RAO_R^2(\omega) d\omega \tag{6.9}$$

The equation above can be rewritten in the following way:

$$m_n(h_s, t_z) = \alpha_n(t_z) h_s^2 \tag{6.10}$$

where

$$\alpha_n(t_z) = \frac{4\pi^3}{t_z^4} \int_0^\infty \omega^{n-5} \exp\left(\frac{-16\pi^3}{\omega^4 t_z^4}\right) RAO_R^2(\omega) d\omega \tag{6.11}$$

Note that the n^{th} spectral moment is a parabolic function of the significant wave height. Then, for a given value of T_z, i.e., $T_Z = t_z$, it is necessary just one crossing of

the RAO with the wave spectrum to obtain the corresponding α_n which can be used to compute the n^{th} spectral moment for any value of H_s. In other words, for a given $T_Z = t_z$ it is necessary just one structural frequency domain analysis to get the true behavior of the response spectral moments for any value of H_s. The same behavior is obtained by other wave spectra, such as JONSWAP model (HASSELMANN et al., 1973).

By substituting Eq. (6.10) into Eq. (6.3) it is possible to see that the frequency of maxima also depends only on the wave zero up-crossing period:

$$\nu^+(h_s,t_z) = \nu^+(t_z) = \frac{1}{2\pi}\sqrt{\frac{\alpha_4(t_z)}{\alpha_2(t_z)}} = \frac{1}{2\pi}\beta^+(t_z) \tag{6.12}$$

For a given $T_Z = t_z$, $\beta^+(t_z)$ is a constant.

Then the integral for the long-term cumulative distribution of peaks can be solved using a single simulation for each value of t_z as follows:

$$\begin{aligned} F_R(r) &= \int_{t_z}\int_{h_s} \frac{\beta^+(t_z)}{2\pi\bar{\nu}^+}\left[1-\exp\left(-\frac{1}{2}\frac{r^2}{\alpha(t_z)h_s^2}\right)\right] f_{H_s,T_z}(h_s,t_z)\,dh_s\,dt_z \\ &= \sum_{i=1}^{N_{Hs}}\sum_{j=1}^{N_{Tz}} \frac{\beta^+(t_{z_j})}{2\pi\bar{\nu}^+}\left[1-\exp\left(-\frac{1}{2}\frac{r^2}{\alpha(t_{z_j})h_{s_i}^2}\right)\right] f_{H_s,T_z}(h_{s_i},t_{z_j})\Delta h_s\,\Delta t_z \end{aligned} \tag{6.13}$$

where the term $\bar{\nu}^+$ is given

$$\begin{aligned} \bar{\nu}^+ &= \int_{t_z}\int_{h_s} \nu^+(h_s,t_z) f_{H_s,T_z}(h_s,t_z)\,dh_s\,dt_z = \int_{t_z}\int_{h_s} \frac{1}{2\pi}\beta^+(t_z) f_{H_s,T_z}(h_s,t_z)\,dh_s\,dt_z \\ &= \int_{t_z} \frac{1}{2\pi}\beta^+(t_z) f_{T_z}(t_z)\,dt_z = \sum_{j=1}^{N_{Tz}} \frac{1}{2\pi}\beta^+(t_{z_j}) f_{T_z}(t_{z_j})\Delta t_z \end{aligned} \tag{6.14}$$

The parameters $\alpha(t_z)$ and $\beta^+(t_z)$ can be computed once for each discrete value of $T_Z = t_{z_j}$ in the equations above or they can be computed for some few specific points and interpolated by means of a parametric equation. Once again, it must be emphasized that in this particular situation just a single frequency domain structural analysis is

required for any T_z since the distributions parameters can be written analytically as an explicit function of H_s.

Finally, the most probable response extreme value can be found using Eq. (4.14) for a given long-term period.

6.1.2 Non-Gaussian processes

The above approach cannot be applied when the structural response is not a narrow-banded and Gaussian process. For example, usually the time-series of dynamic responses of steel catenary risers do not follow the Gaussian distribution. In such cases, another approach must be addressed to optimize the extreme response calculation when the long-term method is used.

In this work, the Weibull distribution is assumed to describe the short-term response peaks. This choice is based on previous experiences; for instance, BAARHOLM & MOAN (2000) pointed that, if the response deviates too much from the Gaussian process, the Weibull distribution may be used instead of Rayleigh's equation. Other authors such as CRAMER (1994), NASCIMENTO (2009), GASPAR *et al.* (2016) and ORIMOLADE *et al*. (2016) adopted this consideration in the analysis of marine structures.

The cumulative probability distribution function of short-term response peaks modelled as the 2-parameter Weibull distribution is defined as:

$$F_{R|(H_s,T_z)}(r|h_s,t_z) = 1 - \exp\left[-\left(\frac{r - u_{Static}(h_s,t_z)}{\alpha(h_s,t_z)}\right)^{\lambda(h_s,t_z)}\right] \tag{6.15}$$

and the corresponding probability density is:

$$f_{R|(H_s,T_z)}(r|h_s,t_z) = \frac{[r - u_{Static}(h_s,t_z)]^{\lambda(h_s,t_z)-1}}{\alpha(h_s,t_z)^{\lambda(h_s,t_z)}}\lambda(h_s,t_z)\exp\left[-\left(\frac{r - u_{Static}(h_s,t_z)}{\alpha(h_s,t_z)}\right)^{\lambda(h_s,t_z)}\right] \tag{6.16}$$

where $u_{Static}(h_s,t_z)$ is the static mean, i.e. the process mean. $\alpha(h_s,t_z)$ and $\lambda(h_s,t_z)$ are the scale and shape parameters respectively.

By adopting the method of moments, the two parameters of this distribution can be evaluated based on the peaks sample mean and standard deviation using the following relationships:

$$\mu(h_s,t_z) = \alpha(h_s,t_z)\Gamma\left(1+\frac{1}{\lambda(h_s,t_z)}\right) \tag{6.17}$$

$$\sigma(h_s,t_z) = \alpha(h_s,t_z)\sqrt{\Gamma\left(1+\frac{2}{\lambda(h_s,t_z)}\right)-\Gamma^2\left(1+\frac{1}{\lambda(h_s,t_z)}\right)} \tag{6.18}$$

where $\mu(h_s,t_z)$ and $\sigma(h_s,t_z)$ are the mean value and the standard deviation of the peaks sample for the short-term response $\mathbf{S}=\mathbf{s}=(h_s,t_z)$.

The frequency of maxima for a given short-term condition can be calculated approximately as:

$$\nu^+(h_s,t_z) = \frac{n_p(h_s,t_z)}{T_{ST}} \tag{6.19}$$

where $n_p(h_s,t_z)$ is the number of peaks identified in the response time series for the given short-term condition and T_{ST} is time-series length (or simulation length).

The average long-term frequency of maxima can be calculated in its discrete form as:

$$\overline{\nu}^+ = \sum_{i=1}^{N_{H_s}}\sum_{j=1}^{N_{T_z}} \nu^+\left(h_{s_i},t_{z_j}\right) f_{H_s,T_z}\left(h_{s_i},t_{z_j}\right)\Delta h_s \Delta t_z \tag{6.20}$$

Based on the previous development, the purpose of the proposed method is to predict the static mean, the peaks mean, the peaks standard deviation and the number of peaks for any value of H_s giving a known value of T_z, i.e., $T_z = t_z$ by means of a parametric interpolation equation which is defined by a minimum number of numerical simulations.

As a compromise between the number of numerical simulations and accuracy of the results, a parabolic function, based on only three numerical simulations for each

zero up-crossing period $T_z = t_z$, has been used to predict the static mean, the peaks mean and the peaks standard deviation. Regarding the number of peaks, it was considered the average of the three numerical simulations results:

$$n_p(h_s|t_{z_i}) = \frac{1}{3}\left[n_p(h_{s_1}, t_{z_i}) + n_p(h_{s_2}, t_{z_i}) + n_p(h_{s_3}, t_{z_i})\right] \tag{6.21}$$

The following parabolic equation is used to predict the mean of the peaks for any significant wave height, given a zero up-crossing wave period $T_Z = t_{z_i}$:

$$\mu(h_s|t_{z_i}) = a_0(t_{z_i}) + a_1(t_{z_i})h_s + a_2(t_{z_i})h_s^2 \tag{6.22}$$

To calibrate the constants $a_0(t_{z_i})$, $a_1(t_{z_i})$ and $a_2(t_{z_i})$ of the above equation, it is necessary to find the mean of the peaks sample for the three distinct simulations, i.e. $\mu(h_{s_1}, t_{z_i})$, $\mu(h_{s_2}, t_{z_i})$ and $\mu(h_{s_3}, t_{z_i})$. The constants are then calculated as follows:

$$a_2(t_{z_i}) = \frac{\mu(h_{s_3}, t_{z_i}) - \mu(h_{s_2}, t_{z_i}) - b_1(t_{z_i})\cdot(h_{s_3} - h_{s_2})}{(h_{s_3} - h_{s_2})(h_{s_3} - h_{s_1})} \tag{6.23}$$

$$a_1(t_{z_i}) = b_1(t_{z_i}) - a_2(t_{z_i})h_{s_1} - a_2(t_{z_i})h_{s_2} \tag{6.24}$$

$$a_0(t_{z_i}) = \mu(h_{s_1}, t_{z_i}) - b_1(t_{z_i})h_{s_1} + a_2(t_{z_i})h_{s_1}\ h_{s_2} \tag{6.25}$$

where:

$$b_1(t_{z_i}) = \frac{\mu(h_{s_2}, t_{z_i}) - \mu(h_{s_1}, t_{z_i})}{h_{s_2} - h_{s_1}} \tag{6.26}$$

The expressions above can also be used in a similar way to establish the parametric equations for the static mean and standard deviation of peaks. Then, given that these expressions have been established for all N_{Tz} values of T_z of the discretized integration domain, it is possible to predict the time series peaks statistical parameters for any short-term condition in the integration domain; consequently, the scale and shape parameters of Weibull distribution for the short-term response peaks. Finally, it is possible to compute the long term cumulative distribution of peaks in the discrete form:

$$F_R(r) = \sum_{i=1}^{N_{Hs}} \sum_{j=1}^{N_{Tz}} \frac{\nu^+\left(h_{s_i}, t_{z_j}\right)}{\overline{\nu}^+} F_{R|(H_s,T_z)_i}\left(r\middle|\left(h_{s_i}, t_{z_j}\right)\right) f_{H_s,T_z}\left(h_{s_i}, t_{z_j}\right) \Delta h_s \, \Delta t_z \qquad (6.27)$$

Note that the number of time domain numerical simulations required for calculating the above equation is $3xN_{Tz}$ where N_{Tz} is the number of up-crossing periods considered in integration mesh.

As mentioned before, the most probable extreme response value can be computed using Eq. (4.14) for a given long-term period.

It must be stressed that the interpolation scheme is conditioned on values of T_z because it is more or less intuitive that for a given value of this parameter any time-series statistical parameter could follow some soft variation with respect to H_s since any resonant variation will not be induced by the value assumed by H_s.

6.2 Parametric Interpolation Method (PIM) for probabilistic fatigue analysis of marine structures

The total damage caused by fatigue is calculated using the Eq. (5.20). Such multidimensional long-term integral requires a great amount of structure numerical simulations to be solved; since, it is necessary to perform a dynamic analysis to obtain each short-term fatigue damage.

As for the long-term extreme response prediction, an interpolation method based on the short-term behavior of fatigue damage is proposed in order to reduce the number of simulations mentioned above,

In what follows some details will be presented for the case where the stress processes are Gaussian and non-Gaussian.

6.2.1 Gaussian and narrowband stress processes

For a Gaussian narrow-banded short-term stress process, the short-term fatigue damage for a single-slope S-N curves given by:

$$d(h_s, t_z) = \frac{\nu_0(h_s, t_z) T \left(2\sqrt{2}\right)^m \left(m_0(h_s, t_z)\right)^{\frac{m}{2}}}{K} \Gamma\left(1 + \frac{m}{2}\right) \tag{6.28}$$

By considering the same hypothesis assumed in the item 6.1.1 of the present work, it is possible to calculate the zero up-crossing response (stress) frequency by substituting Eq.(6.10) into Eq.(3.4). This leads to

$$\nu_o = \frac{1}{2\pi} \beta_0(t_z) \tag{6.29}$$

where

$$\beta_0(t_z) = \sqrt{\frac{\alpha_2(t_z)}{\alpha_0(t_z)}} \tag{6.30}$$

The equation of the short-term fatigue damage can be re-written by substituting Eq. (6.30) into Eq. (5.8) as follows:

$$d(h_s, T_z = t_z) = \frac{\beta_0(t_z) T_S \left(2\sqrt{2}\right)^m \alpha_0(t_z)^{\frac{m}{2}} h_s^m}{2\pi K} \Gamma\left(1 + \frac{m}{2}\right) \tag{6.31}$$

Thus equation can be re-written again in a more compact way as follows:

$$d(h_s, T_z = t_z) = \psi(t_z) h_s^m \tag{6.32}$$

where

$$\psi(t_z) = \frac{\beta_0(t_z) T_S \left(2\sqrt{2}\right)^m \alpha_0(t_z)^{\frac{m}{2}}}{2\pi K} \Gamma\left(1 + \frac{m}{2}\right) \tag{6.33}$$

Note that for a given value of T_z, i.e.. $T_Z = t_Z$,it is possible to identify a single constant $\psi(t_z)$. This constant is obtained from a single dynamic analysis; therefore, any other short-term damage value for this wave up-crossing period can be determined without performing another simulation.

The computational cost reduction is considerable because just a single frequency domain structural analysis is required for any T_z since the short-term fatigue damage can be written analytically as an explicit function of H_s.

The total fatigue damage in the long-term will be calculated by substituting Eq. (6.33) in Eq.(5.19), which results in.

$$D_{1-yr} = 2920 \sum_{i=1}^{N_{Hs}} \sum_{j=1}^{N_{Tz}} \psi\left(t_{Z_j}\right) h_s^m f_{Hs,Tz}\left(h_{S_j}, t_{Z_j}\right) \Delta hs \, \Delta tz \tag{6.34}$$

In this case one structural analysis is needed for each T_z used in the discretization of integration domain. However, this approach cannot be applied when the structural response is not Gaussian or narrowband. Structures such as metallic risers have a highly non-linear behavior; therefore another approach must be addressed to optimize the probabilistic fatigue calculation.

6.2.2 Non-Gaussian processes

As in the previous section, the objective of the proposed method is to predict the short-term fatigue damage for any value of H_s given a known value of T_z, i.e., $T_Z = t_Z$ using a parametric interpolation equation which is defined by a minimum number of structure numerical simulations. Based on the short-term fatigue behavior identified for a Gaussian narrow-banded stress process and on some tests performed in the development of the work, a linear-exponential function has been chosen. The interpolating equation proposed is the following:

$$d\left(h_s | t_{Z_i}\right) = \alpha\left(t_{Z_i}\right) h_s^{\beta\left(t_{Z_i}\right)} + \lambda\left(t_{Z_i}\right) h_s \tag{6.35}$$

In order to calibrate the constants α, β and λ of the above equation, it is necessary to find the short-term fatigue damage for the three distinct simulations (three values of H_s giving a known value of $T_z = t_z$), i.e. $d_1 = d\left(h_{s_1}, t_{z_i}\right)$, $d_2 = d\left(h_{s_2}, t_{z_i}\right)$ and $d_3 = d\left(h_{s_3}, t_{z_i}\right)$. The constants are the solution of the following equations system:

$$d_1 = \alpha\, h_{s1}^{\beta} + \lambda\, h_{s1} \tag{6.36}$$

$$d_2 = \alpha\, h_{s2}^{\beta} + \lambda\, h_{s2} \tag{6.37}$$

$$d_3 = \alpha\, h_{s3}^{\beta} + \lambda\, h_{s3} \tag{6.38}$$

From Eq. (6.36) it is possible to write:

$$\alpha = \frac{d_1 - \lambda\, h_{s1}}{h_{s1}^{\beta}} \tag{6.39}$$

By substituting Eq. (6.39) into Eq. (6.38) results in:

$$\beta = \frac{\ln\left(\dfrac{d_3 - \lambda\, h_{s3}}{d_1 - \lambda\, h_{s1}}\right)}{\ln\left(\dfrac{h_{s3}}{h_{s1}}\right)} \tag{6.40}$$

By substituting Eq. (6.39) and Eq. (6.40) into Eq.(6.37) the following implicit equation can be obtained:

$$\frac{d_1 - \lambda\, h_{s1}}{h_{s1}^{\frac{\ln\left(\frac{d_3 - \lambda\, h_{s3}}{d_1 - \lambda\, h_{s1}}\right)}{\ln\left(\frac{h_{s3}}{h_{s1}}\right)}}} h_{s2}^{\frac{\ln\left(\frac{d_3 - \lambda\, h_{s3}}{d_1 - \lambda\, h_{s1}}\right)}{\ln\left(\frac{h_{s3}}{h_{s1}}\right)}} - d_2 = 0 \tag{6.41}$$

The only unknown term in the above equation is λ. The solution of this equation can be found by any appropriate method for find the root of a single nonlinear equation. In this work the Levenberg-Marquardt algorithm (PRESS *et al.*, 2007) was used. Afterwards, by substituting λ into Eq. (6.40) it is possible to find β, and by substituting λ and β into Eq.(6.39) it is possible to find α. Having the three constants α, β and λ it is possible to calculate the short-term fatigue damage for any H_s value giving that $T_z = t_z$

6.3 Special case: TDZ of a SCR

In the case studies performed in this work, which will be described in the next chapter, it was observed that the interpolation equations described above did not perform well for the touchdown zone (TDZ) of a steel catenary riser (SCR) considering either extreme or fatigue analysis. Then, a more detailed study was performed for this specific region.

In the riser analysis methodology used in this work, static offsets are applied at the top riser for taking into account the floater mean offset, low frequency wind and wave motions. The floater mean offset value is the calculated by taking into account the steady forces from current, wind and waves. Typically, the offset is considered in the same direction as the wave. The adopted hypothesis used to calculate the offset for each fatigue load case ($Offset_i$) is defined as follows:

$$Offset_i = Offset_{max} \frac{h_{si}}{h_{max}} \tag{6.42}$$

where $Offset_{max}$ is the mean displacement of the floater obtained by a distinct analysis where it is subject to wave, wind and current loads; h_{si} is the significant wave height of the short-term environmental condition and h_{max} is usually taken as the maximum 1 year wave height. It is common practice, to consider as a percentage of the water depth which varies between 1% and 5%.

As shown in Fig. 9, the offset changes the riser TDP position from one load case to another. Therefore, the variation of short-term statistical response parameters with H_s is not parabolic, and the variation of short-term fatigue damage with H_s is not exponential in this SCR location.

To clarify the aspect highlighted above, the position variation of the point P in Fig. 9 is analyzed. This position depends on the static offsets of the three load states represented by three significant wave heights ($h_{s1} < h_{s2} < h_{s3}$). For the offset due to h_{s1}, the point P is located on the sea floor, where stresses and fatigue damage are usually very small. Instead, for the offset due to h_{s2}, the point P is located in the TDP,

where stresses and fatigue damage are more critical. Finally, for the offset due to h_{s3}, the point P is located in the suspended riser segment where stresses and fatigue damage are lower than in the TDP.

So, based on this stresses response behavior observed in the study cases, the parametric equation with best performance to predict short-term statistical response parameters for riser sections located in the TDP region, for any value of H_s given a known value of $T_z = t_z$, is a bilinear function. For the peaks mean it is written as follows:

$$\mu\left(h_s|t_{z_i}\right)=\begin{cases}\dfrac{\mu_2-\mu_1}{h_{s2}-h_{s1}}\left(h_s-h_{s1}\right)+\mu_1 & \text{if} \quad h_{s1}\le h_s<h_{s2}\\ \dfrac{\mu_3-\mu_2}{h_{s3}-h_{s2}}\left(h_s-h_{s2}\right)+\mu_2 & \text{if} \quad h_{s2}\le h_s\le h_{s3}\end{cases} \tag{6.43}$$

The same equation format is used for the other statistical parameters.

The bi-linear equation presented also the best performance for the fatigue assessment. and in the same way, for the short-term fatigue damage the equation reads:

$$d\left(h_s|t_{z_i}\right)=\begin{cases}\dfrac{d_2-d_1}{h_{s2}-h_{s1}}\left(h_s-h_{s1}\right)+d_1 & \text{if} \quad h_{s1}\le h_s<h_{s2}\\ \dfrac{d_3-d_2}{h_{s3}-h_{s2}}\left(h_s-h_{s2}\right)+d_2 & \text{if} \quad h_{s2}\le h_s\le h_{s3}\end{cases} \tag{6.44}$$

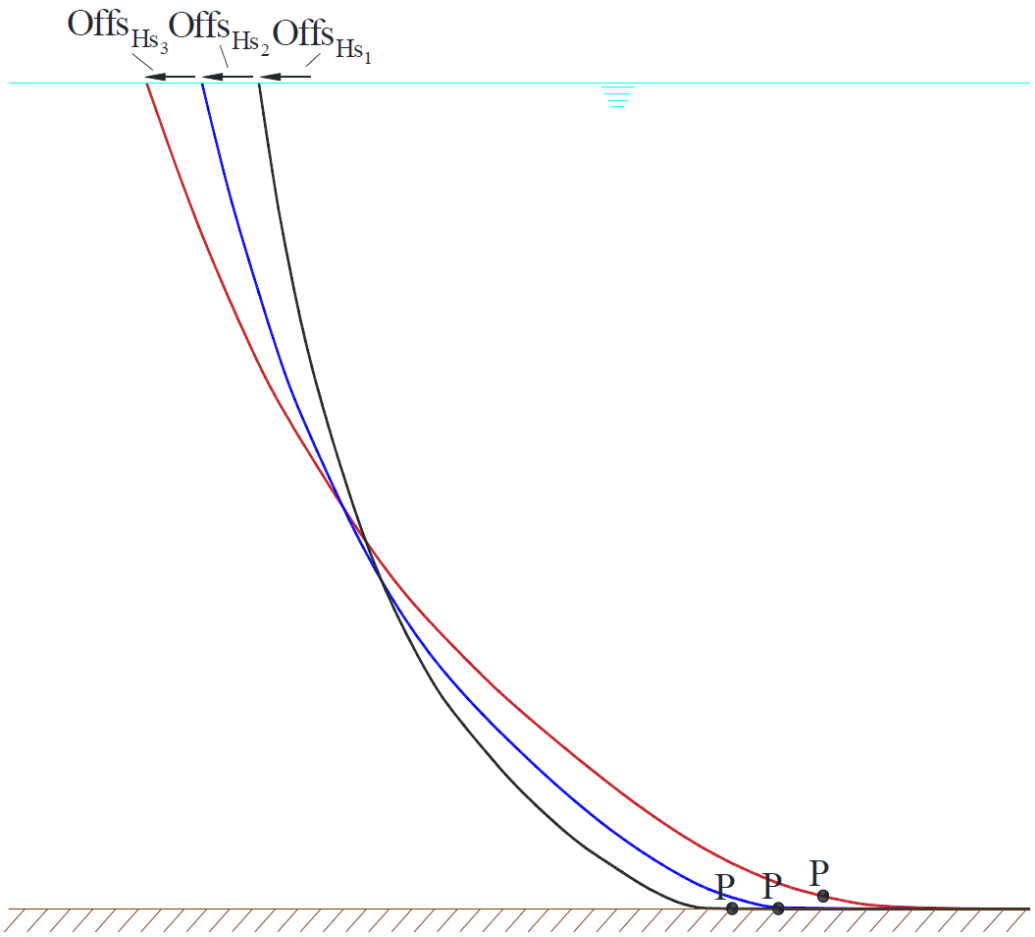

Figure 9. TDP position variation with the applied offsets

6.4 Integrated analysis of long-term extreme response and probabilistic fatigue using the PIM

As commented previously in this work long-term response and probabilistic fatigue analyses are performed over the same integration domain. Moreover, the interpolation schemes presented before these analyses are both based on three structure numerical simulations for each value of the T_z in the discretized integration domain. So, the same structure numerical simulations, which are nonlinear time domain stochastic finite element-based analysis, can be used for the prediction of the long-term response as well as for the fatigue life estimation. This allows for the simultaneous evaluation of both design criteria. This integrated scheme has been implemented in the present work.

Another important aspect is the definition of the integration domain for numerical analyses. By some numerical tests, it has been identified that the integration

domain suitable to perform probabilistic fatigue analysis of marine structures is given by the environmental contour of 100 yr. Besides, VIDEIRO *et al*. (2019) pointed that the key region of the joint probability distribution of significant wave heights and wave periods that most contributes to the long-term response is located between the environmental contours of 10 yr and 10,000 yr. From these two premises it is possible to affirm that an integration domain delimited by the 10,000-yr Hs-Tz environmental contour is suitable for simultaneous probabilistic fatigue analysis and long-term extreme response. This contour is defined from the H_s-T_z joint probability function as described in the Appendix A.

The methodology to determine the most probable extreme response value and the fatigue life using the PIM is summarized in Fig. 10. Initially, the joint probability function for the riser location is informed and used to define the integration domain. The T_z mesh points are defined and for each of these values, three corresponding H_s values are selected. The structure must be simulated for all these short-term conditions. The simulation length is needs to be sufficient to guarantee reliable short-term statistics (at least 10,800s long). The response time series are then processed to obtain the fatigue damage and the statistical parameters of the peaks (mean, standard deviation, and number of peaks) of the response of interest. Afterwards, the interpolation constants are established for obtaining the short-term parameters for each design criterion (Weibull distribution parameters for extreme analysis and short-term fatigue damage for the fatigue life assessment). Then the long-term integrals (for fatigue and extreme analyses) are computed for all points of discretized H_s-T_z mesh using the interpolated parameters and the corresponding results are computed: the N-yr most probable extreme response and the fatigue life.

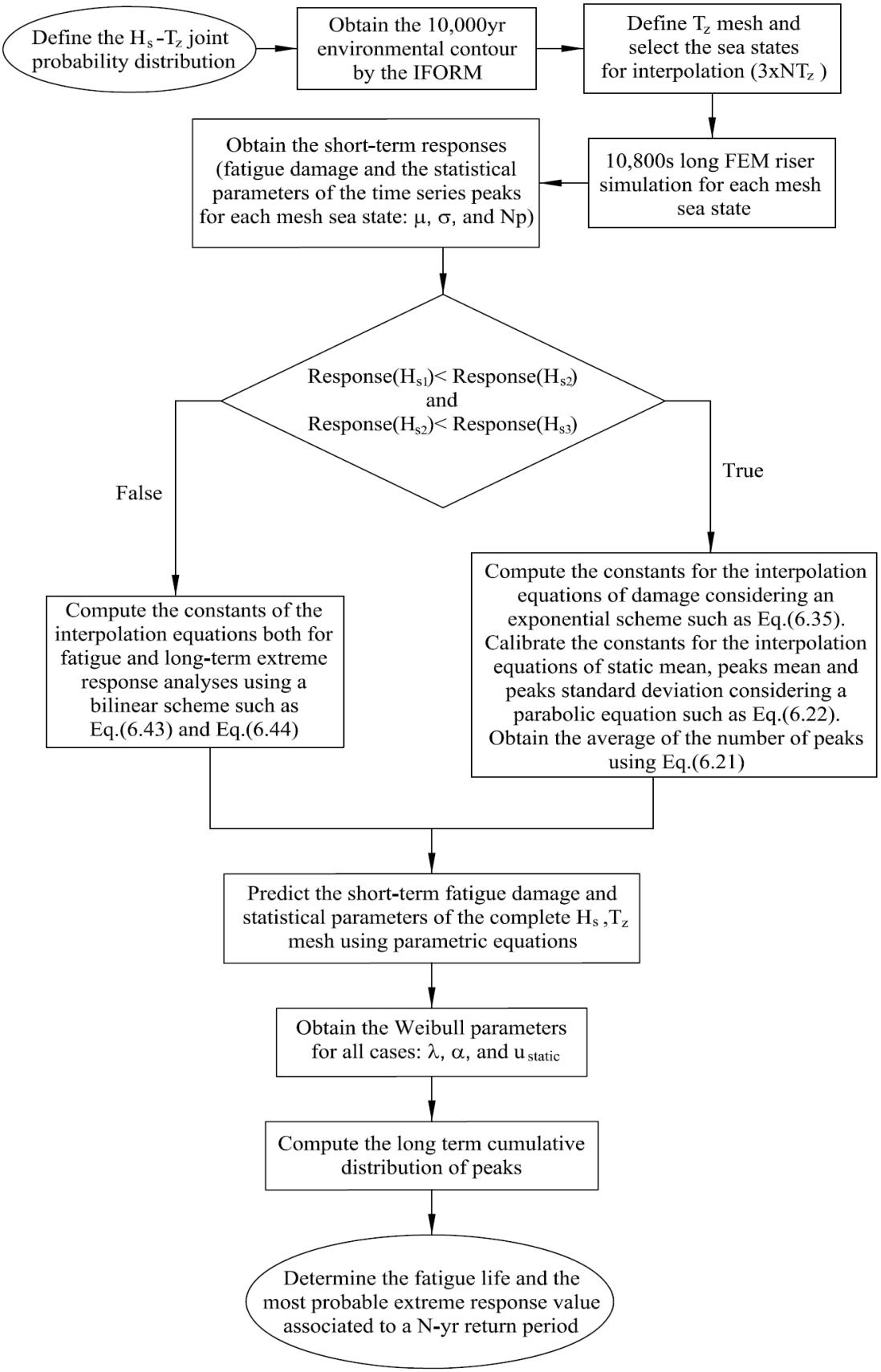

Figure 10. Flow chart of algorithm used to determine the fatigue life and the most probable extreme response value using the PIM

Chapter 7

Examples

Three examples are used to assess the accuracy of the Parametric Interpolation Method applied in long-term extreme response and probabilistic fatigue prediction. In all examples, the waves were considered omnidirectional. The same joint probability distribution model of the environmental parameters is employed for the three examples analyzed. This joint model is based on the conditional modelling described in Chapter 2. The marginal probability density function of H_S is given by a Lognormal distribution:

$$f_{Hs}(h_s) = \frac{1}{\sqrt{2\pi}\,\xi_{Hs}\,h_s}\,\exp\left(-\left(\frac{\ln(h_s)-\lambda_{Hs}}{\xi_{Hs}}\right)^2\right) \tag{7.1}$$

where the location and scale parameters are, respectively, $\lambda_{Hs} = 9.375918\times10^{-1}$ and $\xi_{Hs} = 3.579696\times10^{-1}$.

The conditional probability density of T_P is given by a Weibull-3P distribution:

$$f_{Tp|Hs}(t_p \mid h_s) = \frac{(t_p - u_w(h_s))^{\lambda_w - 1}}{\alpha_w^{\lambda_w}}\,\lambda_w\,\exp\left(-\left(\frac{t_p - u_w(h_s)}{\alpha_w}\right)^{\lambda_w}\right) \tag{7.2}$$

where the location parameter is given by the following equation:

$$u_w(h_s) = -2.329473 + 4.307667\times\ln(h_s) \tag{7.3}$$

and the scale and shape parameters are, respectively, $\alpha_w = 9.313608$ and $\lambda_w = 4.921465$

A breaking wave limit is considered for the above probabilistic model, i.e. a relationship between the significant wave height and the spectral peak period, which defines the waves that can be physically unreal. In this paper, the criterion presented by HAVER & NYHUS (1986) is taken into account. It is represented by the following empirical equation:

$$T_p > 3.2\sqrt{H_s} \tag{7.4}$$

The breaking wave criterion is imposed in the model by changing the conditional distribution of T_p as:

$$f_{Tp|Hs}(t_p \mid h_s) = \begin{cases} \dfrac{\dfrac{(t_p - u_w(h_s))^{\lambda_w - 1}}{\alpha_w^{\lambda_w}} \lambda_w \exp\left(-\left(\dfrac{t_p - u_w(h_s)}{\alpha_w}\right)^{\lambda_w}\right)}{1 - F_{Tp|Hs}(t_p = 3.2\sqrt{hs} \mid h_s)} & \text{if } t_p > 3.2\sqrt{hs} \\ 0 \quad \text{otherwise} \end{cases} \tag{7.5}$$

where $F_{Tp|Hs}(t_p \mid h_s)$ is the cumulative probability function of T_p conditional on H_s.

The following relationship between the zero-crossing period T_z and the peak period T_p was applied:

$$T_z = T_p\left(\frac{5+\gamma}{11+\gamma}\right)^{1/2} \tag{7.6}$$

where γ is the JONSWAP peakedness parameter. In the case of $\gamma = 1$, the JONSWAP spectrum reduces to the Pierson–Moskowitz model; i.e., $T_z = T_p/1.414$. However, in this work this parameter has been assumed as $\gamma = 6.4\, T_p^{-0.491}$ in order to be representative of the Brazilian offshore coast.

The joint probability function is then:

$$f_{Hs,Tz}(h_s, t_z) = f_{Hs}(h_s)\, f_{Tz|Hs}(t_z \mid h_s) \tag{7.7}$$

The limit of the integration domain is defined using the 10.000-yr environmental contour. The 100-yr and 10.000-yr contour lines associated to the H_s-T_p joint probability model is shown in Fig. 11.

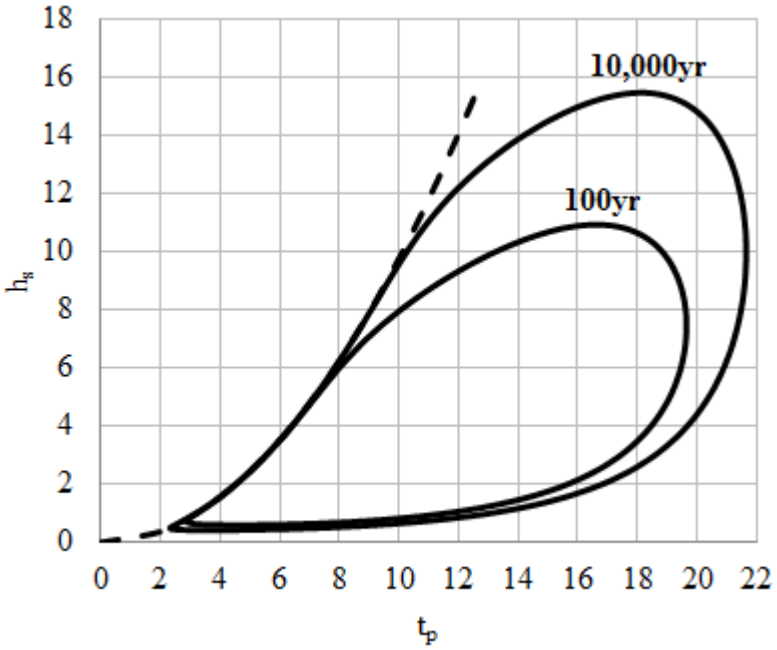

Figure 11.10,000-yr and 100-yr environmental contours

7.1 Example1: An idealized theoretical linear SDOF model

In this first example, the long-term extreme response and fatigue assessment are investigated for an idealized theoretical case. The model is represented by an analytical response amplitude operator (RAO) associated to a single-degree-of-freedom (SDOF) system under wave loading. This model allows a theoretical and fast investigation about the performance of the Parametric Interpolation Method (PIM) when compared with the complete integration of the long-term integrals. For the sake of simplicity, the stress spectrum will be considered equivalent to the response spectrum for the fatigue analysis.

The response amplitude operator (RAO) is described by the following equation:

$$RAO_R(\omega) = \frac{1}{\left[\left(1-\left(\frac{\omega}{\omega_n}\right)^2\right)^2 + \left(2\xi\frac{\omega}{\omega_n}\right)^2\right]^{1/2}} \tag{7.8}$$

where ω_n represents the system natural frequency and ξ is the critical damping ratio of the model. In this example the following values were assumed: $\omega_n = 0.5$ and ξ=0.05.

Under the linear assumption, the spectral density of the system displacement (response) for a given stationary short-term condition $\mathbf{S}=\mathbf{s}=(h_s, t_z)$ is given by

$$S_{R|\mathbf{S}}(\omega|\mathbf{s}) = RAO_R(\omega)^2 \, S_{\eta|\mathbf{S}}(\omega|\mathbf{s}) \tag{7.9}$$

where $S_{\eta|S}(\omega|s)$ is the spectral density of the sea surface elevation $\eta(t)$ for the short-term condition $\mathbf{S}=\mathbf{s}$ represented in this example by the modified Pierson–Moskovitz spectrum.

As the sea surface elevation is assumed to be a Gaussian stochastic process, the system response is also Gaussian. Under the narrow band assumption, the short-term response peaks are Rayleigh-distributed and the procedure described in the section 6.1.1 can be used.

For this example, Δ_{Tz}=1.0s and Δ_{Hs}=0.5m are, respectively, the spacing of wave zero up-crossing periods and significant wave heights considered in the division of the integration domain highlighted in Fig.11. All the sea states considered for the full integration and the sea states considered for the Parametric Interpolation Method are identified in Fig. 12.

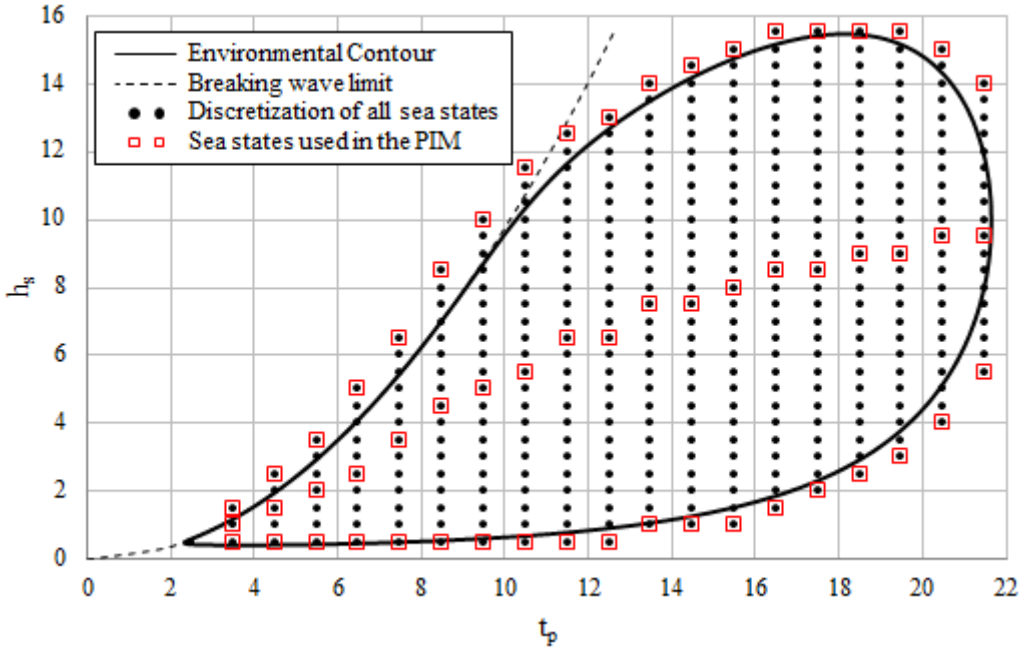

Figure 12. 10,000-yr environmental contour and sea states used in the analyses.

7.1.1 Long-term extreme response

The parameter $\alpha_n(t_z)$ is calibrated by using Eq. (6.11). The behavior of this parameter as a function of T_p is shown in Fig. 13.

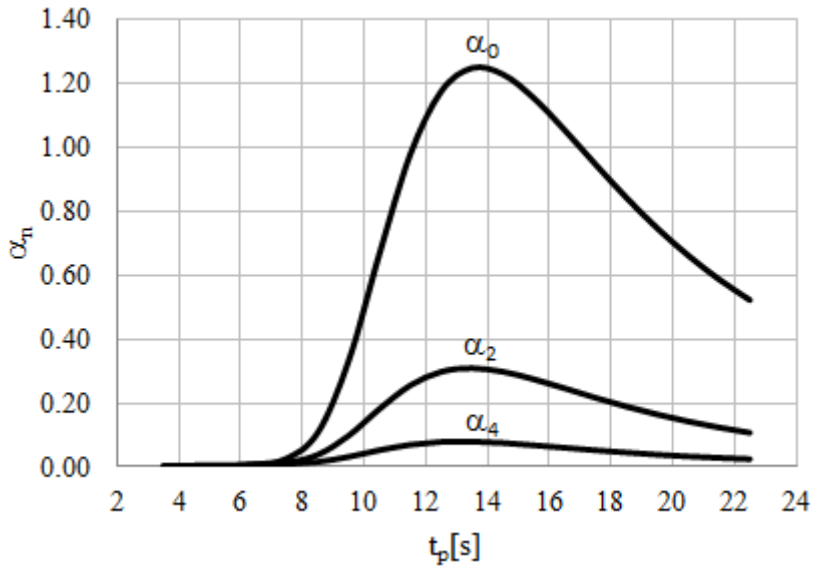

Figure 13. Relation between the parameter α_n and the wave peak up-crossing period T_p.

The spectral moments are obtained using Eq. (6.10). Fig. 14 shows a comparison of these results with those obtained using Eq. (6.6). As expected the results are the same. The frequency of maxima ν_m is calculated using Eq. (6.12). This parameter just depends of T_p. Fig. 15 shows the variation of ν_m with T_p for this example.

By solving Eq. (6.14), the average frequency of maxima obtained is $\bar{\nu}^+ = 0.09893$ peaks/s. The long-term cumulative probability distribution of response peaks is obtained by evaluating numerically the long-term integral (see Eq. (6.13)) using a "structural analysis" for each integration point and using the interpolation functions where just one structural analysis is performed for each T_p of the integration grid. Fig. 16 shows the results obtained. Both curves are exactly the same.

The return period considered in this example to calculate the long-term extreme value is 100 years. Therefore, the expected number of peaks is N_L =100years $\bar{\nu}^+$ N_s T_{ST} = 100years$\times$ 0.09893 peaks/s$\times$2920states/year$\times$10800s/states = 3.11997*10^8peaks. Then, the most probable long-term extreme response calculated with Eq.(4.14) using the

Parametric Interpolation Method is R_{100}^{Parab}=53.22 and the value obtained using full numerical integration is exactly the same. As expected, the accuracy obtained is 100%.

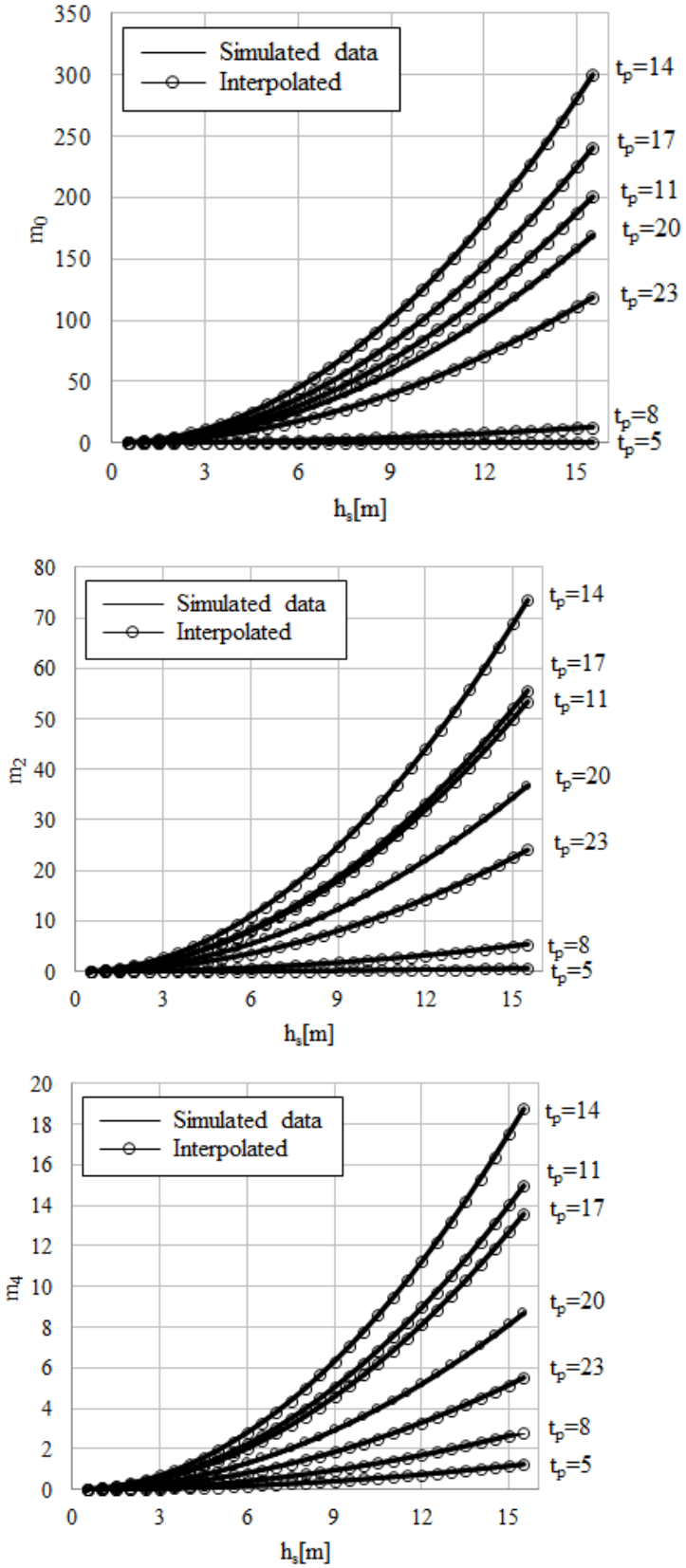

Figure 14. Comparison of simulated and interpolated spectral moments.

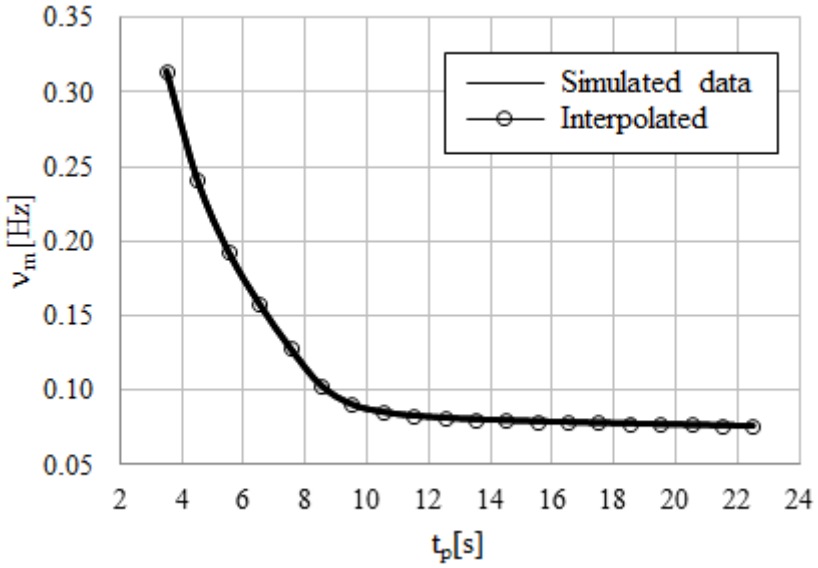

Figure 15. Comparison of simulated and interpolated frequency of maxima

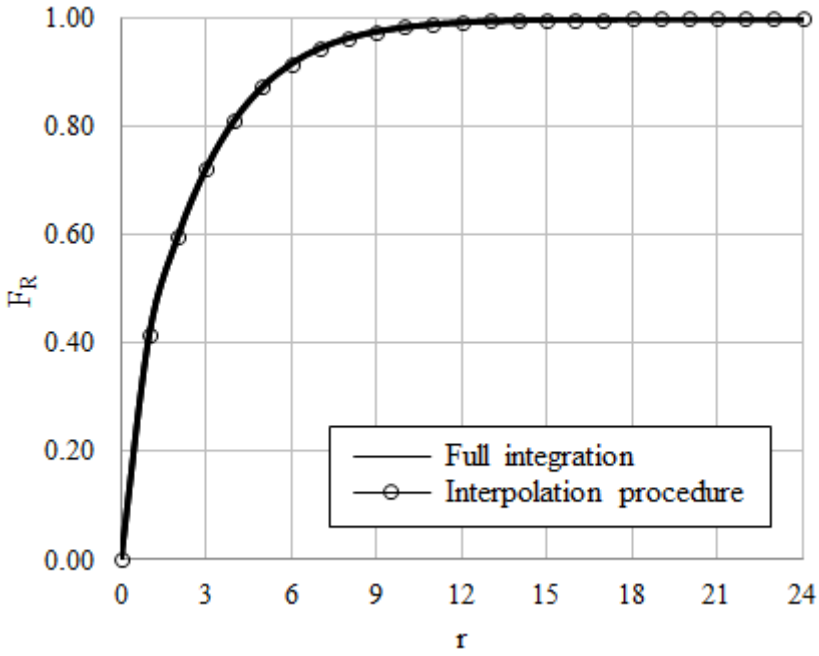

Figure 16. Long-term cumulative probability distributions of peaks obtained by full integration and interpolation procedure.

Note that 392 frequency domain analyses were used when the long-term integral was evaluated by means of the full numerical integration approach. Using the interpolation curves, i.e., Parametric Interpolation Method (PIM), just 20 simulations were necessary for the solution. This means a huge computer saving (≅ 95%) for solving using the long-term approach.

7.1.2 Probabilistic fatigue analysis

The behavior of the parameter ψ (see Eq. (6.33)) varies with T_p and the SN-Curve exponent m as shown in Fig. 17. The S-N curve parameter K is equal to $K=5x10^{10}$. In this figure it can be seen that the parameter ψ reaches its maximum value at a peak period of $T_p=13.5s$ for all the values considered of the SN-curve parameter m. This peak period value is close to the natural period of the considered SDOF, $T_n = \frac{2\pi}{0.5 rad/s} = 12.6 s$.

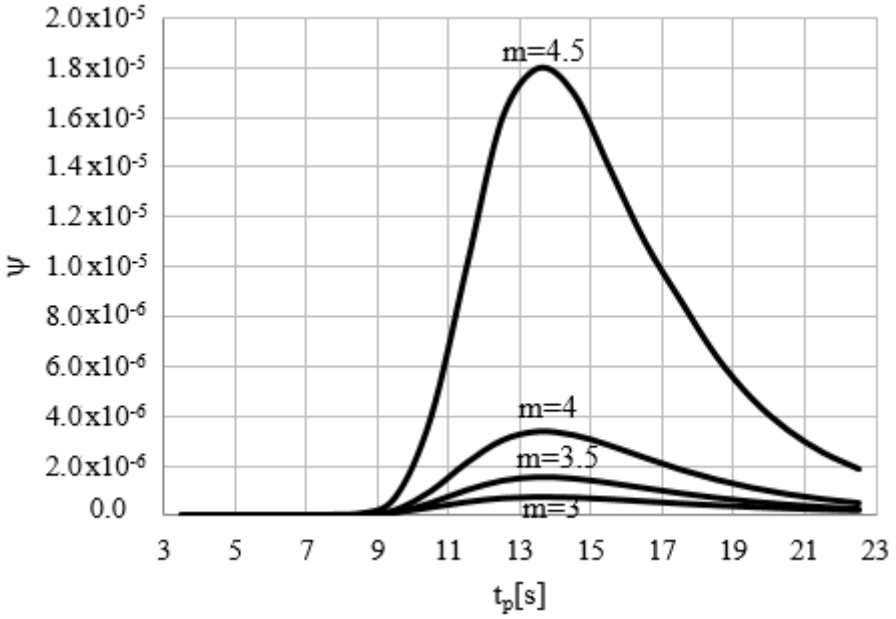

Figure 17. Relation between the parameter ψ and the wave peak period T_p and the SN-Curve exponent m .

Fig. 18 shows the variation of the short-term damage with the significant height H_s considering a fix peak period equal to $T_p=13.5s$, for different values of the SN-curve parameter m. As expected, the damage increases as this parameter increases. Note that the values obtained by the PIM are exactly the same as those obtained by the full integration points.

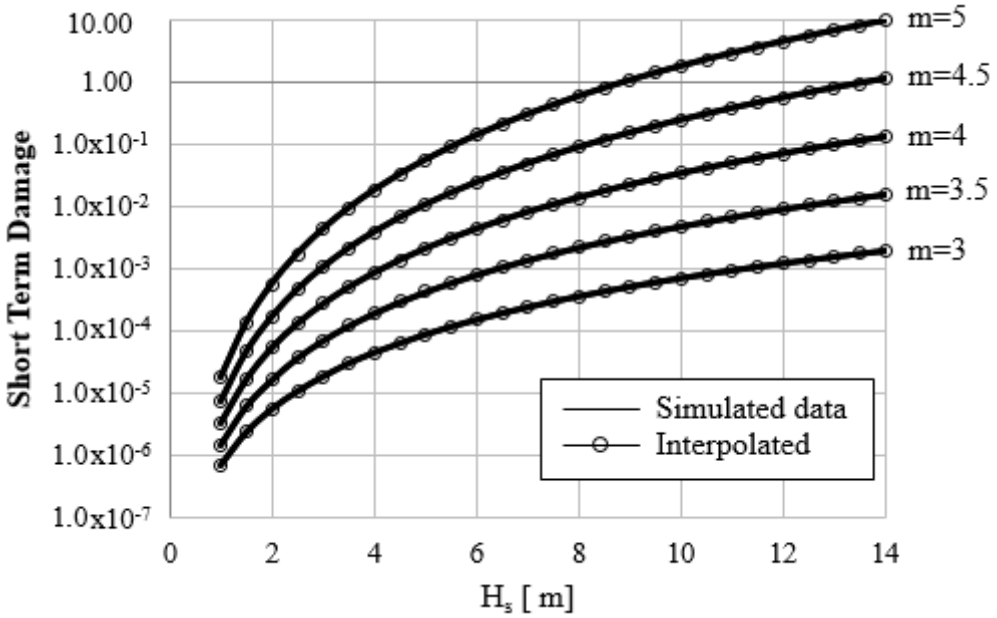

Figure 18. Comparison between the short-term damage obtained by the PIM and the obtained by the full integration.

Evidently, the fatigue life depends on different factors, such as: the natural frequency of the SDOF and the SN curve used. Fig. 19 shows that fatigue life does not have a linear relationship with the natural frequency of the system; for the present case, it can be clearly seen that as this frequency increases its the fatigue life also increases. On the other hand, as the SN curve parameter m increases the fatigue decreases. Note again that the values obtained by the PIM are exactly the same as those obtained by the full integration.

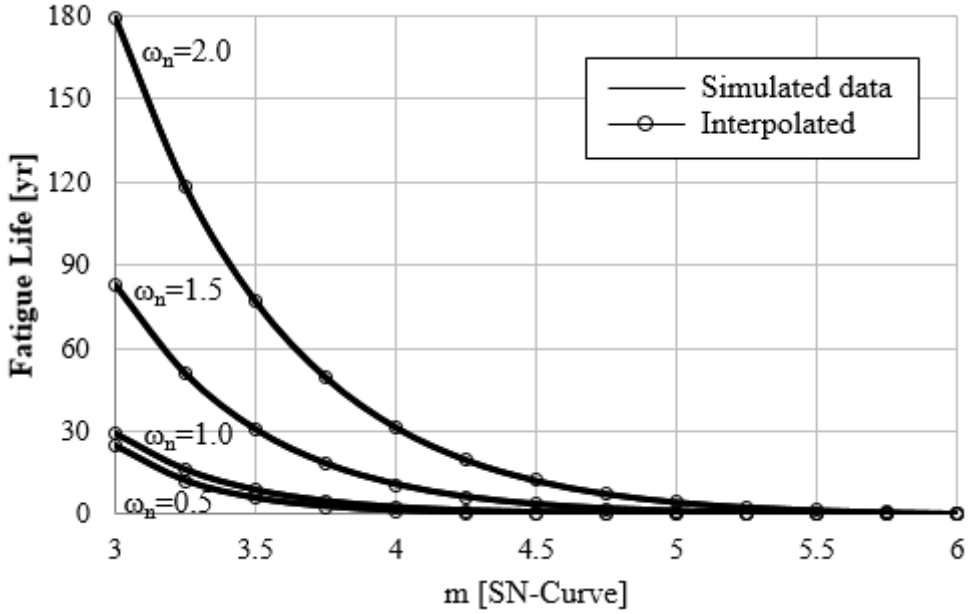

Figure 19. Comparison between the fatigue life obtained by the PIM and by the full integration ("brute force" approach).

As the integration and interpolation points used to perform the probabilistic fatigue assessment are the same as those used previously in extreme response analysis, the computer saving is the same. However, the most important aspect is that both analyses can be performed in parallel without the need of extra short-term structural analysis.

7.2 Example2: SCR installed in deep waters

In this example, the computer efficiency and accuracy of the Parametric Interpolation Method (PIM) is evaluated in the estimation of the long-term extreme response and probabilistic fatigue of an oil production, 4090m long Steel Catenary Riser (SCR) connected to an FPSO located in a water depth of 2100m. The elasticity modulus considered for the steel is 207 GPa and the specific weight is 77 kN/m^3. The FE mesh used in the model is shown in Table 2. The riser properties are shown in Table 3. The top angle is 14º. The connection with the vessel is a flex-joint whose properties are shown in Table 4.

Table 2. FE Mesh for each SCR segment

Seg.	Length (m)	Number of FE	First FE length (m)	Last FE length (m)	Element type
1	1200	461	5	1	Bottom
2	530	530	1	1	Touch down zone
3	192	64	1	5	Suspended
4	1352	272	5	5	Suspended
5	500	167	5	1	Suspended
6	300	571	1	0.05	Suspended
7	12	240	0.05	0.05	Stress Joint
8	-	-	-	-	Flex joint

Table 3. Riser properties for each SCR segment

Seg.	OD (in)	ID (in)	Internal Fluid Density (kN/m^3)	CM	CD
1	14	12	5.9	2.0	1.2
2	14	12	5.9	2.0	1.2
3	14	12	5.9	2.0	1.2
4	14	12	5.9	2.0	1.2
5	14	12	5.9	2.0	1.2
6	14	12	5.9	2.0	1.2
7	16	12	5.9	2.0	1.2

Table 4. Flex joint properties

Parameter	Value
Translational Stiffness (kN/m)	$2.0x10^7$
Torsional Stiffness (kN.m/deg)	200
Bending Stiffness (kN.m/deg)	47

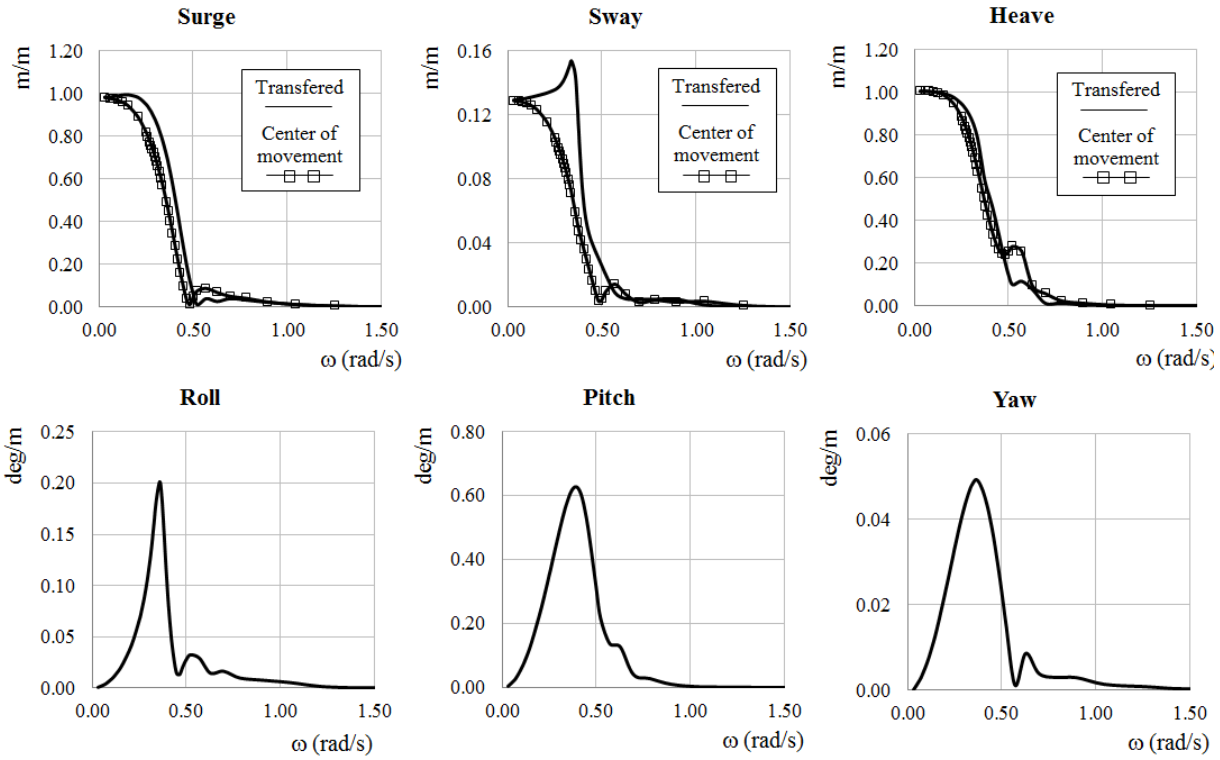

Figure 20. Translational and rotational vessel motions RAOs at the center of motion and at the riser top connection

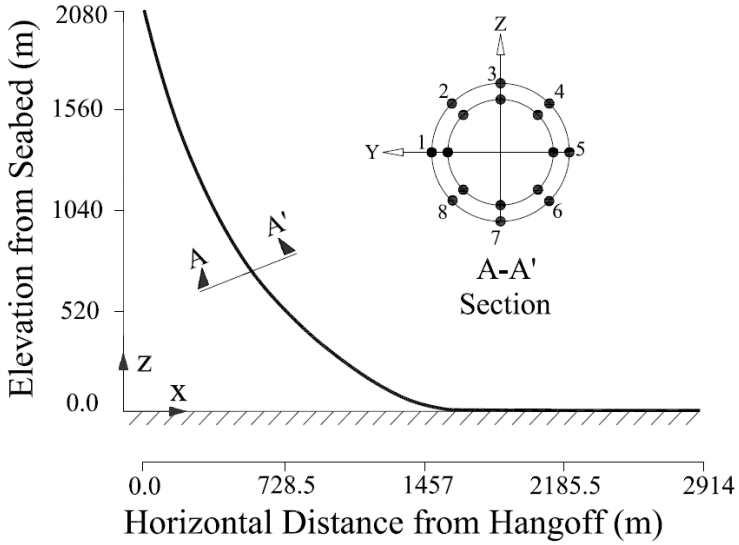

Figure 21. SCR model

The vessel first order motions RAOs are shown in Fig. 20. The SCR model is shown in Fig. 21. The incidence directions of the wave loading and the triangular current velocity profile considered in this example are shown in Fig. 22. Note that the wave and current are aligned. The current velocity at the top is 0.4m/s and the bottom

velocity is 0.0m/s. This current profile is considered to be the same for any short-term wave condition. Fig. 23 shows additional information such as the riser and vessel azimuths, local and global coordinates and the RAO direction. Furthermore, the JONSWAP spectrum was employed to model sea surface elevation in this example.

Regarding the stochastic time-domain riser analyses, each short-term time-domain simulation was taken as 10800s long. Moreover, the wave spectrum was decomposed in 500 wave components for the numerical simulations.

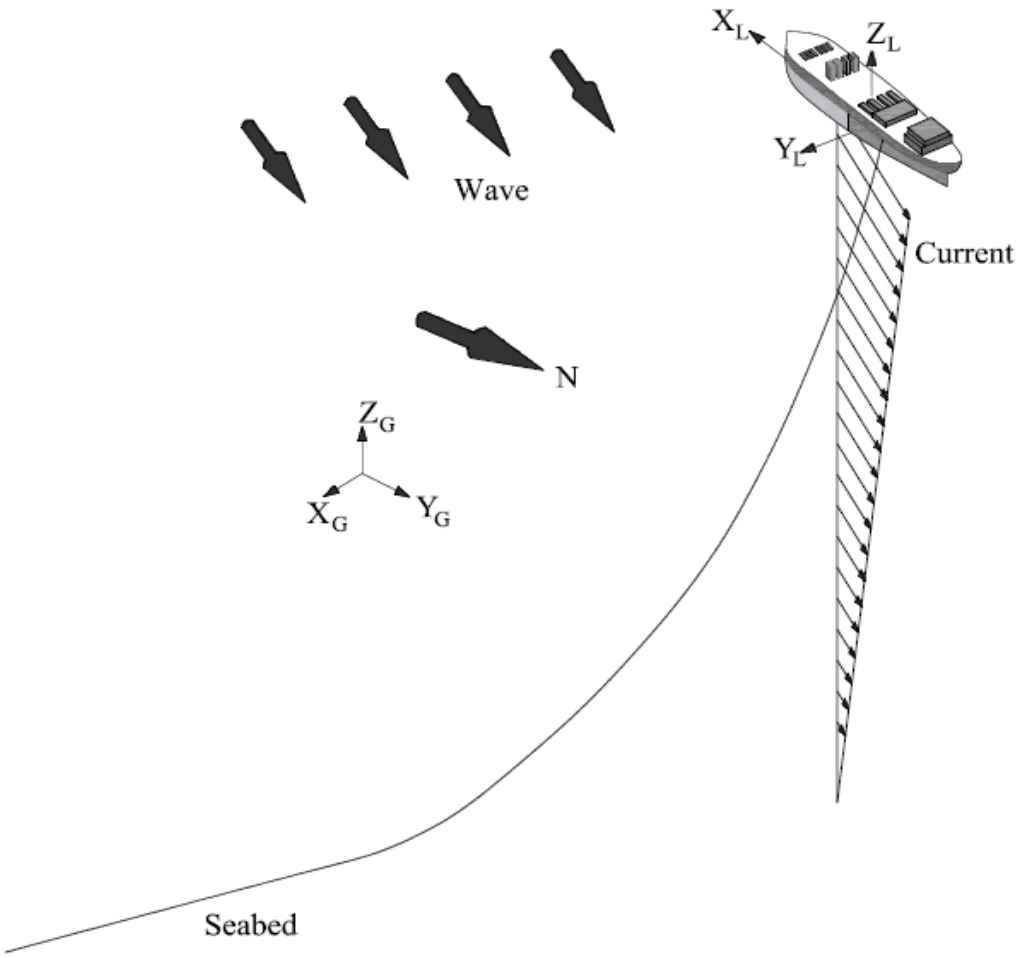

Figure 22. Environmental loading acting on the SCR

For this example, the joint probability function for the wave environmental parameters is the same described in Eq. (7.7). Moreover, the integration domain is the same specified in Fig.11 and the sea states for both, full integration and parametric interpolation, are those illustrated in Fig.12. Consequently, 392 finite elements non-linear numerical simulations in the time domain were performed.

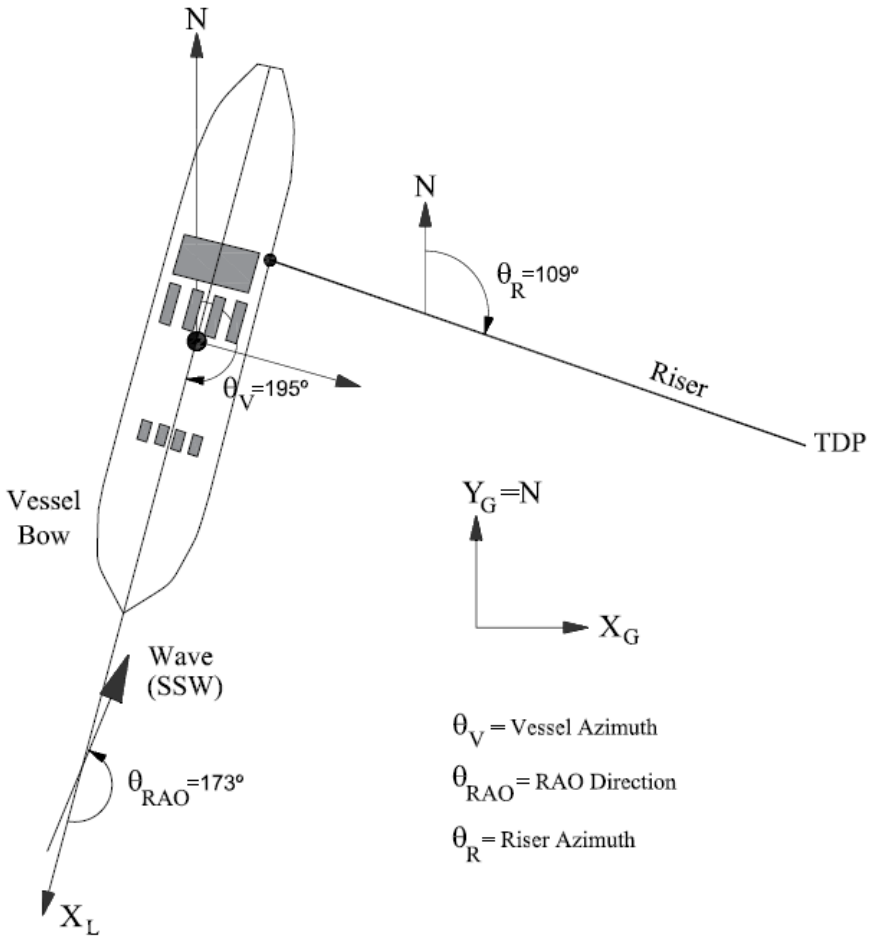

Figure 23. Riser and vessel azimuths, local and global coordinates and RAO direction.

7.2.1 Long-term extreme response

In the analysis of metallic risers, different extreme long-term responses can be studied, for example, axial force, radius of curvature, von Mises stress, among others. In this work, the assessed response was the cross-section utilization factor (UF) of a riser cross section considering the ultimate limit state (ULS) according to DNV-OS-F201 (2010). For steel pipe cross sections subjected to net internal overpressure, the utilization factor is evaluated as:

$$UF(t) = (\gamma_{SC} \cdot \gamma_m) \cdot \left[\frac{|M_d(t)|}{M_k} \sqrt{1 - \left(\frac{p_{ld} - p_e}{p_b(t_2)} \right)^2} + \left(\frac{T_{ed}(t)}{T_k} \right)^2 \right] + \left(\frac{p_{ld} - p_e}{p_b(t_2)} \right)^2 \qquad (7.10)$$

where M_d is the design bending moment time-series, T_{ed} is the design effective axial tension time series, p_{ld} is the local internal design pressure, p_e is the local external

pressure, M_k is the plastic bending moment resistance, T_k is the plastic axial force resistance and $p_b(t_2)$ is the burst resistance, γ_{SC} e γ_m are partial safety factors. All these parameters are defined in DNV-OS-F201 (2010). For net external overpressure case, the utilization factor definition is:

$$UF(t) = (\gamma_{SC} \cdot \gamma_m)^2 \cdot \left[\left(\frac{|M_d(t)|}{M_k} \right) + \left(\frac{T_{ed}(t)}{T_k} \right)^2 \right]^2 + (\gamma_{SC} \cdot \gamma_m)^2 \cdot \left(\frac{p_e - p_{min}}{p_c(t_2)} \right)^2 \quad (7.11)$$

where $p_c(t_2)$ is the hoop buckling capacity of the pipe and p_{min} is the minimum internal working pressure. Considering a long-term analysis, the design is accepted when the utilization factor is lower or equal to the unitary value:

$$UF_k \leq 1 \quad (7.12)$$

where UF_k is most probable value for 100-yr utilization factor of the analyzed riser section.

γ_{SC} and γ_m are safety factors related to uncertainties associated to a safety class and to the material properties, respectively. Safety class is defined by DNV-OS-F201 (2010) as follows:

- **Low**: When riser failure implies low risk of human injury and minor environmental and economic consequences.
- **Normal**: For conditions where riser failure implies risk of human injury, significant environmental pollution or very high economic or political consequences.
- **High**: For operating conditions where riser failure implies high risk of human injury, significant environmental pollution or very high economic or political consequences.

The safety class resistance factor γ_{SC} is obtained from the Table 5 (DNV-OS-F201, 2010).

Table 5. Safety class resistance factor

Safety class	Low	Normal	High
γ_{SC}	1.04	1.14	1.26

The material resistance factor γ_m depends of the limit state considered. The limit states are grouped into the following four categories by DNV-OS-F201 (2010):

- **Serviceability Limit State (SLS)**: requires that the riser must be able to remain in service and operate properly. This limit state corresponds to criteria limiting or governing the normal operation (functional use) of the riser.
- **Ultimate Limit State (ULS):** requires that the riser must remain intact and avoid rupture, but not necessary be able to operate. For operating condition this limit state corresponds to the maximum resistance to applied loads with 10-2 annual exceedence probability.
- **Accidental Limit State (ALS):** is a ULS due to accidental loads or infrequent loads.
- **Fatigue Limit State (FLS):** is an ultimate limit state from accumulated excessive fatigue crack growth or damage under cyclic loading.

Following the classification above, the material resistance factor is defined according to Table 6 (DNV-OS-F201, 2010).

Table 6. Material resistance factor

Limit State	ULS & ALS	SLS & FLS
γ_m	1.15	1.0

For the development of this example, the safety factors used were $\gamma_{SC} = 1.26$ and $\gamma_m = 1.15$, respectively.

Fig. 24 shows the utilization factors (UF) along the entire SCR. The values obtained using the Parametric Interpolation Method (PIM) are compared with those obtained using the full integration and the 100-year environmental contour method which is another design methodology included in DNV-OS-F201 (2010). The values

obtained with the environmental contour were multiplied by a factor of 1.15, since this is a common practice in engineering projects.

Note that the results obtained by the three methods are similar; however, the method of environmental contours presents considerable differences in the touchdown zone (TDZ), which is distant approximately 2800m from the top.

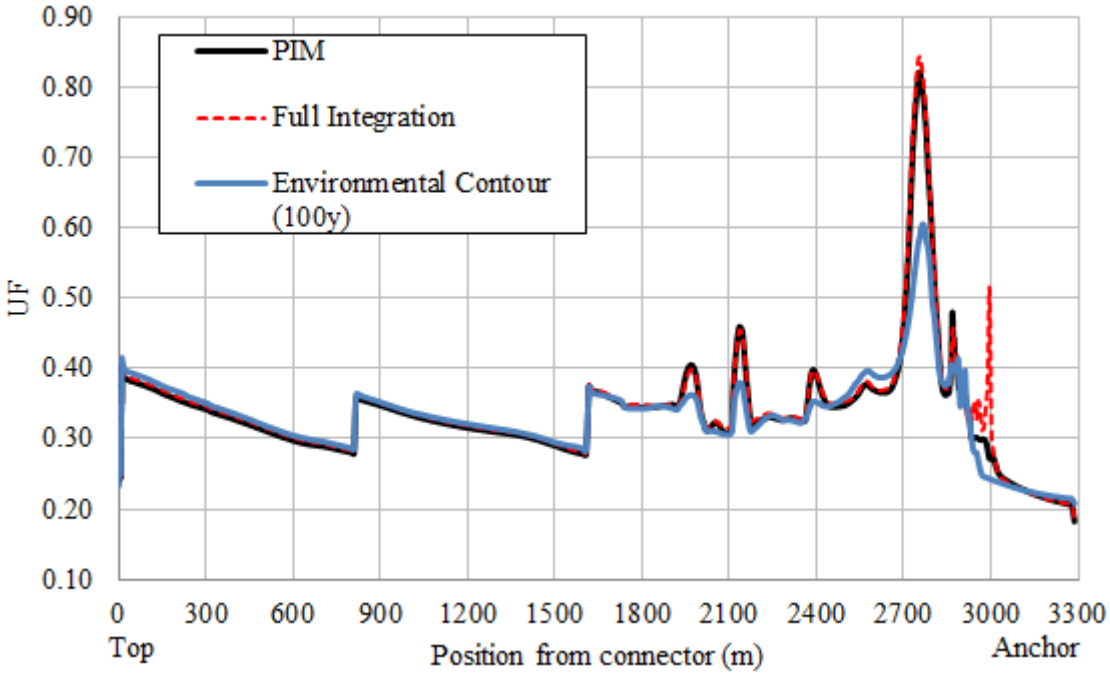

Figure 24. 100-yr utilization factor (UF) assessment along the SCR length.

In the analysis of the SCR long-term response it can be seen that the top region is characterized by presenting mild stress levels. Meanwhile, the suspended section is dominated by the axial tension and the stress behavior is almost linear. In contrast, the stresses along the TDZ are highly influenced by the bending, and soil-structure nonlinearities are significant in this region. Table 7 and Fig. 25 show the critical results for each one of these regions. Note that the proposed method presents good accuracy in all segments; meanwhile, the environmental contour method under predicts considerably the extreme response in the TDZ.

Table 7. Critical values of utilization factor (UF) obtained for each SCR segments and an assessment of the accuracy of methods.

	Full Int	PIM	Env. Contour	Position (m)	Full/PIM	Full/Contour
Stress Joint	0.40	0.39	0.41	11.00	1.01	0.98
Suspended	0.45	0.46	0.38	2134.86	0.99	1.20
Touch down zone	0.84	0.82	0.59	2755.01	1.03	1.44

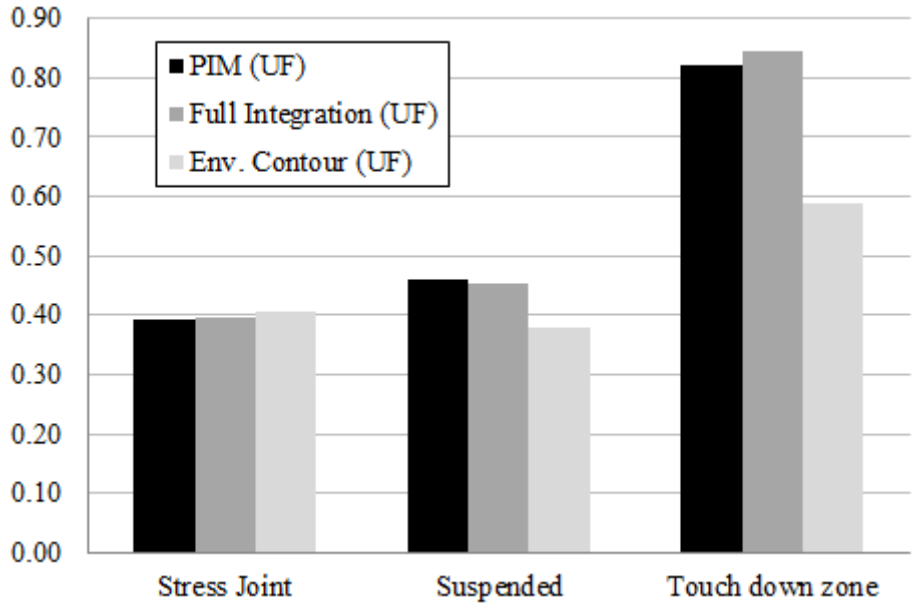

Figure 25. Critical values of utilization factor (UF) obtained for each SCR segment.

The critical element is the TDP, at position 2755.01m from connector where the UF was 0.84 by the full integration, 0.82 by the propossed method and 0.59 by the 100-yr environmental contour approach. For this critical point, four values of T_p (i.e. t_p=4.5s, t_p=9.5s, t_p=15.5s and t_p=21.5s) are selected to show a comparison between the statistical parameters obtained from the numerical simulations and those obtained by using the parametric interpolation (i.e. static mean, peaks mean, peaks standard deviation and number of peaks). Figs. 28 to 31 show this comparison for each of the four wave peak periods mentioned above. It must be noticed that the proposed interpolation equation fits quite well the behavior of the short-term statistical parameters. However, despite showing a clear constant trend, the number of peaks is the most difficult parameter to be predicted, mainly for the T_p=15.5s. However, the results are acceptable because the long-term average peaks frequency obtained by the interpolation method gave

practically the same value as that obtained by the complete integration, i.e. $\overline{\nu^{+}_{PIM}} = 0.13403$ and $\overline{\nu^{+}_{Full}} = 0.13165$, respectively.

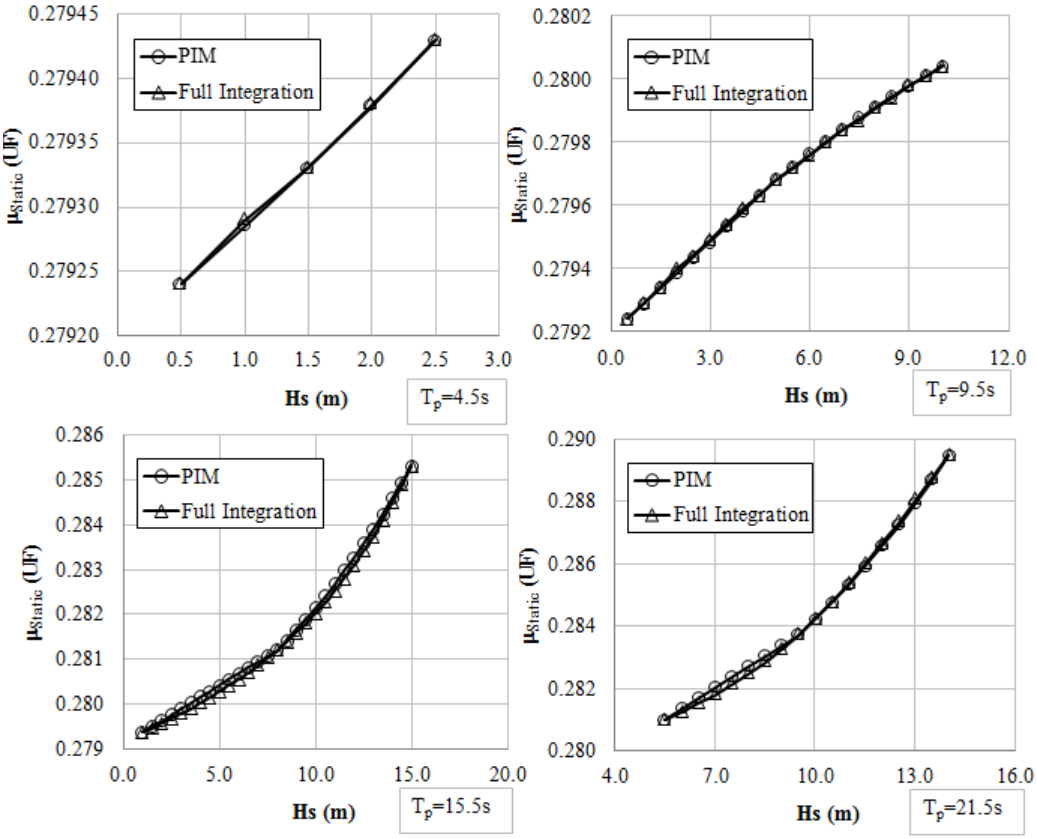

Figure 26. Behavior of the UF static mean in the critical riser point for different wave peak periods.

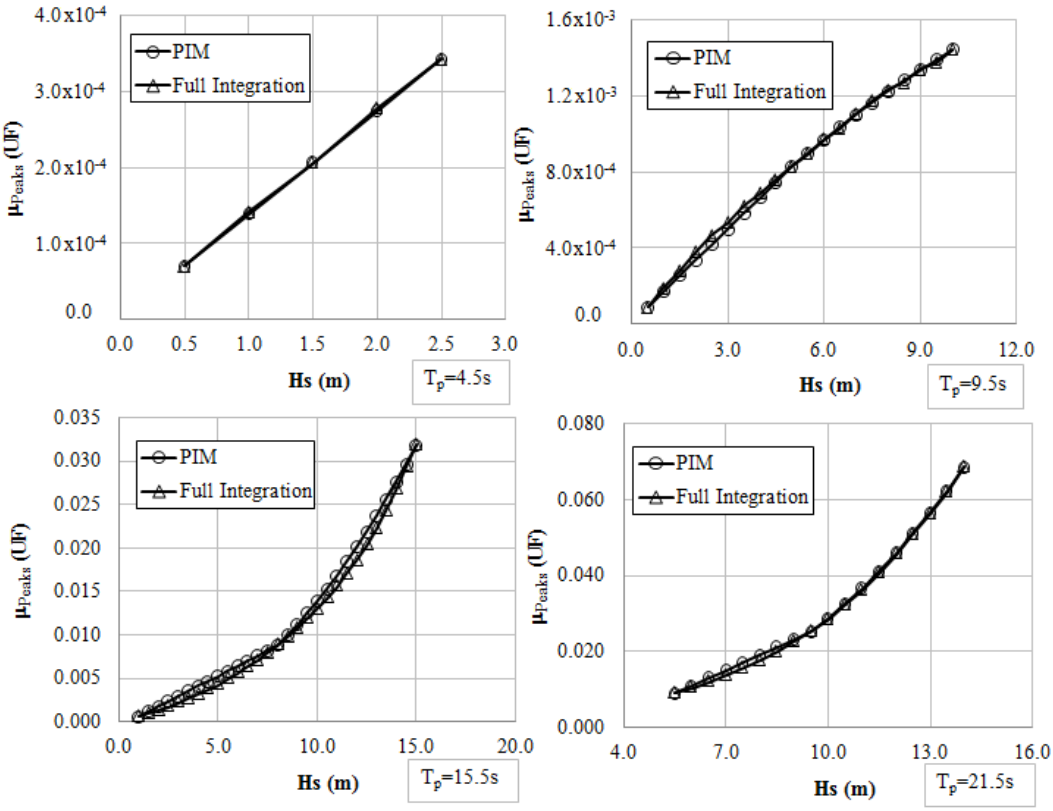

Figure 27. Behavior of the mean of UF peaks in the critical riser point for different wave peak periods

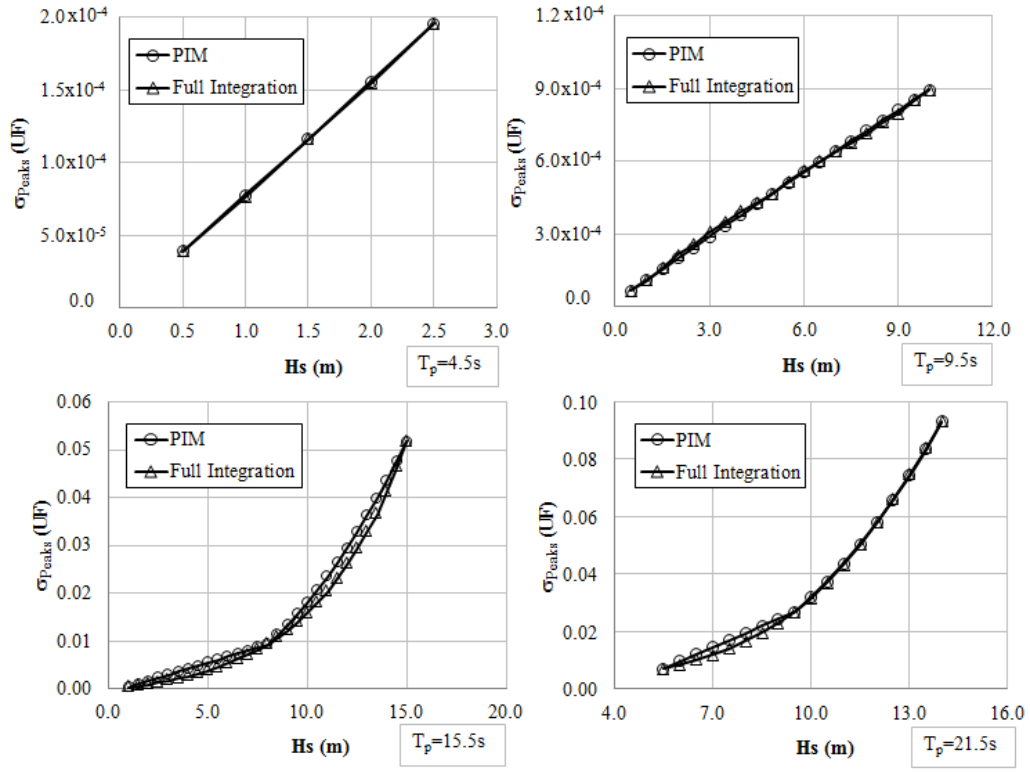

Figure 28. Behavior of the standard deviation of UF peaks in the critical riser point for different wave peak periods.

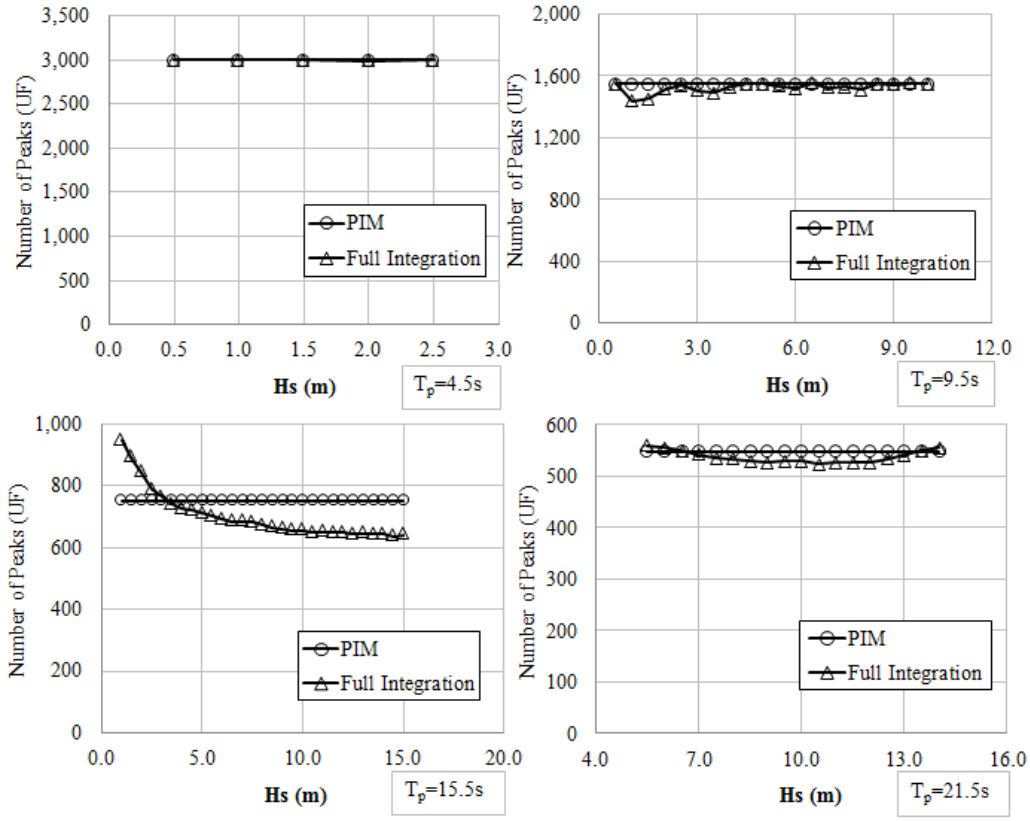

Figure 29. Behavior of the expected number of UF peaks in the critical riser point for different wave peak periods.

The statistical variables estimated by the PIM can be used to determine the Weibull scale, and shape parameters by using Eqs. (6.17) and (8.18), respectively. Then, the probability distribution function of short-term UF response peaks, adopted as the two-parameter Weibull distribution, can be fitted. Five sea states were selected in order to show the accuracy of the PIM when fitting the probability distribution function of short-term UF response. These values are shown in Fig. 30 in blue circles and are also specified in Table 8. Note that such sea states values are located between the three values used to calibrate the parametric equations for each T_p.

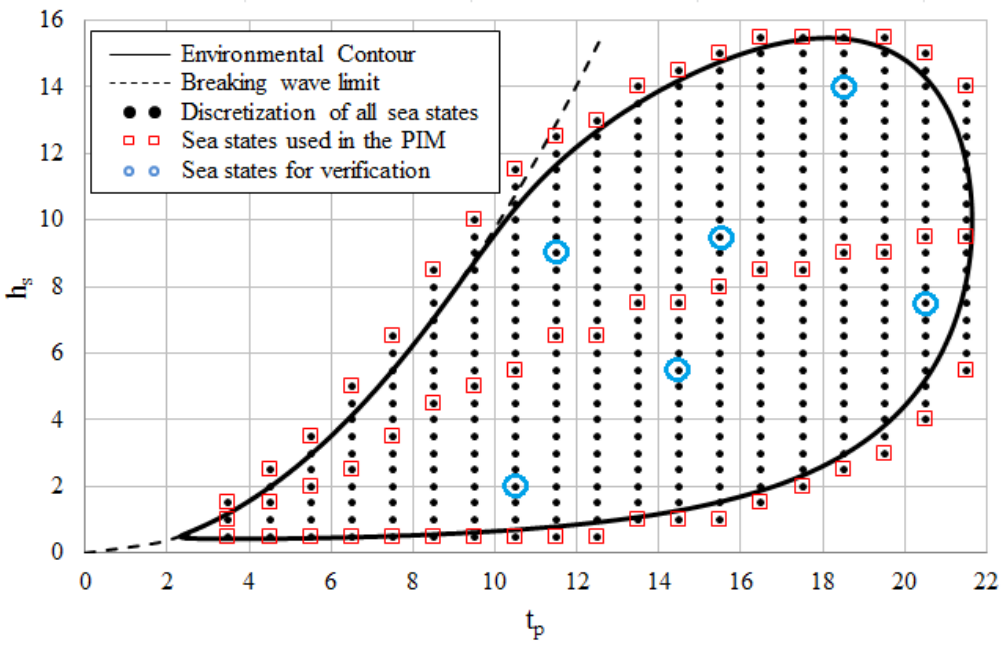

Figure 30. Sea states for verification of short-term peaks distributions obtained with the PIM.

Table 8. Sea states for verification of the short-term peaks distributions obtained with the PIM.

Hs(m)	2.0	9.0	5.5	14.0	7.5
Tp (s)	10.5	11.5	9.5	18.5	20.5

Fig. 31 shows the cumulative probability density function of short-term UF peaks for the critical element investigated, considering the short-term conditions indicated in Table 8. Note that the approximated distribution obtained by the PIM fits quite well the distribution fitted to the true data obtained from the numerical simulation time series.

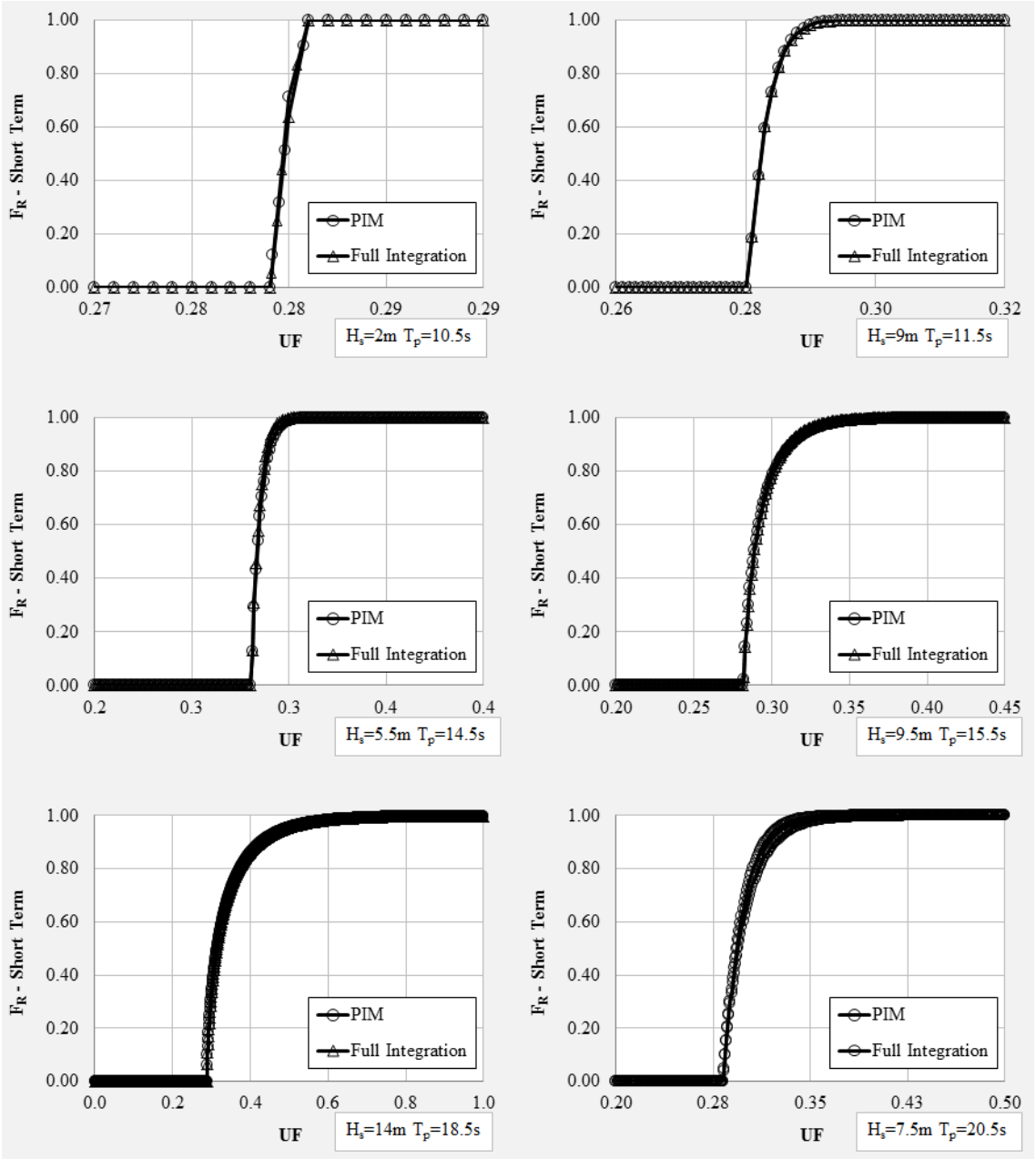

Figure 31. Short-term cumulative probability distribution of utilization ratio peaks

The long-term cumulative probability distribution of the utilization ratio peaks for the critical element identified (i.e., the TDP) was calculated with Eq. (6.1). This equation was computed using the statistical parameters directly from time domain simulations for each point in the integration mesh and also by using the parabolic interpolation method. These results are shown in Fig. 32. It must be noticed that the distribution predicted by using the PIM is in close agreement with that obtained using time domain simulations for each integration point. All the results commented above

just corroborate to show the accuracy of PIM in the estimation of the 100-yr utilization ratio presented in Table 7 and Fig. 25.

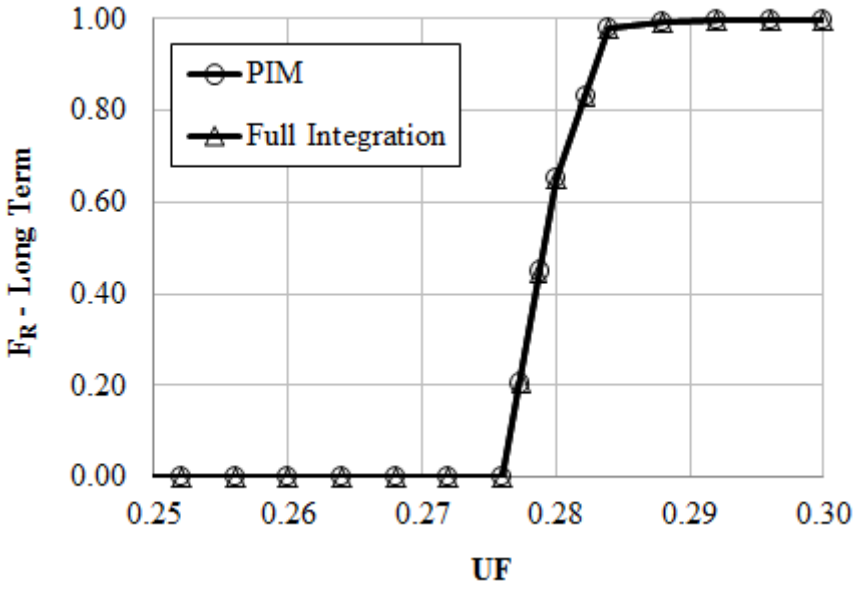

Figure 32. Long-term cumulative probability distribution of peaks

In terms of efficiency it is important to note that 392 simulations were used for the full integration method, and just 60 simulations were by the PIM, i.e., a computer cost saving of almost 85%. Considering that any riser simulation took almost 3-h to run in a modern desk computer, this means a huge effect on the computer demand for long-term analysis.

7.2.2 Probabilistic fatigue analysis

The fatigue damage evaluation was performed for the 8 external section points shown in Fig. 21 of each structural node of the finite element model. For this purpose, the Rainflow cycle counting method and the bi-linear DnV E SN curve with cathodic protection were used (DNV-RP-F204, 2010):

$$N(\bar{S}) = \begin{cases} 10^{11.61}\bar{S}^{-3} \text{ for } & \bar{S} > 74.13\,\text{MPa} \\ 10^{15.35}\bar{S}^{-5} \text{ for } & \bar{S} < 74.13\,\text{MPa} \end{cases} \tag{7.13}$$

Fig. 33 presents the envelope of the most critical fatigue life among the 8 external points for each cross section along the riser. The values obtained using the

Parametric Interpolation Method (PIM) are compared to those obtained with the direct integration approach. From these results it is possible to identify that for the most critical region, i.e. the TDP, the proposed method predict reasonable accurate results using just a few number of SCR numerical simulations.

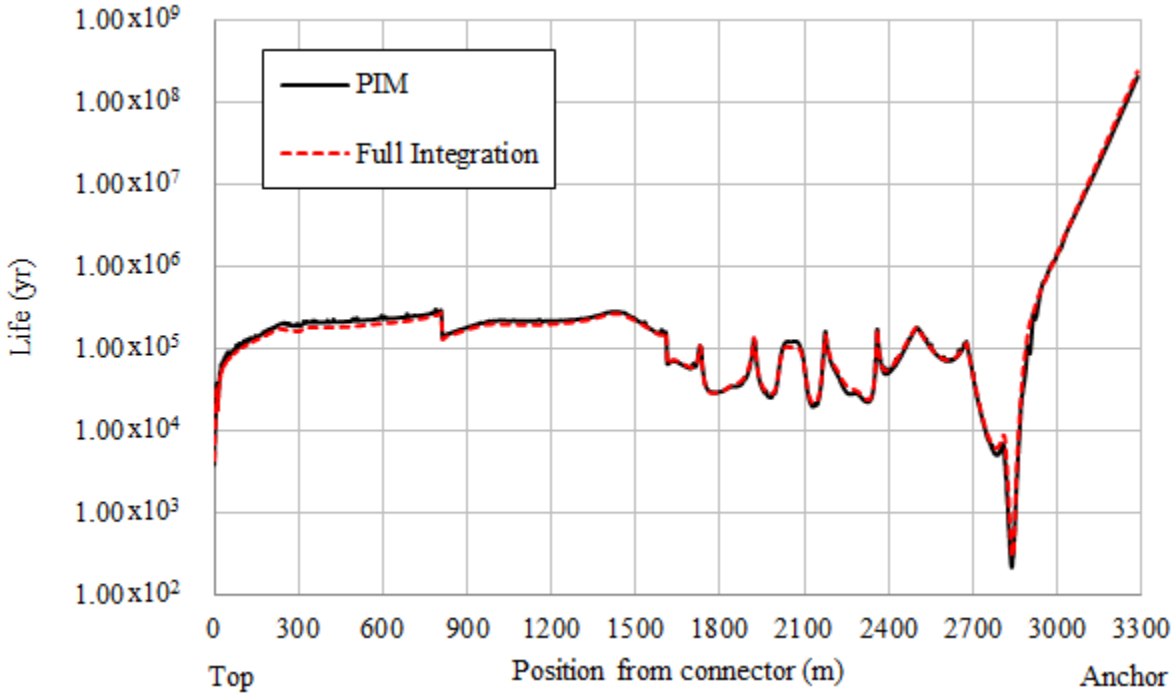

Figure 33. Fatigue life (FL) assessment along the SCR length.

Table 9 and Fig. 34 show the critical results of fatigue life in each riser segment. Note that the proposed method presents good accuracy in all segments but TDZ region. The results, although conservative, are less accurate for the TDZ because the stresses along of this region are highly influenced by bending and soil-structure nonlinear interaction.

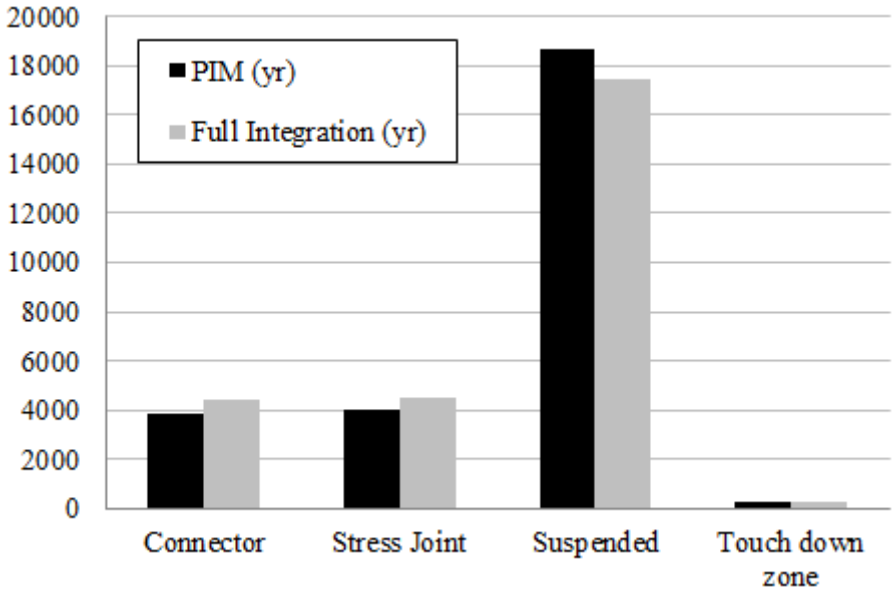

Figure 34. Critical values of fatigue life (FL) obtained for each SCR segments

Table 9. Critical values of fatigue life (FL) obtained for each SCR segments and accuracy

	PIM	**Full Int**	**Position**	**Full/PIM**
Connector	3883.48	4425.40	0.00	1.14
Stress Joint	3993.55	4535.10	0.05	1.14
Suspended	18672.14	17435.00	12.11	0.93
Touch down zone	239.39	293.68	2841.03	1.23

The critical element fatigue joint at TDZ is far 2841.03m from the connector. As shown in Table 9, its fatigue life was estimated as 293.68 yr by the full integration approach and 239.4yr by the proposed method. For this critical joint, the critical point of the cross section was the 5 (see Fig. 21). In order to verify the adopted premise of the exponential tendency of short-term fatigue damage for a given wave period, Figs. 37 to 39 present a comparison between the statistical short-term fatigue damage obtained from the numerical simulations and those obtained by using the parametric interpolation. All the peak periods used in the integration were included in this analysis. Note that all cases present a good fit with the predicted values showing a clear exponential behavior. However, quite small differences in some results led to conservative fatigue life estimation by PIM. Once more, it must be stressed that same riser numerical simulations used in the long-term extreme assessment were used to compute the fatigue life along the riser.

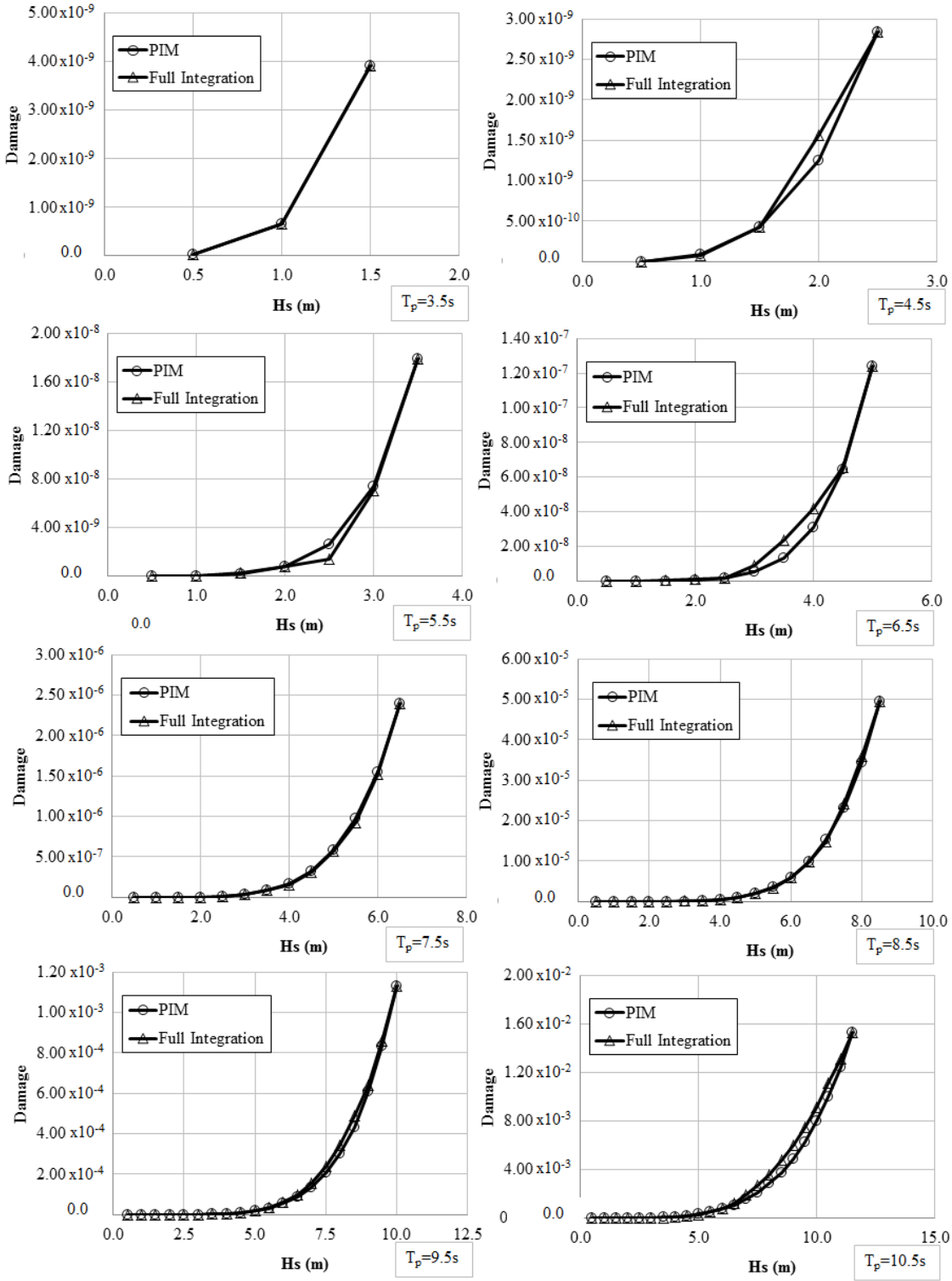

Figure 35. Behavior of the short-term fatigue damage in the critical riser point for different wave peak periods (1/3).

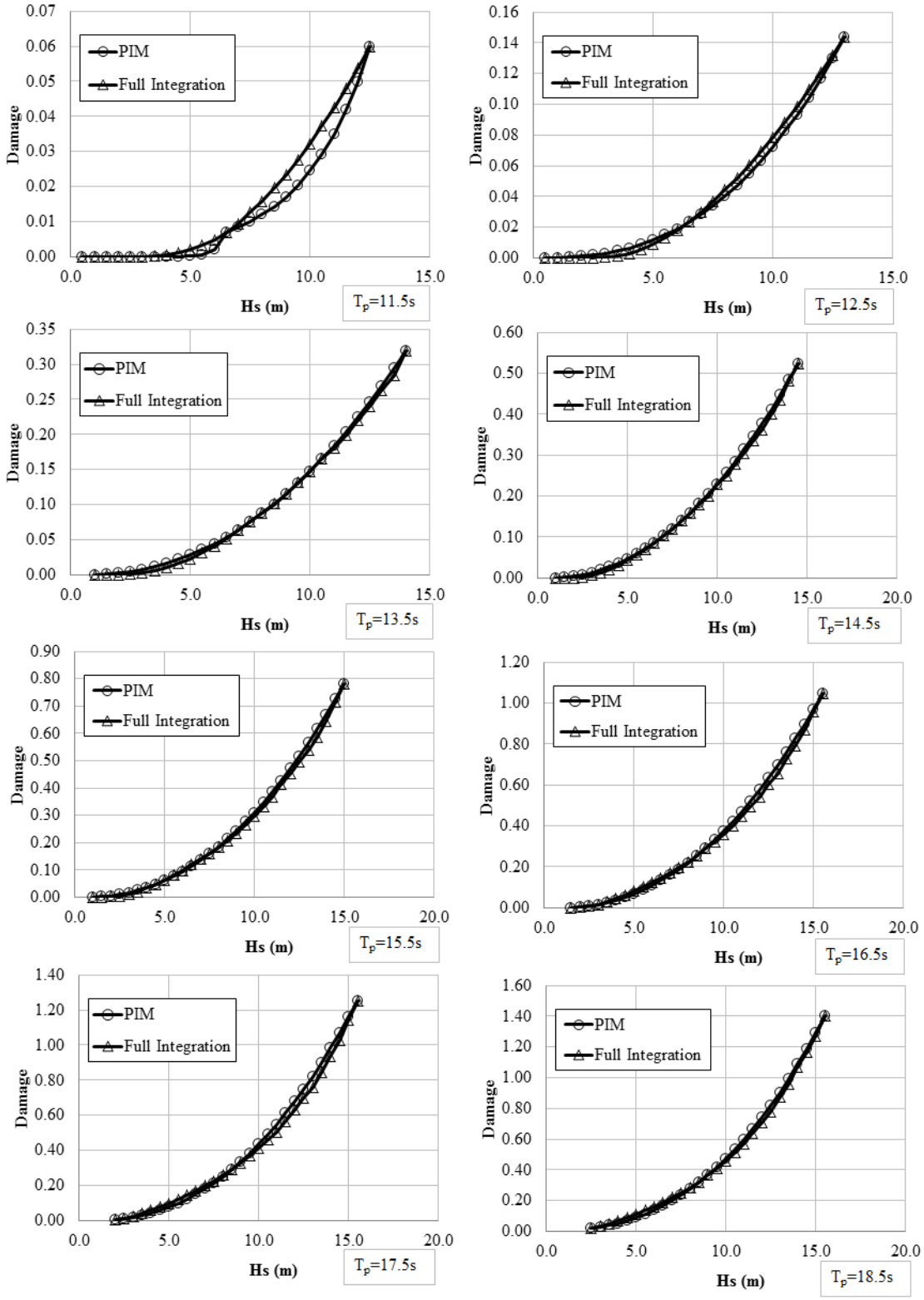

Figure 36. Behavior of the short-term fatigue damage in the critical riser point for different wave peak periods (2/3).

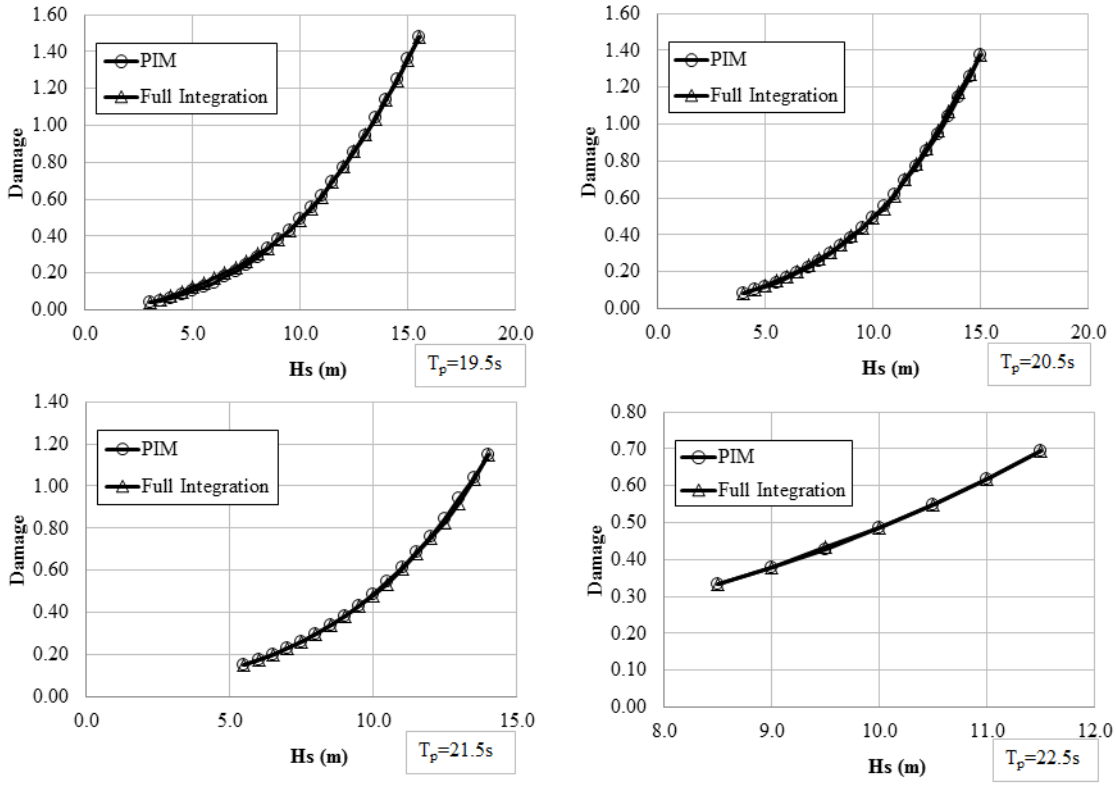

Figure 37. Behavior of the short-term fatigue damage in the critical riser point for different wave peak periods (3/3).

7.3 Example3: SLWR in deep water

In this last example, the Parametric Interpolation Method (PIM) is used in the estimation of the long-term extreme response and probabilistic fatigue for a 4373m long, oil production, Steel Lazy-Wave Riser (SLWR) connected to another FPSO in a water depth of 2200m.

As in the previous example, the elasticity modulus considered for the steel is 207 GPa and the specific weight is 77 kN/m^3. The FE mesh used in the model is shown in Table 10. The riser properties are shown in Table 11. The connection with the vessel is a flex-joint whose properties are shown in Table 12.

Table 10. FE Mesh for each SLWR segment

Seg.	Length (m)	Number of FE	First FE length (m)	Last FE length (m)	Element type
1	500	336	2	0.5	Bottom
2	500	922	0.5	0.5	Touch down zone
3	922	1216	0.5	0.5	Hog
4	700	1274	0.5	0.5	Sag
5	1536	818	0.5	2	Suspended
6	200	214	2	0.05	Suspended
7	10	219	0.05	0.05	Suspended
8	5	219	0.05	0.05	Stress Joint
9	-	-	-	-	Flex joint

Table 11. Riser properties for each SLWR segment

Seg.	OD (in)	ID (in)	Internal Fluid Density (kN/m^3)	Floater Weight (kN/m)	Floater Force (kN/m)	CM	CD
1	24	21	9.0	0.00	0.00	2.0	1.0
2	24	21	9.0	0.00	0.00	2.0	1.0
3	24	21	9.0	8.73	1.56	2.3	1.0
4	24	21	9.0	0.00	0.00	2.0	1.0
5	24	21	9.0	0.00	0.00	2.0	1.0
6	24	21	9.0	0.00	0.00	2.0	1.0
7	24	21	9.0	0.00	0.00	2.0	1.0
8	27.5	21	9.0	0.00	0.00	2.0	1.0

Table 12. Flex joint properties

Parameter	Value
Translational Stiffness (kN/m)	2.00x10^8
Torsional Stiffness (kN.m/deg)	2.00 x10^8
Bending Stiffness (kN.m/deg)	28.9

The first order vessel motions RAOs are shown in Fig. 38. The SLWR model is shown in Fig. 39. The wave loading and the triangular current velocity profile considered in this example are shown in Fig. 40. The riser and vessel azimuths, local and global coordinates and the RAO direction are shown in Fig. 41.

The current profile, the Hs-Tp joint probability function, the wave spectrum model, the number of wave components for the spectral decomposition and the duration of the stochastic time-domain riser analyses were taken the same as in the previous example.

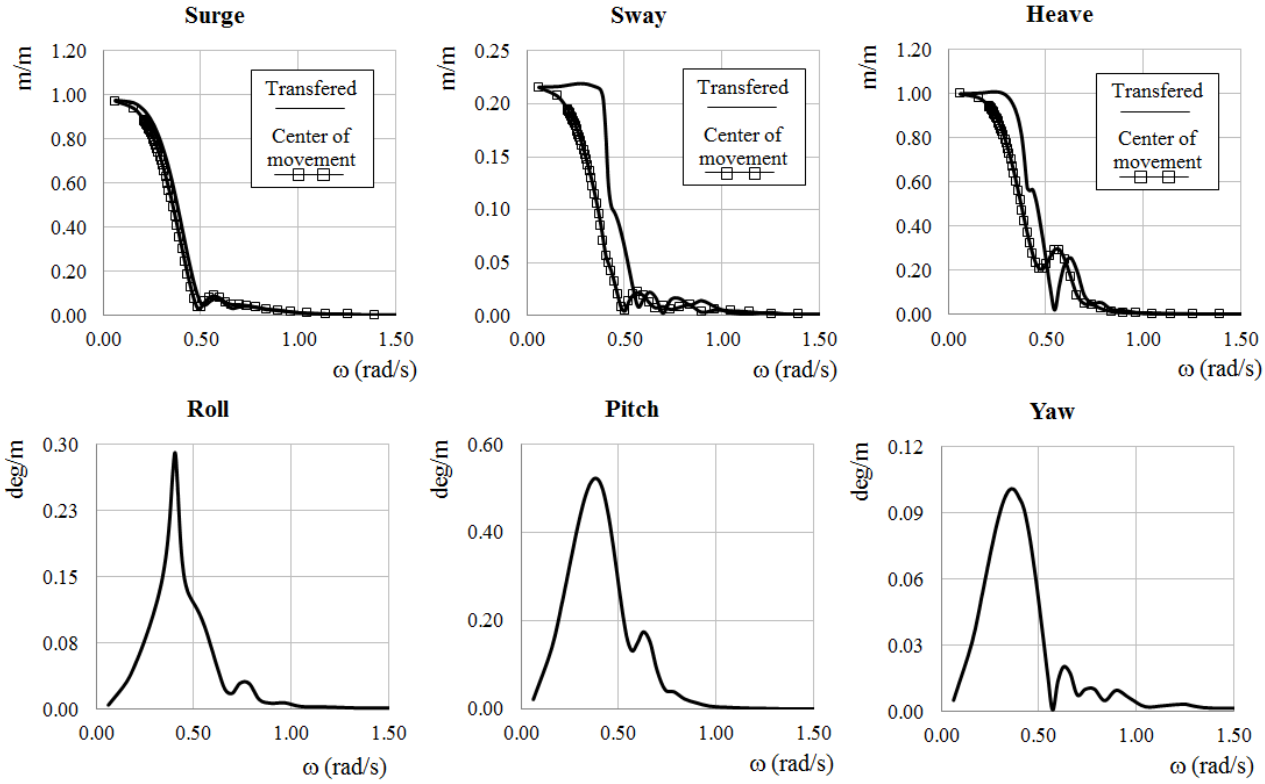

Figure 38. Translational and rotational vessel motions RAOs at the center of motion and at the riser top connection.

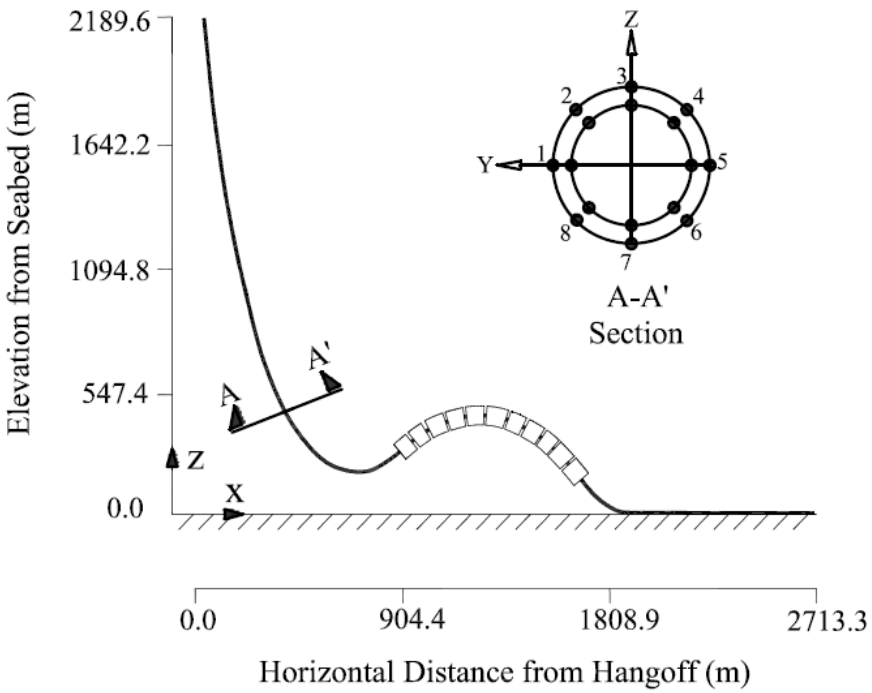

Figure 39. SLWR model.

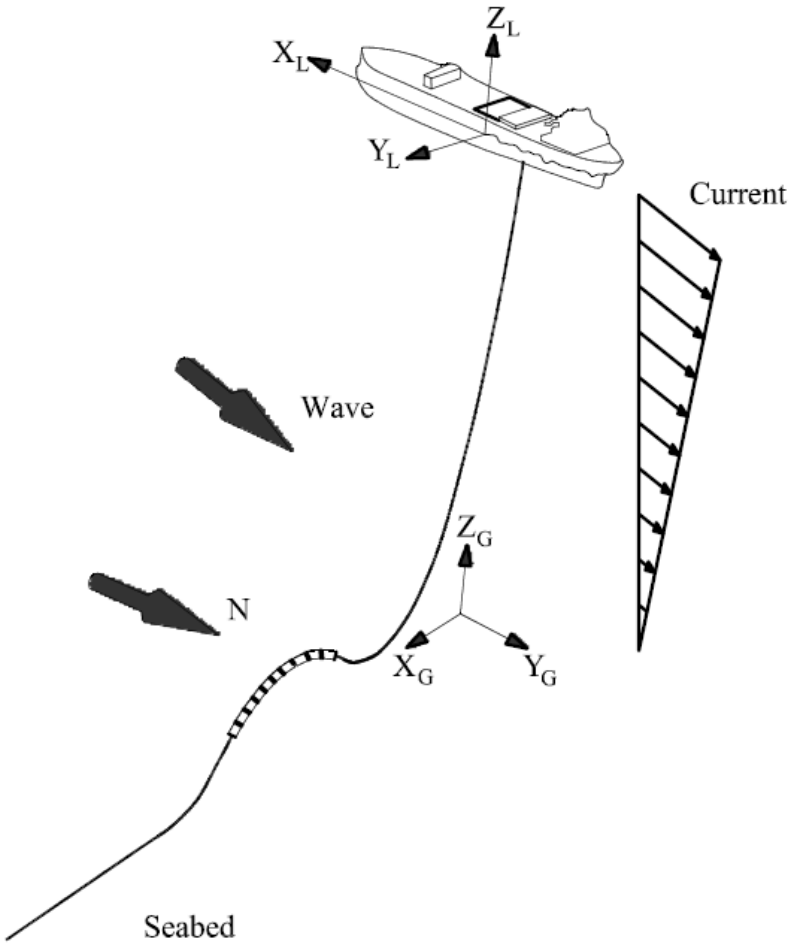

Figure 40. Environmental loading acting on the SLWR.

The structural behavior of the riser varies throughout its all length, for instance, the top region is characterized as the critical zone presenting larger stress levels. Meanwhile, the suspended section is dominated by the axial tension and the stress behavior is almost linear. The stresses along the hump are highly influenced by the bending and nonlinearities are significant in this region. In contrast, the stresses are extremely low for the riser segments from the TDZ to the anchor point.

For this analysis, as in the previous example the joint probability function of H_s and T_p is the same described in Eq. (7.7), the integration domain is the same specified in Fig.11 and the sea states used for full integration and PIM, are the specified in Fig.12.

7.3.1 Long-term extreme response

As in the previous example, the assessed response considered for the SLWR analyzed was the cross-section utilization factor (UF) considering the ultimate limit state (ULS); i.e. Eqs. (7.10) and (7.11).

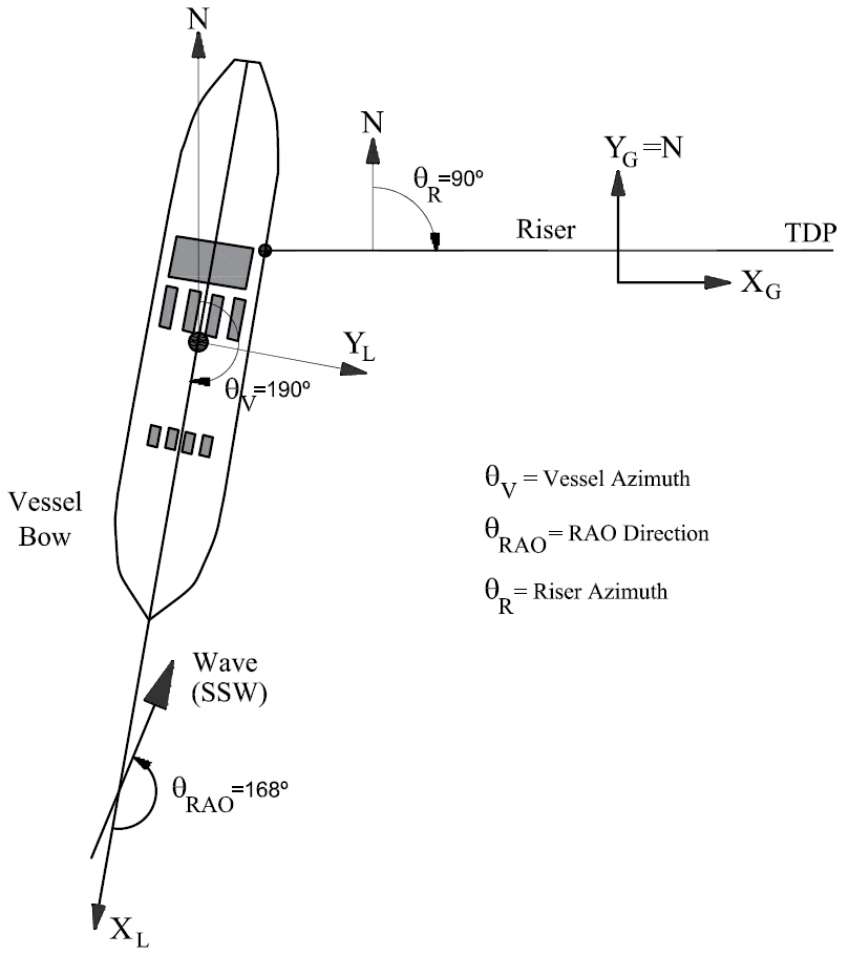

Figure 41. Riser and vessel azimuths, local and global coordinates and RAO direction.

Fig. 42 shows the result of the utilization factor (UF) obtained along the entire SLWR. Three methods are compared in this figure, the long-term full integration, the PIM and the 100-yr environmental contour method. As explained before, the results obtained by the environmental contour were multiplied by a factor of 1.15 looking for a better accuracy of this approach.

It is possible to note in Fig. 42 that the results obtained by the proposed method present a good accuracy along the entire structure when compared to the full integration approach. The results obtained by the environmental contour method present a good accuracy; however, some differences at the critical points of the hump are observed.

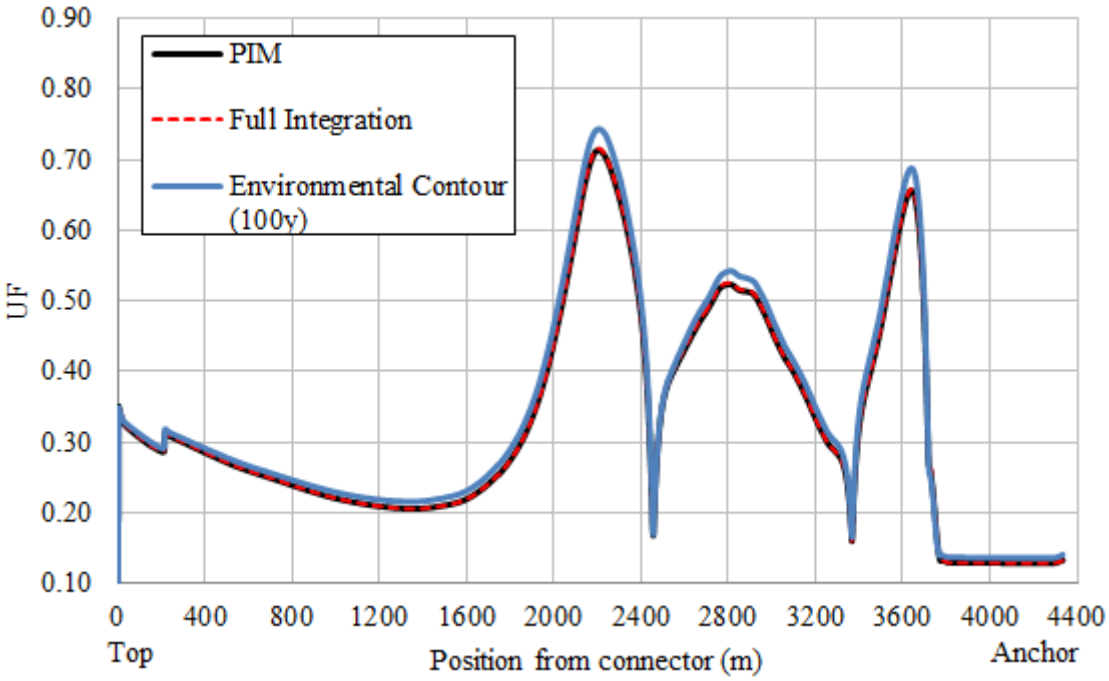

Figure 42. Cross-section utilization factor (UF) assessment along the SLW length.

Table 13 and Fig. 43 show the critical results for each one of the SLWR segments. Note that the proposed method presents good accuracy in all segments; meanwhile, the environmental contour method presents a slight difference for the sag and hog positions and even for points in the TDZ.

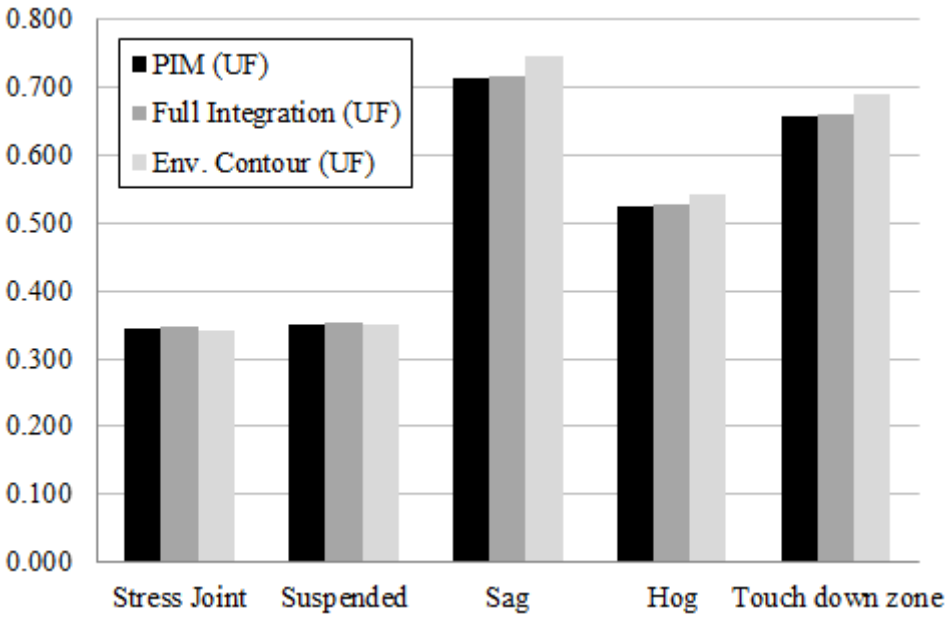

Figure 43. Critical values of cross-section utilization factor (UF) obtained for the SLWR segments.

Table 13. Critical values of cross-section utilization factor (UF) obtained for the SLWR segments, comparing the accuracy of the estimation methods.

Position	PIM	Full Int	Env. Contour	Position (m)	Full/PIM	Full/Contour
Stress Joint	0.344	0.346	0.342	5.0	1.01	1.01
Suspended	0.351	0.353	0.349	5.05	1.01	1.01
Sag	0.714	0.716	0.744	2205.0	1.00	0.96
Hog	0.524	0.526	0.542	2801.0	1.00	0.97
Touch down zone	0.657	0.658	0.688	3639.0	1.00	0.96

The critical element is in the sag point, at position 2205m from the connector. This region includes the initial part of the hump where the concavity is positive. The bending effects are extremely important in such riser region and affect directly the value of the utilization factor. As shown in Table 13, the UF obtained was 0.716 using the full integration methodology, 0.714 the proposed method and 0.744 by the 100-yr environmental contour approach. As in the previous example, for this critical point, four values of T_p (i.e. t_p=4.5s, t_p=9.5s, t_p=15.5s and t_p=21.5s) are selected to show a comparison between the statistical parameters obtained from the numerical simulations and those obtained by using the parametric interpolation (i.e. static mean, peaks mean, peaks standard deviation and number of peaks).

Figs. 46 to 49 show such comparison for each of the four peak periods. Note that for all the peak periods considered, all the statistical parameters present a good accuracy with those ones predicted by PIM. For T_p=4.5s and 15.5s the tendency of all statistical parameters follows a clear linear behavior. For T_p=9.5s the static mean presents a linear performance while the peak mean and the standard deviation presents a parabolic behavior. The UF static value is relatively high when compared to its dynamic variation for this riser point. In the case of the T_p=21.5s, the static mean and the peak mean presents a linear behavior while the standard deviation presents a parabolic tendency. The number of peaks has a clear constant trend for all the peak periods considered. The long-term average peaks frequency obtained by the interpolation method gave practically the same value that the obtained by the complete integration, i.e., $\overline{\nu^{+}_{\mathrm{PIM}}} = 0.10533$ and $\overline{\nu^{+}_{\mathrm{Full}}} = 0.10515$, respectively.

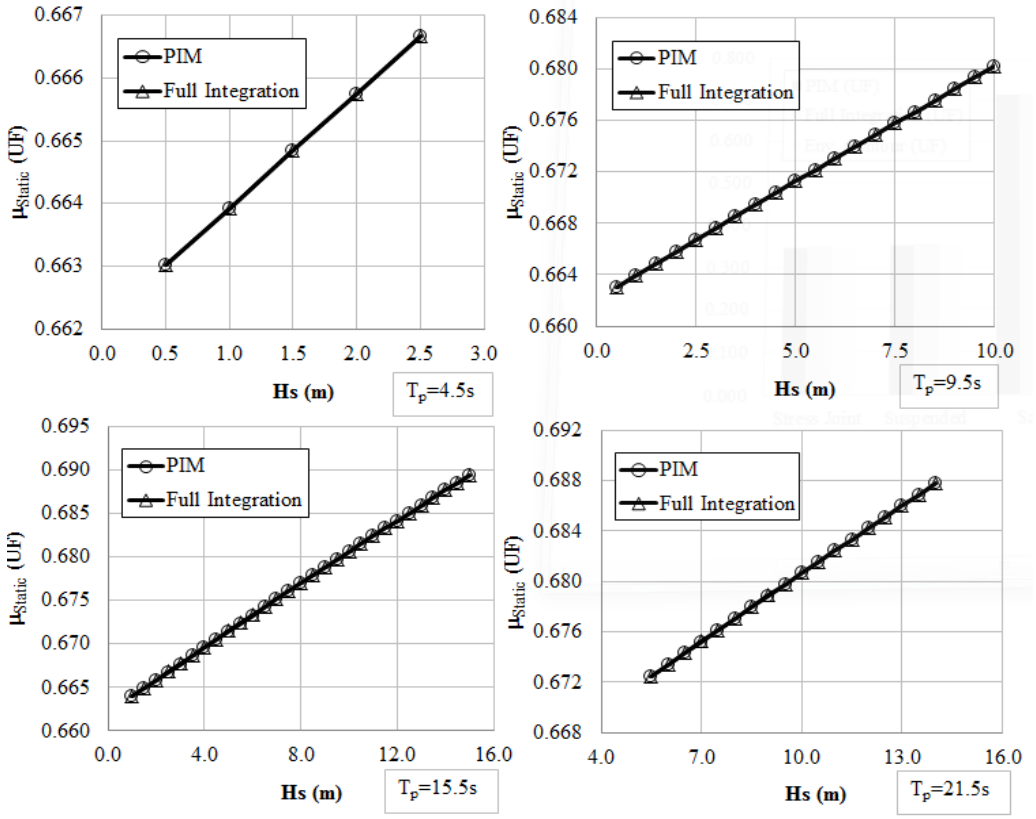

Figure 44. Behavior of the UF static mean in the critical riser point for different wave peak periods.

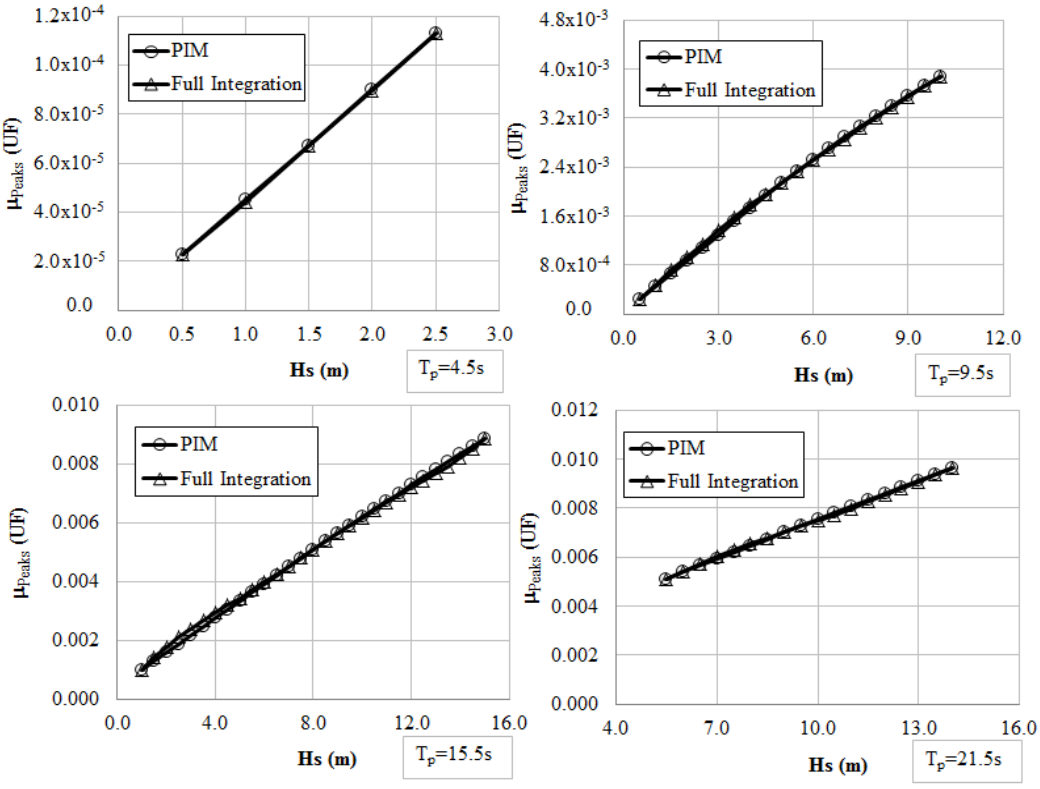

Figure 45. Behavior of the mean of UF peaks in the critical riser point for different wave peak periods.

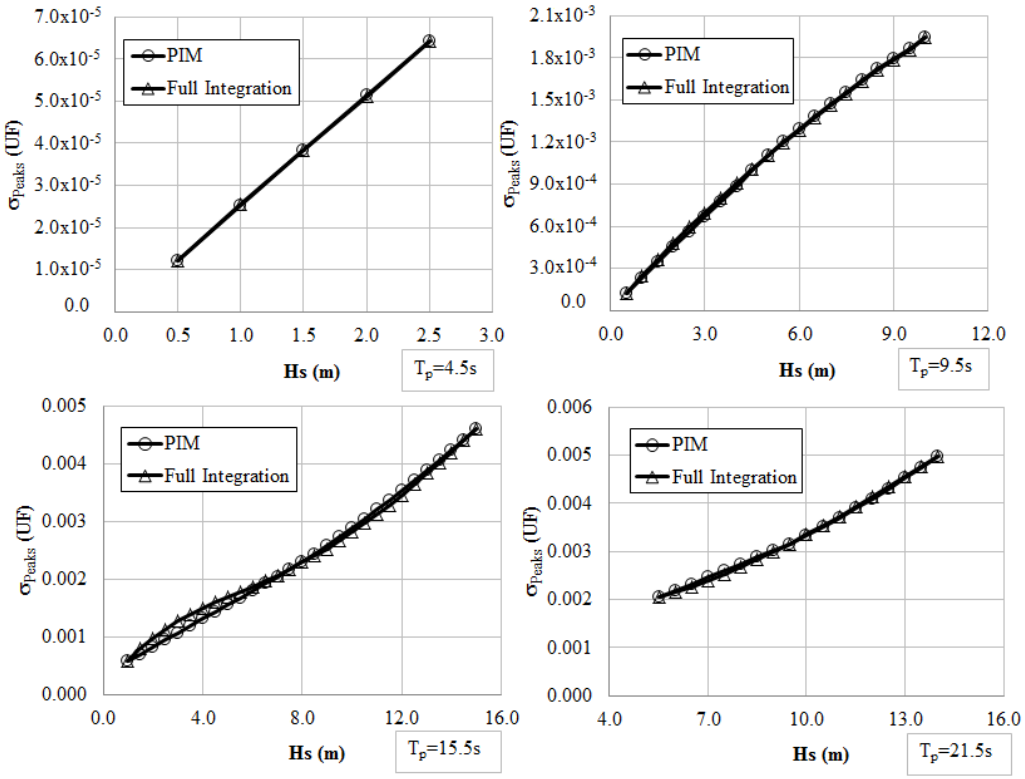

Figure 46. Behavior of the standard deviation of UF peaks in the critical riser point for different wave peak periods.

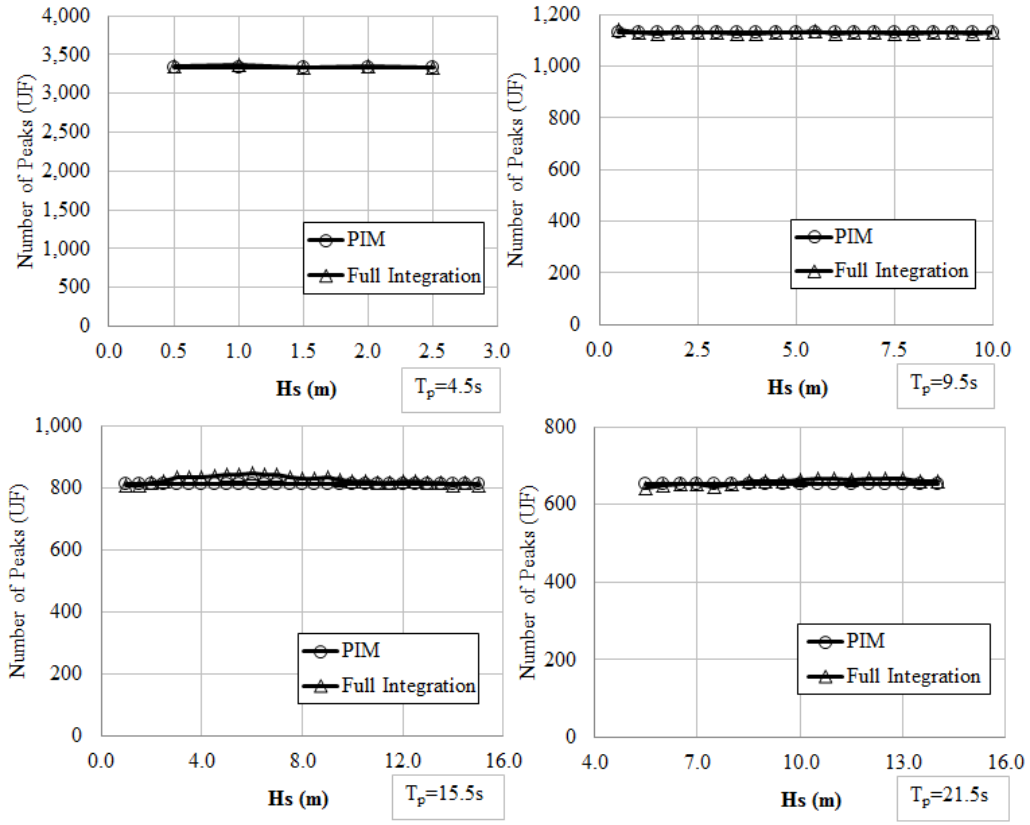

Figure 47. Behavior of the expected number of UF peaks in the critical riser point for different wave peak periods.

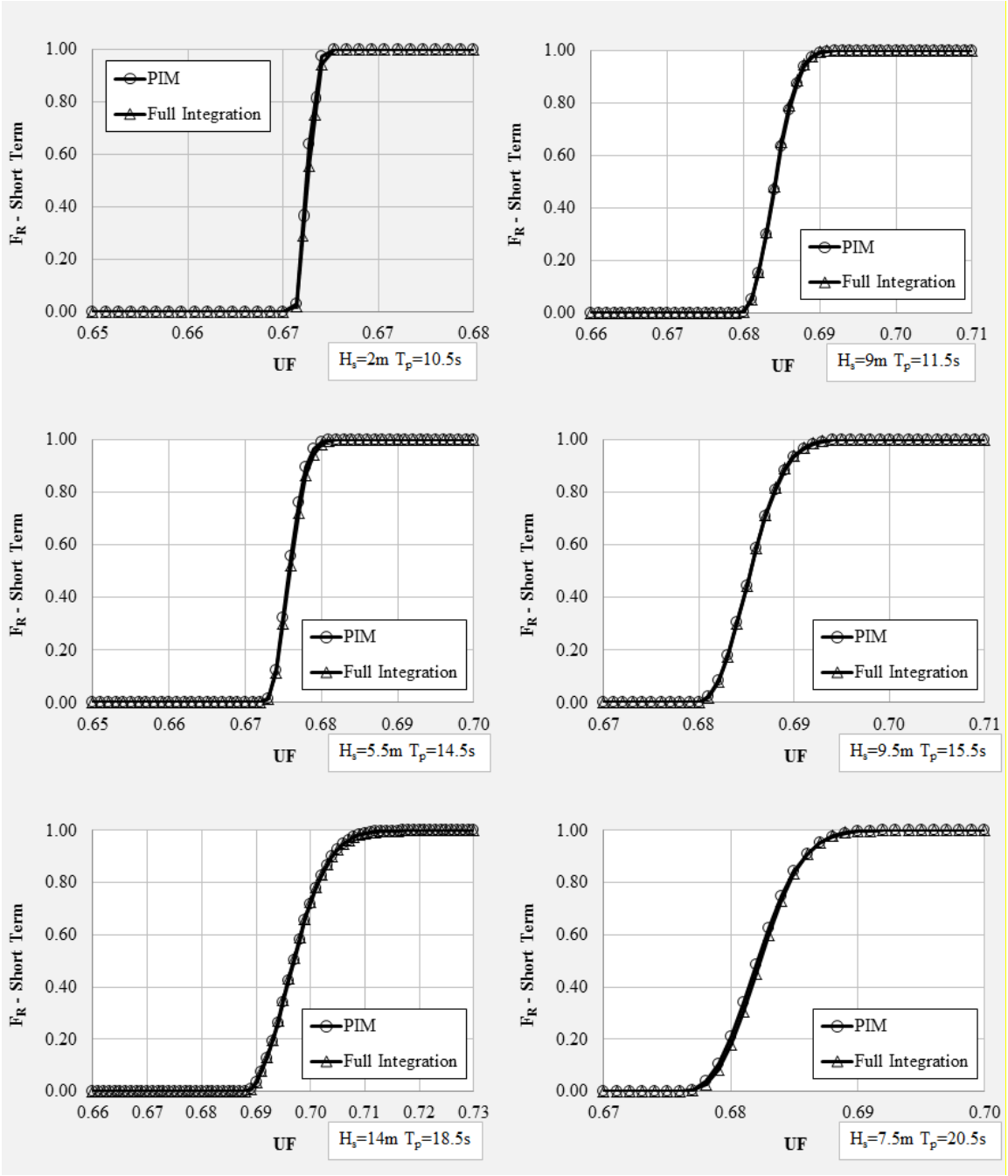

Figure 48. Short-term cumulative probability distribution of UF peaks for the most critical riser point.

In the same way as it was considered in the previous example, some specific sea states are used to show the accuracy of the proposed method when fitting the probability distribution function for the peaks of the short-term UF response. This sea states are the represented by blue circles in Fig. 30 and are indicated in Table 8. This probability distribution function is adopted as the two-parameter Weibull as in the previous example.

Fig. 48 shows the cumulative probability density function of short-term UF peaks for the critical riser point investigated for the sea states mentioned above. As it was expected, the approximated distribution obtained by the proposed method fits quite well with that obtained from numerical simulations.

The long-term cumulative probability distribution of UF peaks for the critical element identified is shown in Fig. 49. As it was expected, the distribution predicted by the proposed method fits well with the distribution calculated with the statistical parameters obtained directly from the numerical simulations associated to each integration mesh point.

Again, very accurate results are obtained using just 15% of the numerical simulations required for the full integration approach.

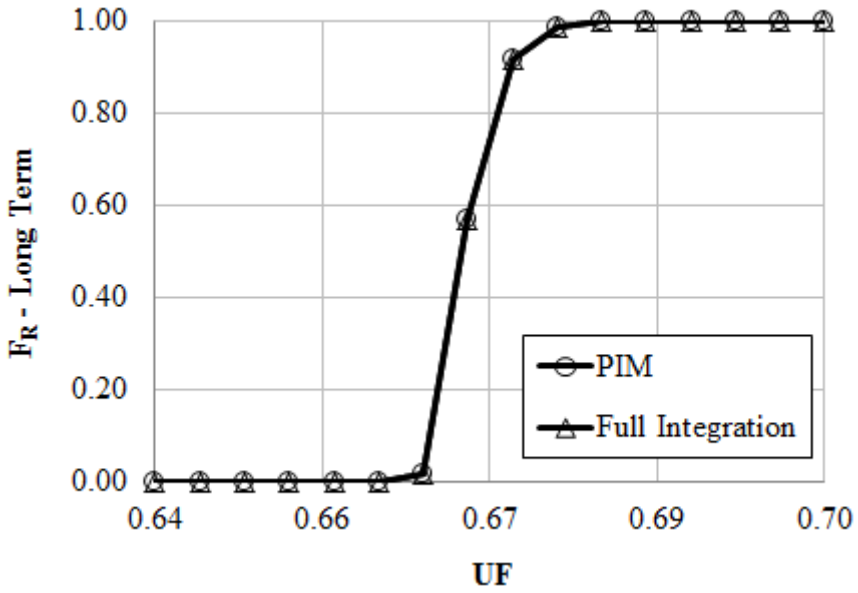

Figure 49. Long-term cumulative probability distribution of UF peaks for the most critical riser point.

7.3.2 Probabilistic fatigue analysis

In the same way that the SCR was analyzed, the 8 external section points shown in Fig. 39 of each structural SLWR node were considered. Likewise, the Rainflow cycle counting method and the bi-linear DnV E SN described in Eq. (7.13) were used for fatigue calculation.

Fig. 50 presents the envelope of the most critical fatigue life among the 8 external points for each cross section along the entire riser. The values obtained using the Parametric Interpolation Method (PIM) are compared to those obtained with the direct integration approach.

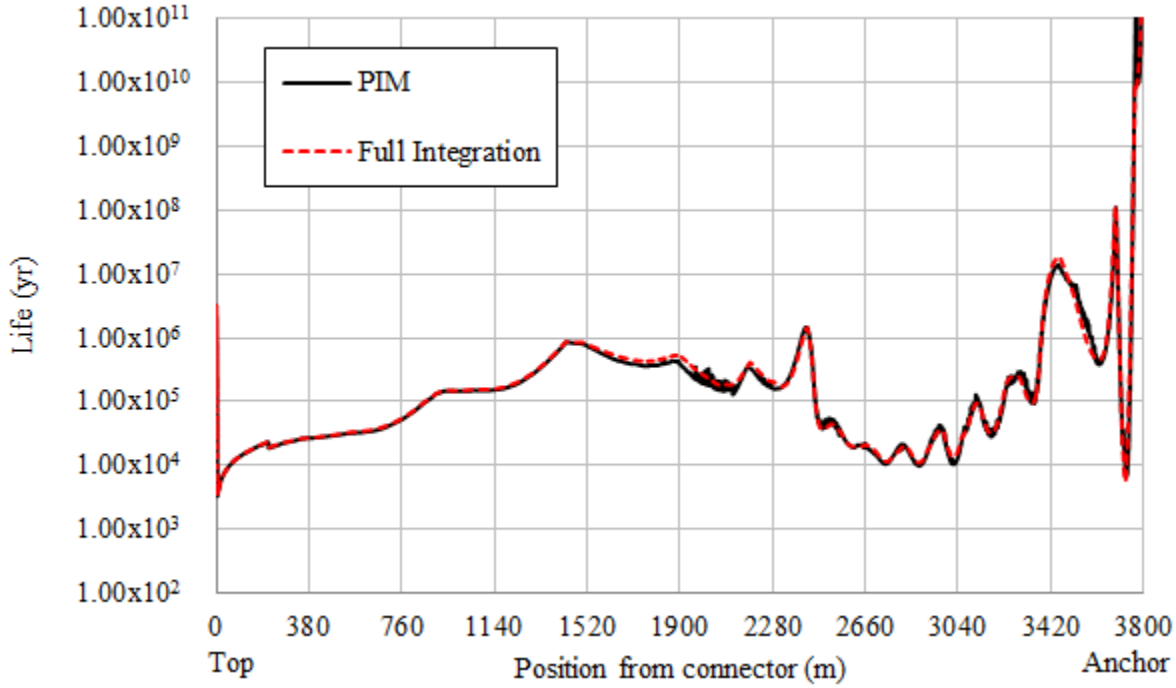

Figure 50. Fatigue life (FL) assessment along the SLWR length.

Table 14 and Fig. 51 show the critical results of fatigue life in each riser regions. Comparing all these results mentioned above, it is possible to observe that the proposed method presents good accuracy in all segments, mainly for those points with lower fatigue life. In the sag and TDZ regions the results are a little bit less accurate due to the distortion of the results generated by the important effects of bending and structural nonlinearities.

Table 14. Critical values of fatigue life (FL) obtained for each SLWR segment and the corresponding PIM accuracy.

Riser location	PIM	Full Int	Position	Full/PIM
Stress Joint	3274.59	3487.30	5.00	1.06
Suspended	3373.04	3551.00	5.45	1.05
Sag	176675.96	152400.00	2451.00	0.86
Hog	9777.90	10986.00	2880.50	1.12
Touch down zone	6768.56	5536.80	3725.00	0.82

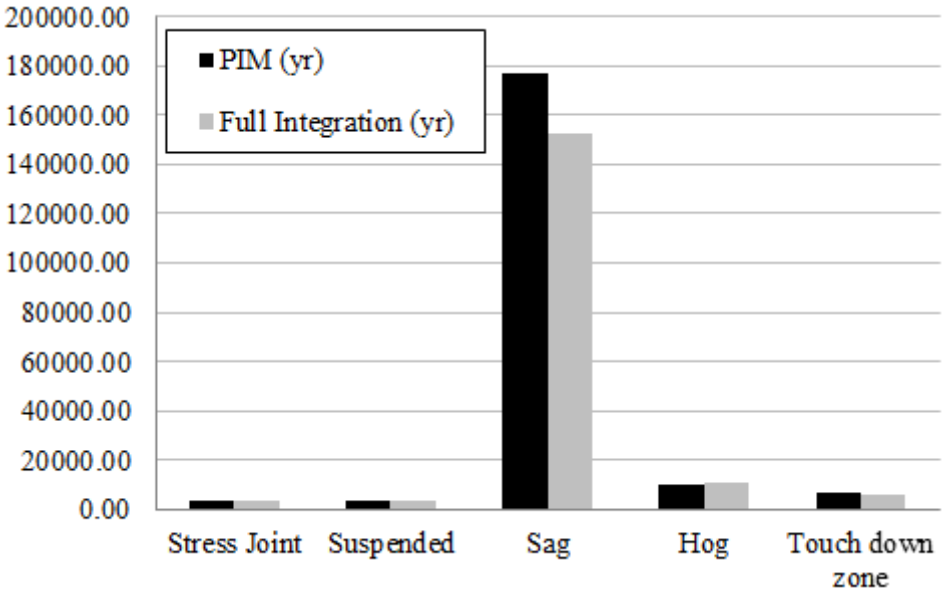

Figure 51. Critical values of fatigue life (FL) obtained for each SLWR segments

The critical riser point for fatigue is located in the stress joint, at position 5.0m from the connector. At this point the estimated fatigue life was 3487.3 yr by the full integration approach and 3274.6 yr by the proposed method. In this location the point 5 (see Fig. 39) on the riser cross section is the most critical. Figs. 54 to 56 present a comparison between the statistical short-term fatigue damages obtained from the numerical simulations and those obtained by using the proposed method. Note that all cases present a good fit showing a clear exponential behavior and a good performance of the interpolation scheme.

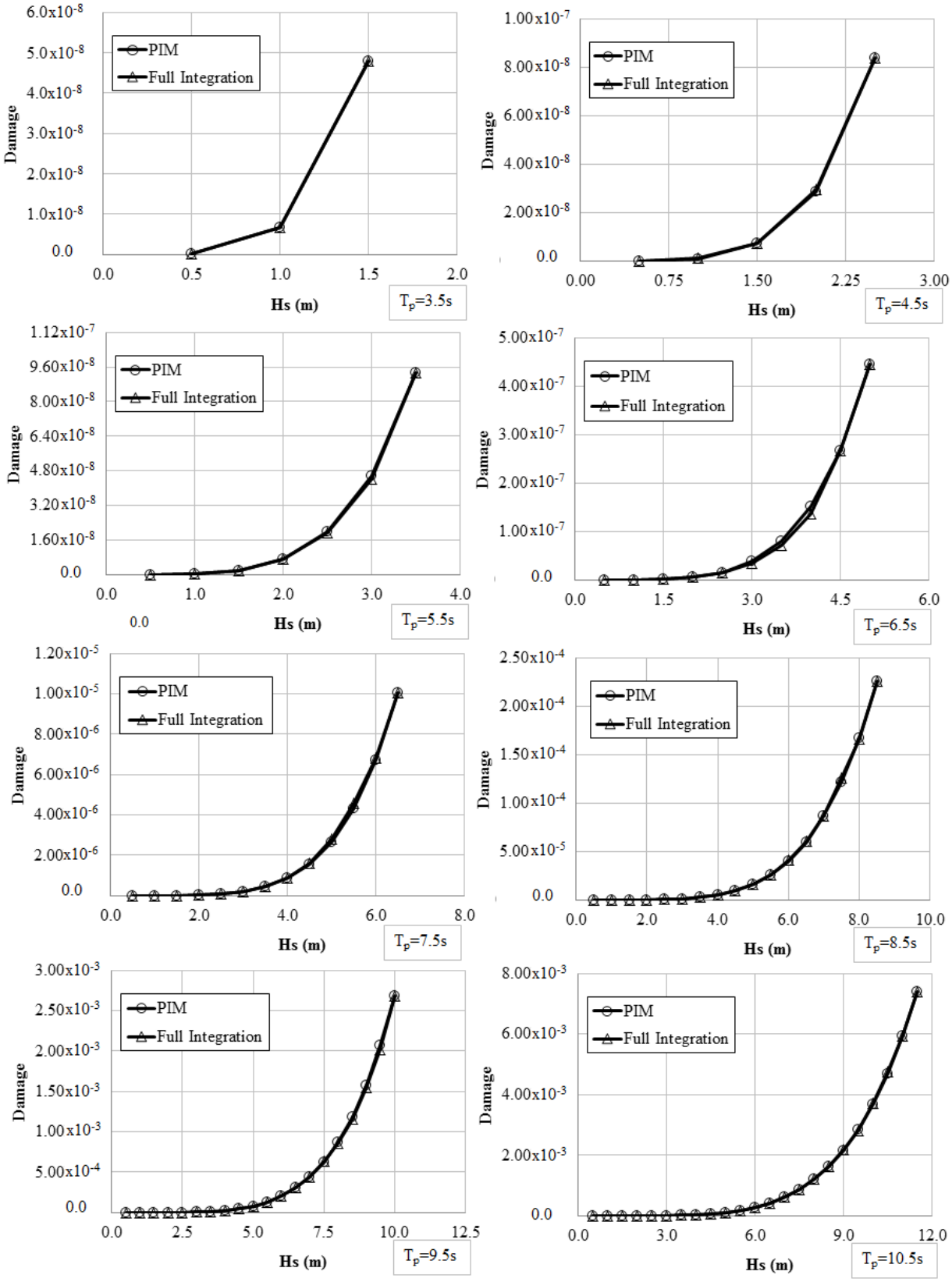

Figure 52. Behavior of the short-term fatigue damage in the critical riser point for different wave peak periods (1/3).

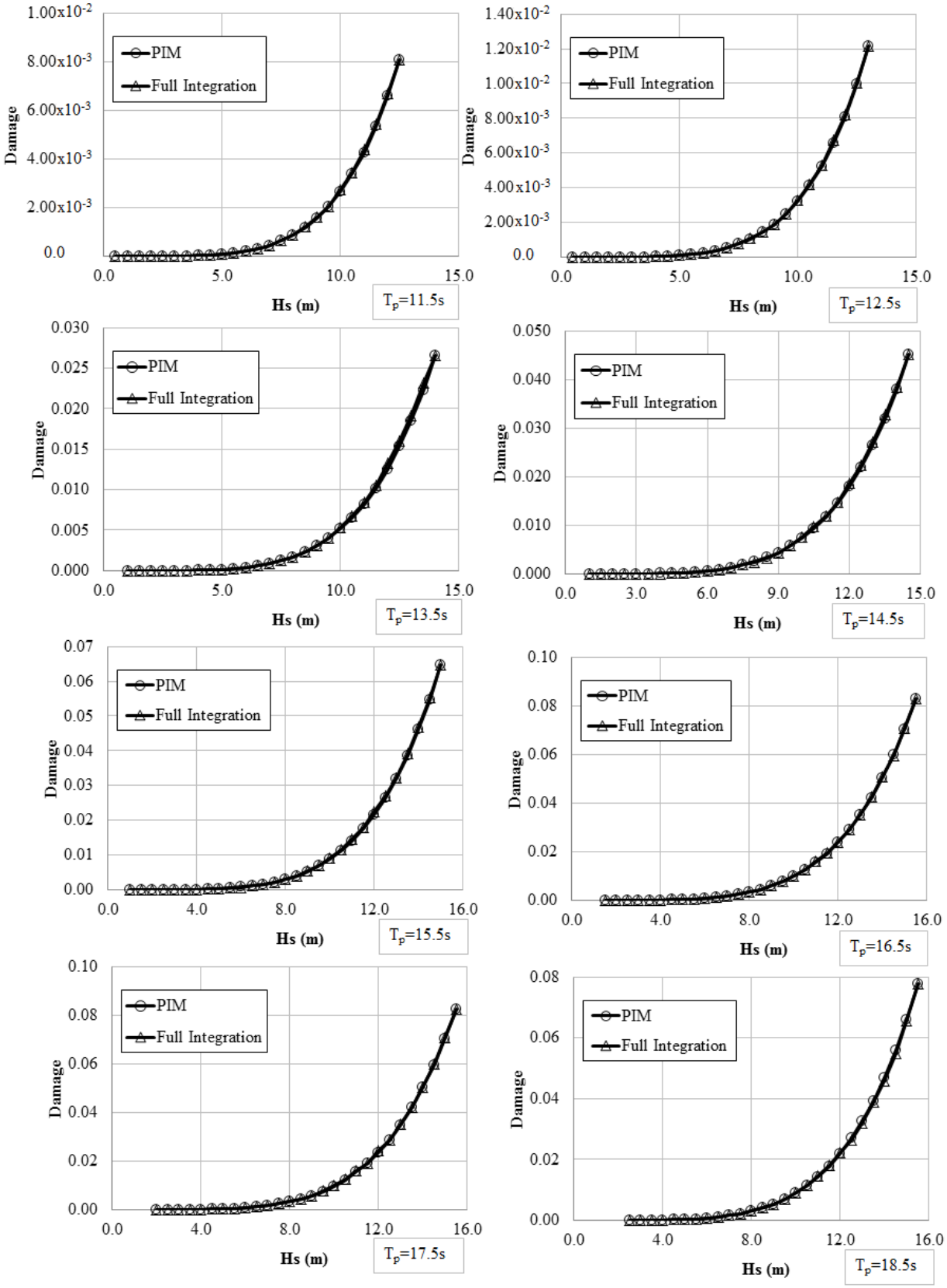

Figure 53. Behavior of the short-term fatigue damage in the critical riser point for different wave peak periods (2/3).

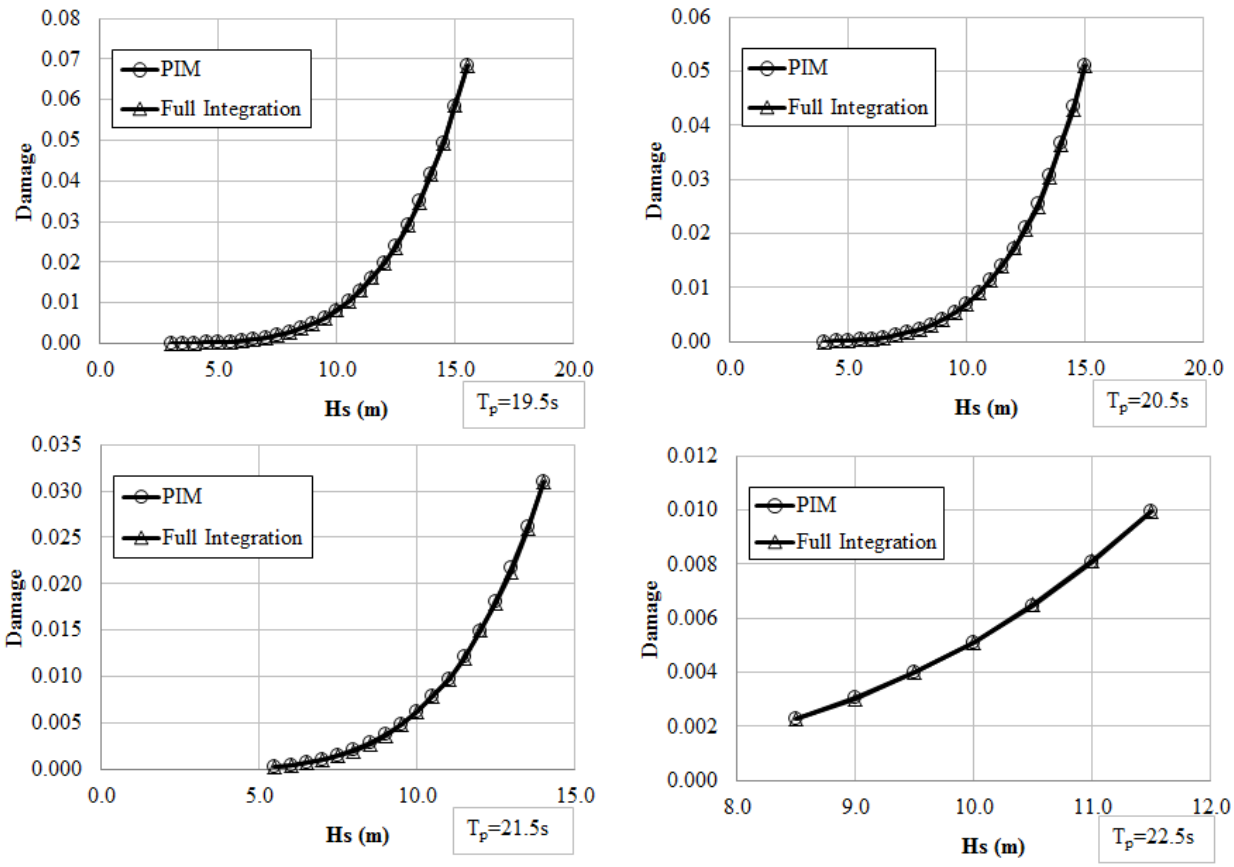

Figure 54. Behavior of the short-term fatigue damage in the critical riser point for different wave peak periods (3/3).

7.4 General comments

In this chapter, three practical examples were studied in which the proposed methodology, the so-called Parabolic Interpolation Method, was applied.

In the first example, we analyzed a linear model of a single degree of freedom in which the response was obtained by crossing a theoretical RAO with the wave spectrum; besides, the environmental load was assumed Gaussian and narrow banded. The results showed a good performance of the proposed method offering good accuracy and reducing considerably the number of dynamic analyzes.

In the second and third example, a SCR and a SLWR were analyzed respectively. Both structures were modeled in finite elements and dynamic analyzes were performed in the time domain. The Parametric Interpolation Method was used to determine both the long-term extreme response and fatigue life along the entire

structures. The results were good, showing acceptable approximations when compared with the complete integrations.

Again, as an overall observation, it must be emphasized that the fatigue analysis used the same numerical simulations defined for the extreme response estimation and the computer cost saving of proposed approach is approximately 85% when compared to full integration approach.

Chapter 8

Conclusions and recommendations for further studies

8.1 Conclusions

Extreme response assessment and fatigue damage analysis are the main design criteria in the everyday design practice of marine structures. Although some structures which have a linear behavior can be analyzed in a simplified way by analytical methodologies or by means of frequency domain procedures, the slender structures such as risers and mooring lines are sensitive to non-linear effects and require more judicious numerical dynamic evaluations.

Regarding the extreme response assessment of metallic risers, this evaluation in the design phase is usually performed by means of some simplified procedure such as the environmental contour method; however, the long-term extreme response method is the recommended methodology for this purpose. In a similar way, the fatigue assessment for such structures requires a long-term methodology. So, both design verifications require a huge number of short-term numerical evaluations of the structure in order to carry out the multi-dimensional integrals related to such calculations. This large number of numerical analyzes represent a high computational cost regarding to processing and data storage.

Aiming at improving the computational efficiency in the long-term extreme response and fatigue damage analysis of metallic risers used in deep and ultra-deep water oil fields, some efficient integration method is urgently required. This work proposed the Parametric Interpolation Method (PIM) for this purpose. This methodology uses a surrogate interpolation scheme which predicts short-term responses, i.e., fatigue damage and the statistical parameters of response peaks. Besides, the numerical simulation needed to calibrate the interpolation equations are used for both long-term response analysis and probabilistic fatigue analysis, so that both analyses can be performed in an integrated form.

Given the possible dynamic response dependency on the wave period, a parametric equation is defined for any wave period (zero-up crossing or peak period) used in the wave parameters integration mesh. For each period, just three numerical simulations are needed. Then, for a given wave direction the total number of numerical simulations required is 3 x NT_z, where NT_z is the number of T_z points needed to cover the integration domain region which is important in the analysis (identified in this work as the 10.000-yr environmental contour).

The Parametric Interpolation Method (PIM) keeps an optimal level of accuracy and needs much less numerical simulations when compared to the long-term integrations used in both the long-term extreme response and fatigue damage analyses. For the risers analyzed in this work, very small errors were identified when the results of the present approach were compared to full integration results. Moreover, these results were obtained using just 15% of the numerical simulations required by the full integration approach.

Based on the results presented in this work, it is concluded that PIM is a promising alternative for more efficient and accurate long-term extreme responses and probabilistic fatigue assessment of metallic risers, at least for early design stages.

8.2 Recommendations for Further Studies

There many research works that can be conducted as a sequence of the present work. Among others, the following ones can be cited:

- Develop an improved method to discretize the wave zero up-crossing period T_z by studying the behavior of short-term response variables (i.e. fatigue damage, static mean, peak mean, standard deviation and number of peaks) fixing H_s and varying T_z and considering the participation of each H_s-T_z pair on the response;
- Implement the Parametric Interpolation Method (PIM) for determining the fatigue damage and the long-term extreme values of traction and radius of curvature for flexible risers;
- Implement the Parametric Interpolation Method (PIM) for determining the long-term response and fatigue damage of other marine structures such as mooring lines, jumpers, wellhead structure, among others.

Bibliography

ANG, A. H-S., and TANG, W. H., 1984. *Probability concepts in engineering planning and design, Volume II Decision, risk, and reliability.* JOHN WILEY & SONS. United States.

ARIDURU S., 2004, *Fatigue Life Calculation by Rainflow Cycle Counting Method*, M.Sc. Thesis, The Graduate School of Natural and Applied Sciences, Middle East Technical University, Ankara, Turkey.

ASTM E-1049, *Standard Practices for Cycle Counting in Fatigue Analysis*, United States, 2005

BAARHOLM, G. S., HAVER, S., and OKLAND, O. D., 2010, *Combining contours of significant wave height and peak period with platform response distributions for predicting design response*. Marine Structures, Volume 23, Pp147–63.

BAARHOLM, G.S., and MOAN, T., 2000, *Estimation of nonlinear long-term extremes of hull girder loads in ships*. Marine structures, Volume 13, Pp 495-516.

BATTJES, J. A., 1970, *Long-term wave height distribution at seven stations around the British Isles*, Godalming: National Institute of Oceanography, Report no. A 44.

CHAKRABARTI, S.K., 2005. *Handbook of Offshore Engineering*, ELSEVIER, Pp. 106-118, 197-216.

CHAKRABARTI, S.K., 1987. *Hydrodynamics of Offshore Structures*, Computational Mechanics Publications, Wessex England.

CLOUGH, R. W., and PENZIEN, J., 1993. *Dynamics of Structures*, 2nd Edition. McGraw-Hill, New York, United States.

CRAMER, E.H., 1994, *Stochastic modeling of long term wave induced responses of ship structures*. Marine structures; Volume 7, Pp 537-566.

DIRLIK, T., 1985, *Application of Computers in Fatigue Analysis*, Ph.D. Thesis, Department of Engineering, University of Warwick, Coventry, England.

DNV-RP-F204 (DNV), *Riser Fatigue*, Det Norske Veritas, Hovik, Norway, 2010.

DNV-OS-F201 (DNV), *Dynamic Risers*, Det Norske Veritas, Hovik, Norway, 2010.

ETUBE, L. S., 2001. *Fatigue and Fracture Mechanics of Offshore Structures*. Duncan

Dowson, Professional Engineering Publishing Limited, London and Bury St Edmunds, UK.

FALTINSEN, O. M., 1990. *Sea loads on ships and offshore structures*. Cambridge University Press, Cambridge, England.

FARNES, K.A., and MOAN, T., 1994, *Extreme dynamic, non-linear response of fixed platforms using a complete long-term approach*. Applied ocean research, Volume 15, Pp 317-326.

GAIDAI, O., and NAESS, A., 2008, *Extreme response statistics for drag dominated offshore structures*. Probabilistic engineering mechanics, Volume 23, Pp 180–187.

GASPAR, B., TEIXEIRA, A. P., and GUEDES-SOARES, C., 2016, *Effect of the non-linear vertical wave-induced bending moments on the ship hull girder reliability.* Ocean engineering, Volume 119, Pp 193-207.

GONG, K., DING, J., and CHEN, X., 2014, *Estimation of long-term extreme response of operational and parked wind turbines: Validation and some new insights.* Engineering structures, Volume 81, Pp 135-147

HAVER, S.K., and NYHUS, K.A., 1986, "A Wave Climate Description for Long Term Response Calculations". *Proceedings of the 5th International Offshore Mechanics and Artic Engineering Symposium*, Vol. IV, New York, pp. 27-34

HASSELMANN, K., BARNETT, T.P., BOUWS, E., CARLSON, H., CARTWRIGHT, D.E., EAKE, K., EURING, J.A., GICNAPP, A., HASSELMANN, D.E., KRUSEMAN, P., MEERBURG, A., MULLEN, P., OLBERS, D.J., RICHREN, K., SELL, W., WALDEN, H. 1973. *Measurements of wind-wave growth and swell decay during the joint North Sea wave project (JONSWAP).* Deutschen Hydrographischen Institut, Hamburgo.

LOW, Y. M., 2008, *Prediction of extreme responses of floating structures using a hybrid time/frequency domain coupled analysis approach*. Ocean engineering, Volume 35, Pp 1416-1428.

LOW, Y. M., and CHEUNG, S. H., 2012. *On the Long-term Fatigue Assessment of Mooring and Riser Systems*. Ocean Engineering, ELSEVIER, pp. 60-71.

LOW, Y. M., and LANGLEY, R. S., 2008, *A hybrid time/frequency domain approach for efficient coupled analysis of vessel/mooring/riser dynamics.* Ocean engineering, Volume 35, Pp 433-446.

MANUEL, L., NGUYEN, P. T. T., CANNING, J., COE, R. G., ECKERT-GALLUP, A.C., and MARTIN, N., 2018, *Alternative approaches to develop environmental contours from metocean data.* Journal of Ocean Engineering and Marine Energy.

MATSUISKI, M., and ENDO, T., 1968, *Fatigue of Metals Subject to Varying Stress*, Japan Society of Mechanical Engineers, Fukuoka, Japan.

MONSALVE GIRALDO, J. S., 2014, *Efficient methods for probabilistic fatigue analysis of marine structures*, M.Sc. Thesis, Department of Civil Engineering, COPPE/UFRJ, RJ, Brazil.

MONSALVE GIRALDO, J. S., CORTINA, J. P. R., SOUSA F. J. M., VIDEIRO, P. M., and SAGRILO, L. V. S., 2018, *Hybrid Parabolic Interpolation – Artificial Neural Network Method (HPIANNM) for long-term extreme response estimation of steel risers.* Applied Ocean Research, Volume 76, Pp 221–234.

MONSALVE GIRALDO, J. S., DANTAS, C. M. S., and SAGRILO, L. V. S., 2016, *Probabilistic fatigue analysis of marine structures using the univariate dimension-reduction method*. Marine Structures, Volume 50, Pp 189-204.

MOSQUERA, I. A. M., 2013, *Modelo de função de probabilidade conjunta de parâmetros ambientais usando a transformada de Nataf*, M.Sc. Thesis, Department of Civil Engineering, COPPE/UFRJ, RJ, Brazil.

NAESS, A., and ENGESVIK, K., 1985. *Fatigue Handbook Offshore Steel Structures, Chapter 3 Fracture Mechanics as a Tool in Fatigue Analysis*, TAPIR.

NAESS, A., and MOAN, T., 2013. *Stochastic Dynamic of Marine Structures*, CAMBRIDGE UNIVERSITY PRESS, New York, United States.

NASCIMENTO, L. S., 2009, *Extreme values analysis of dynamic response parameters of self-elevating platforms*, M.Sc. Thesis, Department of Civil Engineering, COPPE/UFRJ, RJ, Brazil.

NEJAD, A.R., GAO, Z., and MOAN. T., 2013, *Long-term analysis of gear loads in fixed offshore wind turbines considering ultimate operational loadings*. Energy Procedia, Volume 35, Pp 187-197

NEWLAND, D.E., 1993. *An Introduction to Random Vibrations, Spectral & Wavelet Analysis*, 3rd Edition. Longman Scientific and Technical, Harlow, England.

NOLTE, K.G., HANSFORD, J. E., 1976. *Closed-Form Expressions for Determining the Fatigue Damage of Structures Due to Ocean Waves*. Offshore Technology Conference. Paper number OTC 2606, pp. 862-870.

NUGTEREN, F., 2015, *Flexible riser fatigue analysis, studying conservatism in flexible riser fatigue analysis and development of an engineering model to study influencing parameters of local wire stress*, M.Sc. Thesis, Faculty of Mechanical, Maritime and Materials Engineering, Delft University of Technology, South Holland, Netherlands.

ORIMOLADE, A. P., HAVER, S., and GUDMESTAD, O. T., 2016, *Estimation of*

extreme significant wave heights and the associated uncertainties: A case study using NORA10 hindcast data for the Barents Sea. Marine structures, Volume 49, Pp 1-17.

PAPALEO, A., 2009, *Metodologia para definição de casos de carregamentos ambientais equivalentes para o projeto de risers em catenária*, D.Sc. Thesis, Department of Civil Engineering, COPPE/UFRJ, RJ, Brazil.

PIERSON JR W.J. and MOSKOWITZ L. 1964. *A proposed spectral form for fully developed wind seas based on the similarity theory of S.A. Kitaigorodskii*. Journal of Geophysical Research, 69, 24, 5181-5203.

PEREIRA, L. O. C., 2018, *Métodos simplificadores para análise de fadiga em risers*, M.Sc. Thesis, Department of Civil Engineering, COPPE/UFRJ, RJ, Brazil

PRESS, W. H., TEUKOLSKY, S. A., VETTERLING, W. T., and FLANNERY, B. P., 2007. *Numerical Recipes*, 3rd Edition. Cambridge University Press, Cambridge, UK.

SILVA, P. B. A., 2018, *Modelagem probabilística de parâmetros de onda para análise de estruturas marítimas*, M.Sc. Thesis, Department of Civil Engineering, COPPE/UFRJ, RJ, Brazil.

REN, N., GAO, Z., MOAN, T., and WAN, L., 2015, *Long-term performance estimation of the Spar–Torus-Combination (STC) system with different survival modes*. Ocean engineering, Volume 108, Pp 716-728.

SAGRILO, L.V.S., 2016, *Lecture notes - Probabilistic analysis of offshore structures*, PEC/COPPE/UFRJ,Rio de Janeiro, RJ, Brasil.

SAGRILO, L. V. S., NAESS, A., and DORIA, A. S., 2011, *On the long-term response of marine structures*. Applied Ocean Research, Volume 33, Pp 208-214.

TAN, Z., QUIGGIN, P., and SHELDRAKE, T., 2007, "Time domain simulation of the 3D bending hysteresis behaviour of an unbonded flexible riser". *Proceedings of the 26th International Conference on Offshore Mechanics and Artic Engineering*, San Diego, Californa, USA.

TRIM, A.D., 1992, *Extreme responses of flexible risers*. Marine structures, Volume 5, Pp 367-385.

VARGAS-BAZÁN, J. A., 2012, *Response statistics of ocean structures due to non-linear effects of wave loads*. M.Sc. Thesis, Department of Civil Engineering, COPPE/UFRJ, RJ, Brazil.

VIDEIRO P. M., MONSALVE GIRALDO J. S., SOUSA F. J. M., DOS SANTOS C. M. P. M. and SAGRILO L. V. S., 2019, *Long-term analysis using a scatter diagram key*

region to evaluate the extreme response of steel risers. Marine Structures, Volume 64, Pp 322-340.

WINTERSTEIN SR, U de TC, CORNELL CA, BJERAGER P, HAVER S., 1993. "Environmental parameters for extreme response: inverse FORM with omission sensitivity". *Proceedings of the international conference on structural safety and reliability*, Innsbruck, Austria.

WIRSCHING, P. H., and CHEN, Y. N., 1987. "Consideration of Probability-Based Fatigue Design for Marine Structures". *Marine Structural Reliability Symposium,* The Society of Naval Architects and Marine Engineers. pp. 35-37.

WIRSCHING, P. H., LIGHT, M. C., 1980. *Fatigue under wide band random stresses.* Journal of the Structural Division. Volume 106, Issue 7, Pp 1593-1607

Appendix A

Environmental Contour Method

The Environmental Contour Method (ECM) is a practical approach used to estimate extreme responses of offshore structures subjected to wave loads by using only some short-term analyses. Different codes such as DNV-OS-F201 (2010) accept this methodology for the evaluation of this type of structures. Through this procedure it is possible to determine characteristic structure responses, obtaining approximate values which are usually acceptable for basic project requirements, without the need to perform the full integration on the H_s-T_z domain that demands the long-term response methodology.

The Inverse First-Order Reliability Method (known as I-FORM) is an efficient method to obtain the environmental contours (BAARHOLM *et al*., 2010), which indeed represent a set of characteristic environmental parameters associated to a specified return period of N years. The main requirement for use of the environmental contour method, is the availability of a joint probability density function of H_s and T_z such taht described in Eq. (2.5).

The approach to determine the contour lines considers an exceedance probability of $p_e = \frac{1}{Ns}$ in a transformed bi-dimensional U_1-U_2 standard normal space. Ns is the number of expected sea states in N years. The environmental contour in the Gaussian standard space U_1-U_2 is a circle with radius equal to $\beta = -\Phi^{-1}(p_e)$, where each pair (u_1, u_2) along this circle corresponds to an N-yr exceedance probability event. $\Phi(.)$ corresponds to the cumulative probability function of a standard normal variable and $\Phi^{-1}(.)$ to its inverse.

The contour line in the H_s-T_z space may be obtained by using the Rosenblatt transformation, the Nataf transformation, or a copula-based transformation (MANUEL *et al*., 2018). In this work, a full joint distribution on H_s ant T_z is available; therefore, the Rosenblatt transformation was used to obtain the characteristic sea states. In this technique, as explained in details by BAARHOLM *et al*. (2010) and MANUEL *et al*.

(2018), a relation between the significant wave height, the up-crossing (or peak) period and the standard Gaussian variables U_1 and U_2 is given by:

$$\begin{aligned} u_1 &= \Phi^{-1}\left[F_{Hs}(h_s)\right] \\ u_2 &= \Phi^{-1}\left[F_{Tz|Hs}(t_z|h_s)\right] \end{aligned} \tag{A.1}$$

or

$$\begin{aligned} h_s &= F_{Hs}{}^{-1}\left[\Phi(u_1)\right] \\ t_z &= F_{Tz|Hs}{}^{-1}\left[\Phi(u_2)\right] \end{aligned} \tag{A.2}$$

By applying this transformation, it is possible to determine in the Hs-Tz space the so called N-yr contour line or N-yr environmental contour.